

CZECH TECHNICAL UNIVERSITY IN PRAGUE

Faculty of Mechanical Engineering

Department of Automotive, Combustion Engine, and Railway

Engineering

Study program: Master of Automotive Engineering

Field of study: Advanced Powertrains



APPLICATION OF AN AUTOMATED OPTIMIZATION SYSTEM ON AN ENGINE TESTBED

Author: Ashwin Srinivasa Raghavan

Supervisor : Ing. Jiří Vávra, Ph.D

Tutor : Ing. Vít Doleček, Ph.D.

Year: 2021

I. Personal and study details

Student's name: **Srinivasa Raghavan Ashwin** Personal ID number: **490520**
Faculty / Institute: **Faculty of Mechanical Engineering**
Department / Institute: **Department of Automotive, Combustion Engine and Railway Engineering**
Study program: **Master of Automotive Engineering**
Branch of study: **Advanced Powertrains**

II. Master's thesis details

Master's thesis title in English:

Automated optimization of parameters of a gas spark ignition engine

Master's thesis title in Czech:

Automatizované optimalizace parametrů plynového zážehového spalovacího motoru

Guidelines:

Make a survey of available systems for automated offline and online optimization applicable to an engine test bed. Study documentation of the available automated optimization system. Prepare documentation for the necessary steps and modifications of the current test setup for the application of an automated optimization system on an engine test bed. Couple a 1-D model of a SI turbocharged gas engine in a GT-Suite with the external optimization tool and perform optimization of engine performance and fuel consumption. Consider the practical constraints of the SI engine as a knock, turbocharger speed, exhaust gas temperature, and thermal and mechanical stress of the engine components.

Bibliography / sources:

AVL CAMEO documentation
GT-Suite manuals


Name and workplace of master's thesis supervisor:

Ing. Jiří Vávra, Ph.D., Department of Automotive, Combustion Engine and Railway Engineering, FME

Name and workplace of second master's thesis supervisor or consultant:

Date of master's thesis assignment: **16.04.2021** Deadline for master's thesis submission: **13.08.2021**

Assignment valid until: **19.09.2021**

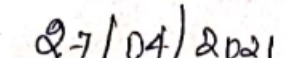

Ing. Jiří Vávra, Ph.D.
Supervisor's signature

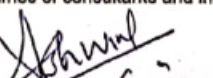

doc. Ing. Oldřich Vlček, Ph.D.
Head of department's signature


prof. Ing. Michael Valášek, DrSc.
Dean's signature

III. Assignment receipt

The student acknowledges that the master's thesis is an individual work. The student must produce his thesis without the assistance of others, with the exception of provided consultations. Within the master's thesis, the author must state the names of consultants and include a list of references.

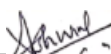

Date of assignment receipt


Student's signature

Disclaimer

I hereby declare that the following thesis is my independent work and to the best of my knowledge. I have only used the document listed in the attachments. It contains no materials previously published or written by any other person.

In Prague :13/08/2021



Ashwin Srinivasa Raghavan.

Acknowledgment

I would like to convey my sincere gratitude to my supervisor Ing. Jiří Vávra, Ph.D., for giving me this opportunity. His guidance, continuous support, knowledge have motivated me throughout my thesis and helped me achieve my goals. Besides my supervisor, I am grateful to Ing. Vít Doleček, Ph.D. & I would like to thank my family & friends for all the love, support, and care throughout my studies.

Abstract

This thesis deals with surveying the modern automated optimization systems applicable to the engine testbed. For this purpose, a series of engine performance optimization software (working) operations were understood using their respective user manuals. Associated with this task was the automated optimization of the Zetor 1605 engine, taking into account the tests and optimization of the turbocharged SI gas engine. For this purpose, the Zetor 1605 engine model was built in GT-Power. Using the Design of Experiments (DOE), the performance data generated is coupled with AVL CAMEO for full load performance optimization. Furthermore, this task was carried out for the Common Mixer system and Multi-Point Fuel Injection (MPFI) system configuration taking into account the practical constraints of the engine, namely knock, turbocharger speed, exhaust gas temperature, thermal and mechanical stress of the components.

Keywords: *GT-Power, AVL CAMEO, Full load Optimization, DOE.*

Abstrakt

Tato práce se zabývá průzkumem moderních automatizovaných optimalizačních systémů použitelných na motorovém zkušebním stanovišti. Za tímto účelem byla prozkoumány možnosti řady softwarových optimalizačních procedur podle příslušných uživatelských příruček. Byla provedena automatizovaná optimalizace plynového přeplňovaného zážehového motoru Zetor 1605. Za tímto účelem byl model motoru Zetor 1605 postaven v GT-Power a pomocí Design of Experiments (DOE) byla v software AVL CAMEO provedena optimalizace výkonu při plném zatížení. Tato úloha byla provedena pro konfiguraci systému v provedení s nízkotlakým směšovačem (Common Mixer) a vícebodovým vstřikováním paliva (MPFI) s přihlédnutím k praktickým omezením motoru, konkrétně klepání, otáček turbodmyhadla, teploty výfukových plynů, tepelného a mechanického namáhání součástí.

Klíčová slova: *GT-Power, AVL CAMEO, Optimalizace plného zatížení, DOE.*

Table of Content

| | |
|--|----|
| 1.Nomenclature | 8 |
| 2.Introduction | 9 |
| 3. Research Motivation & Scope of thesis | 11 |
| 4. Literature survey | 12 |
| 4.3 Engine Energy Split:..... | 13 |
| 4.4 Multi-Point Fuel Injection: | 15 |
| 4.5 Emissions:..... | 16 |
| 5. Make a survey of the available systems for automated optimization systems applicable on an engine testbed | 18 |
| 6. Engine Modelling in GT Power | 26 |
| 6.1 GT Suite software | 26 |
| 6.1.1 GT-Power..... | 26 |
| 6.1.2 GT- SPACECLAIM..... | 26 |
| 6.1.3 GEM3D preprocessor..... | 26 |
| 6.2 Engine model and its aspects | 26 |
| 6.3 Environment..... | 28 |
| 6.4 Cylinder object..... | 28 |
| 6.5 Crank train model | 29 |
| 6.6 Piston object..... | 31 |
| 6.7 Valve object | 31 |
| 6.8 Injector object | 32 |
| 6.9 Air filter | 34 |
| 6.10 Compressed air Intercooler | 35 |
| 6.11 Turbocharger system..... | 36 |
| 6.12 Wastegate control | 37 |
| 6.13 Thermocouple temperature sensor model..... | 37 |
| 6.14 Knock control | 38 |
| 6.14.1 Maximum cylinder pressure..... | 39 |
| 6.14.2 Knock Induction time integral | 39 |
| 6.14.3 Unburnt mass fraction | 40 |
| 6.14.4 Crank angle at knock onset | 40 |
| 6.14.5 Knock Index | 40 |
| 6.15 Exhaust Gas Recirculation System (EGR) | 41 |
| 6.15.1 Low-pressure EGR..... | 41 |

| | |
|--|----|
| 6.15.2 High-pressure EGR | 41 |
| 6.15.3 EGR control | 43 |
| 6.15.4 EGR % recycled | 43 |
| 6.15.5 EGR mass flow rate | 44 |
| 6.16 Throttle position control | 44 |
| 6.17 Heat Transfer Object..... | 45 |
| 6.18 NOx model..... | 45 |
| 6.19 Discretization Length for simulation | 45 |
| 7. Engine model & design of experiments | 46 |
| 7.1 Common Mixer model..... | 46 |
| 7.2 MPFI system model | 46 |
| 7.3 Design of Experiments (DOE)..... | 46 |
| 8. Optimization | 46 |
| 8.1 AVL CAMEO software | 46 |
| 8.2 Common Mixer full load DOE data evaluation..... | 47 |
| 8.3 MPFI system full load DOE data evaluation. | 48 |
| 9. Results & Conclusion | 49 |
| 9.1 Comparison of Common Mixer and MPFI system performance | 49 |
| 10. Further Scope..... | 54 |
| 11. References | 55 |
| 12. List of Figure | 57 |
| 13. List of Tables..... | 58 |
| 14. List of Files in Attached CD..... | 59 |
| 15. Appendix. | 60 |
| 15.1 Common Mixer system..... | 60 |
| 15.2 MPFI system | 61 |
| 15.3 Simulation graphs | 62 |
| 15.3.1 Common Mixer system | 62 |
| 15.3.2 MPFI system full load optimization | 66 |
| 15.4 Zetor Forterra 135 Diesel Datasheet[30] | 70 |

1.Nomenclature

| | |
|------------------|-----------------------------------|
| \dot{m}_{fuel} | Mass Flow Rate of Fuel |
| 1D | One Dimensional |
| 2D | Two Dimensional |
| 3D | Three Dimensional |
| BDC | Bottom Dead Center |
| BP | Brake Power |
| BSFC | Brake Specific Fuel Consumption |
| BSEC | Brake Specific Energy Consumption |
| CH ₄ | Methane |
| CNG | Compressed Natural Gas |
| CO | Carbon Monoxide |
| CO ₂ | Carbon Dioxide |
| c_p | Specific Heat Capacity |
| CR | Common Rail |
| EV | Electric Vehicle |
| ICE | Internal Combustion Engine |
| LNG | Liquefied Natural Gas |
| MEP | Mean Effective Pressure |
| MPFI | Multi Point Fuel Injection |
| NO _x | Oxides of Nitrogen |
| P | Actual Pressure of The Gas |
| RPM | Revolutions Per Minute |
| SI | Spark Ignition |
| TDC | Top Dead Center |
| γ | Specific Heat Ratio |
| λ | Air Excess (lambda) |

2. Introduction

The transportation sector is one of the crucial sectors of an economy. It involves the movement of people and goods across different locations. In the course of the development of this sector, it had reached its pinnacle with the invention of the internal combustion engines 200 years ago. Even now, it is still difficult to find a reliable technology that can completely replace internal combustion engines due to the present-day emission norms and global warming conditions. Every year the pollution norms are becoming very stricter, and the focus is currently either on replacing this technology by going completely electric or improving the efficiency of the engines. However, complete replacement of internal combustion engines is difficult due to the following reasons:

Energy density and weight: Gasoline is about 100 times energy denser than the present-day battery system [33] and weighs lesser than the present-day battery system. For instance, the battery pack of the modern-day Tesla Model S weighed 540 kg.[32]

Cost for the buyer: electric cars are expensive because of the battery costs. However, over the years, it is expected for this cost to reduce due to more people buying more electric cars.

Cost for the seller: “The propulsion-system cost for a long-range EV is around \$16,000, compared with \$6,500 for a conventional internal-combustion powertrain. The consultants expect system design and manufacturing efficiencies to reduce costs by about 10% annually; given this assumption, EVs will take many years to achieve cost parity with ICE. [2]

It is easier to improvise and optimize the existing and proven engine technology at reasonable costs than having a new infrastructure that doesn't suit the customer demographics from an economic point of view.

Charging Infrastructure: Not all countries have the charging infrastructure to go completely electric. E.g., India doesn't possess the necessary infrastructure right now to adapt to electric vehicles, and the present-day market focuses on the development of electric scooters than automobiles.

Therefore, it will take a significant amount of time till we become completely become electric. Before achieving that goal, intermediate steps taken are developing hybrid vehicles, hydrogen fuel cell technology, and further improvement of the internal combustion engines.

Low-temperature combustion, RCCI, Homogenous charge compression ignition(theoretical), exhaust gas recirculation, Turbocharging, and prechamber combustion technologies are some of the present-day improvements to make ICE better.

Both ammonia and hydrogen are carbon-free fuels. Blends of ammonia with hydrogen and Nitrogen are optimized to exhibit premixed laminar flames properties similar to that of methane (CH_4). [3]

However, even these fuel technologies have their drawbacks, i.e., hydrogen requires high storage containers to maintain its energy density, and globally, hydrogen production is from natural gas sources than other methods as it is cost-effective. [4]

Natural gas has been used as a fuel for transportation, and globally about 23 million [5] vehicles are running on natural gas. Compared with gasoline and diesel, natural gas has lower costs and lower pollutant emissions. Also, natural gas has a high-octane number compared to gasoline. Therefore, they can withstand higher compression ratios than gasoline and achieve higher thermal efficiencies than conventional SI engines.[6]

The usage of lean mixtures of natural gas offers additional benefits.[6] The production of NO_x is reduced significantly due to the lower in-cylinder temperatures compared to lambda 1 operation. The world also has higher natural gas reserves compared to crude oil reserves.[7][8]. Also, conversion of existing engines into natural gas engines is cheaper than the development of electric vehicles. Therefore, in this thesis, we are using a Zetor Forterra SI gas engine which has been converted from a diesel engine to a SI engine presently running on natural gas. The goal of this thesis is to perform automated optimization of parameters of the SI gas engine. The optimization has been carried out, taking into account the engine performance, fuel consumption, and safety aspects.

3. Research Motivation & Scope of thesis

The Research and Development Centre of Vehicles of Sustainable Mobility at Czech Technical University has converted an existing diesel tractor engine into a SI gas engine. Therefore, as part of this process, several students have been assisting in the same conversion. Therefore, this thesis is a continuation of the works of the previous students.

Mr.Ing.Pavlíček, the author of “Engine characteristics of a turbocharged natural gas engine with a scavenged prechamber,” worked to build a model of a diesel engine and subsequent conversion to a gas-powered engine with a prechamber.

Mr.Ing.Shubaham Bawkar, the author of “ Mixture homogeneity evaluation for a CNG port fuel injection,” worked to design and develop a fuel injection system for methane injection into inlet ports and evaluated the mixture homogeneity of the port fuel injection system. Simulations were performed on the designed fuel injection location using the AVL FIRE to evaluate the mixture homogeneity of the PFI system.

The goal of the present thesis is to modify the current test setup for applying an automated optimization system on the engine testbed. GT-Power was used for further development of the engine model, and AVL CAMEO was used for engine performance optimization. Here, the performance optimization has been performed for an engine for a common mixer system and an MPFI system.

A theoretical study has been performed to understand the present-day automated engine optimization technologies.

4. Literature survey

Automotive manufacturers are constantly struggling to reduce the amount of engine emissions. Lean burn combustion is one of the viable solutions to reduce the emission levels such that they are within the legislative limits. The lean-burn combustion works in such a way that it reduces the in-cylinder temperature and avoids NO_x formation. On the other hand, slow burn, partial burn, and misfire are some of the problems that arise if the air excess goes beyond the smoke point of the engine (misfire point for a typical CNG engine). Therefore, to quantify lean combustion, we use the concept of air excess.

4.1 Air Excess:

The Fuel Composition is defined by the combustion stoichiometry, which in turn defines the theoretical air for fuel's complete combustion. In engine testing, both the air mass flow rate and fuel mass flow rate are measured. The ratio of these flow rates is useful when defining engine operating conditions.

$$\text{Air/Fuel Ratio (A/F)} = \frac{\dot{m}_a}{\dot{m}_f}$$

Eq 1 Air fuel ratio

Air excess co-efficient (λ) is defined as the ratio between the Actual A/F to Stoichiometric A/F

$$\lambda = \frac{A/F_{\text{Actual}}}{A/F_{\text{Stoichiometric}}}$$

Eq 2 Air excess Co-efficient

We can define whether the combustion was carried out using rich mixture or lean mixture with the above equation.

If $\lambda > 1$, the mixture is lean.

If $\lambda = 1$, the mixture is stoichiometric

If $\lambda < 1$, the mixture is rich mixture.

4.2 Chemical Efficiency:

It is the fraction of fuel energy supplied which is released in the combustion process.

$$\eta_c = \frac{H_R(T_A) - H_P(T_A)}{m_f Q_{HV}}$$

Eq 3 Chemical Efficiency

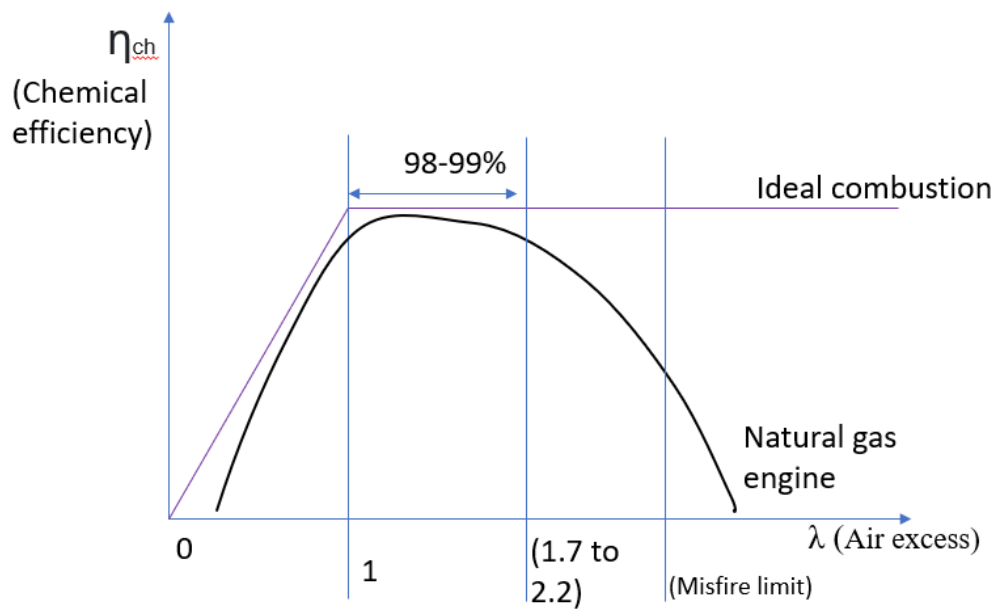


Figure 1 Chemical Efficiency vs. Air excess [13]

In figure 1, we observe the graph between chemical efficiency vs. Air excess for natural gas. The chemical efficiency is maximum slightly after stoichiometric condition as it requires an excessive amount of air for the highest chemical efficiency (for ideal combustion case, it is exactly stoichiometric). It decreases with further increase in air excess. The maximum air excess is limited by the misfire limit[13].

4.3 Engine Energy Split:

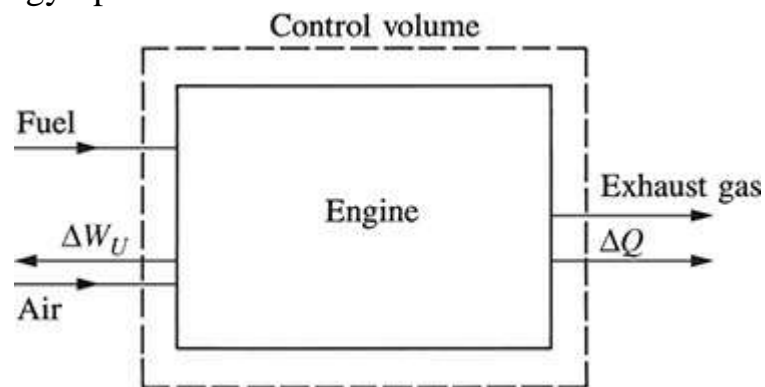


Figure 2 sample engine control volume[11]

For a control volume surrounding the engine, the steady flow energy conservation equation is

$$P_b + \dot{Q}_{cool} + \dot{Q}_{misc} + \dot{H}_{e,ic} + \dot{m}\dot{H}_{e,s} = \dot{m}_f Q_{LHV}$$

Eq 4

Where,

P_b is the brake power [kW]

\dot{m}_f is the mass of fuel [kg/s]

\dot{Q}_{cool} is heat loss due to cooling [J/s]

\dot{Q}_{misc} is the miscellaneous losses [J/s]

$\dot{H}_{e,ic}$ is exhaust enthalpy of losses due to incomplete combustion. [J/K]

$\dot{H}_{e,s}$ is the sensible enthalpy of the exhaust gases. [J/K]

$$\dot{H}_{e,s} = h_e(T) - h_e(T_{ref})$$

$$T_{ref} = 298.15K$$

A considerable part of the Indicated power from the combustion is dissipated in the form of friction to overcome the frictional losses between piston rings and skirt and cylinder walls. The secondary frictional dissipation happens in bearings, valve mechanisms or auxiliary devices. The enthalpy in the exhaust can be further divided into sensible enthalpy, exhaust kinetic energy, incomplete combustion, and heat transfer to the exhaust system.

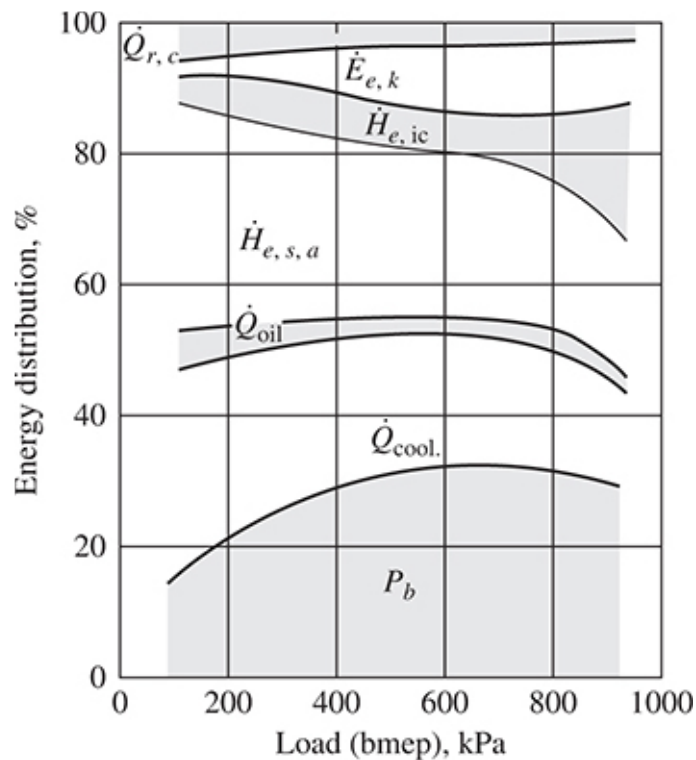


Figure 3 Energy balance for a spark-ignited gasoline engine as a function of load. Operating Conditions:2000 rpm, bmep from 100 to 920 kPa [11]

The above figure shows the energy distribution for a spark ignited gasoline engine. Although heat losses are a substantial part of the fuel energy input, eliminating heat losses would only

allow a fraction of heat transferred to the combustion chamber and exhaust port walls to be converted to useful work. The remainder would leave the engine as sensible exhaust enthalpy.

4.4 Multi-Point Fuel Injection:

Over the last two decades, a steady transition occurred from carburetors to the use of port fuel injection, where the fuel is injected into the intake port of each engine cylinder. Such systems require one fuel injector per cylinder. While there are both mechanical and electromagnetically controlled injection systems, both are electronically controlled. The advantages of port fuel injection are increased power and torque through improved volumetric efficiency and more uniform fuel distribution, the more rapid engine response to changes in throttle position, and more precise control of the in-cylinder air-fuel ratio. Electronically controlled fuel injection allows the amount of fuel injected per cycle for each cylinder to be varied in response to inputs derived from sensors, which define the actual engine operating conditions. Two basic approaches have been developed; the major difference between the two is the method used to determine the airflow rate: direct measurement or estimation based on air density and engine speed.

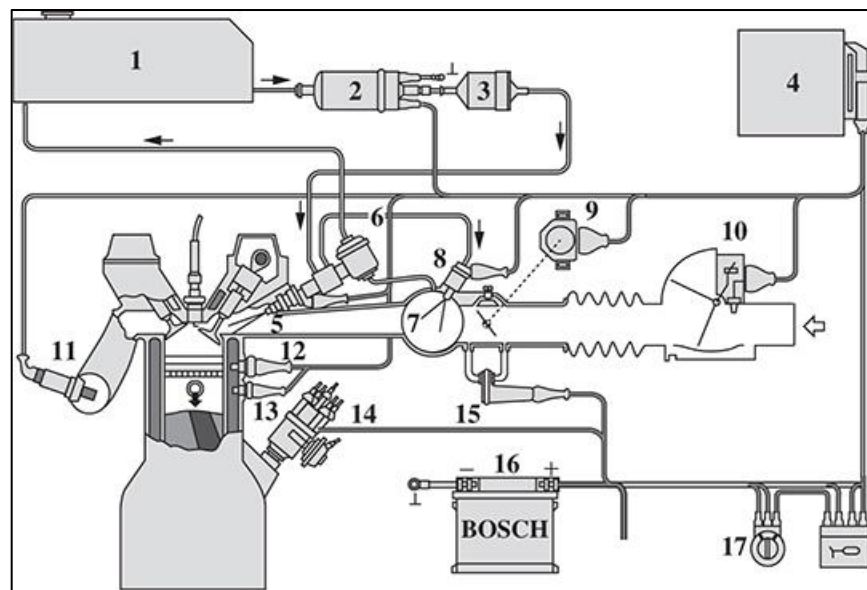


Figure 4 Bosch L-Jetronic Multi point PFI. [11]

Index: 1-Fuel tank; 2- Electric fuel pump ; 3-Fuel Filter ; 4-ECU ;5-Injector ; 6 – Fuel Pressure regulator ; 7-Intake Manifold ; 8-Electric cold start valve ; 9-Throttle valve switch ; 10-Airflow Sensor ; 11- Exhaust oxygen Sensor ; 12- Thermal-Time switch ; 13- Engine Temperature sensor ; 14-Ignition Distributor ; 15-Auxillary Air valve ; 16- Battery ; 17- Ignition switch

Port fuel injection systems offer several options regarding the timing and location of each injection relative to the intake event. The spray is directed towards the back of the intake valves. With electronically controlled injection systems, the fuel is injected intermittently toward the intake valves. The fuel-injection pulse width to provide the appropriate fuel mass for each cylinder air charge varies from about 1.5 to 10 ms over the engine load and speed range. Crank angle degrees vary from 10 to 20° at light load and low speed to up to 300° at maximum speed and load. Thus, the pulse width varies from being much less than to greater than the duration of the intake stroke. In the early fuel injection systems, all injectors were operated

simultaneously. Now, to achieve mixture uniformity, sequential injection timing is used, where the phasing of each injection pulse relative to its cylinder's intake valve lift profile is the same.

4.5 Emissions:

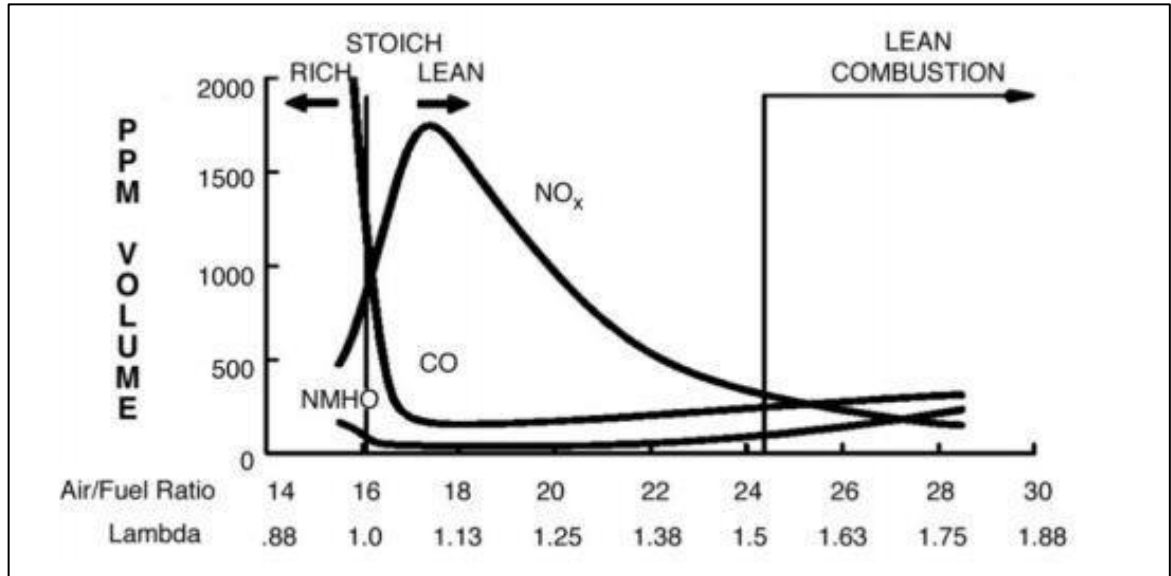


Figure 5 Emission Vs A/F Ratio[11]

The pollutants entering the atmosphere from incomplete combustion can be measured by the main emissions of Carbon Monoxide (CO), Hydrocarbon gas (HC), and Nitrogen Oxide (NO_x). The figure above shows the graphical representation of the emissions in parts per million (ppm) versus the A/F ratio; it can be noticed that running the engine on a lean A/F mixture result in decreased emissions. This happens because enough air is available to burn all the fuel, which means there will be no products from incomplete combustion. However, irrespective of whether the mixture is rich or lean, some amount of A/F mixture gets trapped in the crevices of the compression rings & oil rings, which do not burn and are processed in the catalytic converter [11]. Under cold-start or generally under cold conditions, other HC sources such as lubricating oil films and single-wall flame quenching are believed to become equally important with combustion-chamber crevices [11] [18], which can be seen in the figure below. The combustion of the air-fuel mixture is fast but not instantaneous, resulting in the production of heat and pollutant gases. Lean burn combustion helps to reduce both the in-cylinder temperature as well as pollutants like NO_x. The NO_x formation takes place at very high in-cylinder temperatures; lean burn combustion reduces the in-cylinder, which results in a decrease in NO_x formation. Also, the combustion process is more efficient due to excess oxygen, and more energy is generated from the same amount of fuel [19].

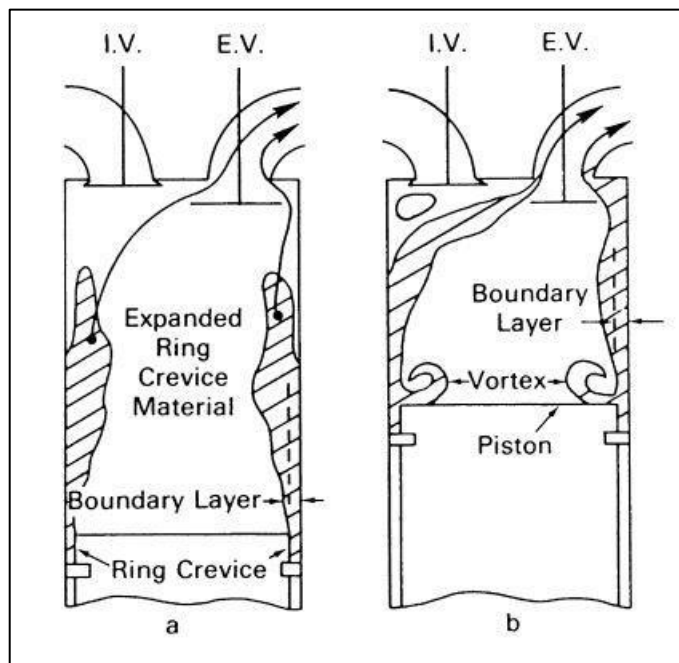


Figure 6 Schematic of Flow process during a) blowdown phase b) exhaust stroke[11]

Even though with all the advantages mentioned above, there are few limitations in using a lean mixture. The disadvantage of this method is it results in low flame speeds, and in actual operating conditions flame speed required to combust the A/F mixture is high. If the flame speed is too low, it might result in a misfire, resulting in high unburnt hydrocarbon (UHC) emissions. Therefore, the lean burn limit is restricted by the capability of the ignition system to ignite the A/F mixture. To overcome the above limitation, an alternative ignition system should be considered. This can be achieved by using any of the following methods - creating high turbulence, turbocharging, and using advanced combustion techniques [20].

5. Make a survey of the available systems for automated optimization systems applicable on an engine testbed

Increasing customer satisfaction and strong emission control limits are putting huge pressure on the transportation sector, leading to a great increase in the number of control variables and higher complex control. As a result, finding the optimum points from the available data is taking greater time and effort. Furthermore, the number of measurements increases exponentially with the increase in an additional input variable, rendering full factorial measurements difficult [21]. Therefore, the DOE process is widely accepted in the present-day transportation sector for engine performance optimization. The purpose of DOE is twofold, i.e., response surface optimization and regression modeling. Our prime focus is on the former as we want to optimize the full-load performance of the engine.

This DOE process mainly involves statistics behind the process for performance optimization, and different companies have developed their own engine performance optimization software package. Presently, we have taken into account AVL CAMEO, GT Power, IAV Orion, MATLAB, ETAS ASCMO for a theoretical study purpose to understand the overall services offered by the software for engine performance optimization. This list is not entirely exhaustive. The selection is based on the availability of the product operation manuals and the popularity amongst the engineering audience.

For all these software packages, the following steps are common (If for model-based offline optimization).

1. Definition of Parameters
2. Experimentation
3. Measurement
4. Modeling
5. Optimization
6. Data Filling in ECU.

1. Definition of Parameters

Initially, we define the input parameters, the output performance parameters, and the constraints of the overall system. The input parameters in the present thesis were evaluated in GT-Power, and the output data is transferred to AVL CAMEO for optimization. We used CA50 & EGR % as the two input parameters to evaluate the output performance, namely Brake torque (Nm), power (kW), Exhaust gas inlet temperature (K), etc. Next, we defined the constraints, namely the Maximum cylinder pressure being 140 bars and mass averaged turbine inlet temperature being 973 K. This step is common for all the software packages as it is the input.

2. Design of Experiments (DOE)

Next, we choose the kind of DOE we want to perform to generate a particular dataset and populate the design space. This dataset generation is one of the most tedious time-consuming processes, and the kind of DOE contributes to computation time. We have Full factorial, Space-filling Designs & Optimal designs (V, A, D). The full factorial design is the simplest design style that estimates the interactions and output parameters. But this method is computationally time-consuming if the number of control parameters is more. In our present study, we used full factorial design as we had only two control parameters, i.e., CA50 & EGR %, and therefore it was computationally feasible.

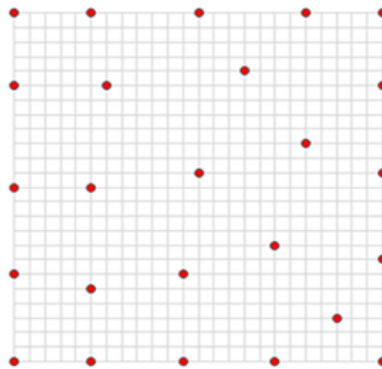


Figure 7 Space Filling Design

Space-filling designs are used for deterministic systems whose output is spread out throughout the design space. Due to the spread of points, they can catch the responses of different regions of the design space, and they should not take more than one input for one design space. One of the types of space-filling design is Latin Hypercube design. Maximum distance and even placement are the main objectives of Latin Hypercube design. The Latin Hypercube covers the boundaries and is also in the center [22].

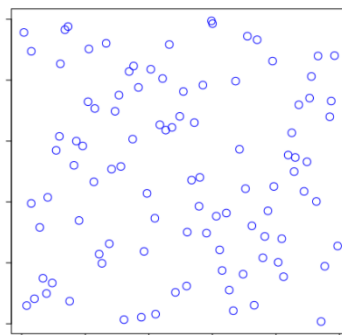


Figure 8 Latin Hypercube design

Lattice is another sub-type of Space-filling design & the point generated in this algorithm uses a prime number per factor. The lattice points are well spread over the design space [23]. A poor choice of numbers can result in a clustered model, resulting in not being able to capture all the effects in the model. Latin Hypercube is preferred over Lattice if the number of points is larger than factors. Otherwise, in the case of a smaller number of points, the number of factors and generators is restricted, leading to the points falling into diagonals.

Another subtype of Space-filling design is Stratified Latin Hypercube which is used to separate the hypercube into different levels or when the number of levels is unknown. Also, they are useful when certain factors can be run only at a given level.

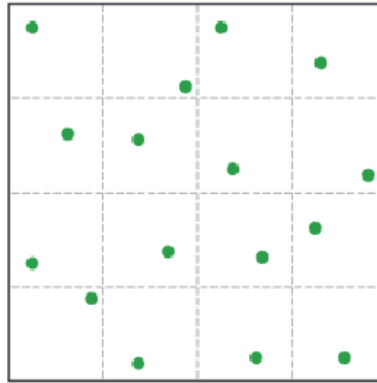


Figure 9 Stratified Latin Hypercube sampling

The optimal design is used in these terms because they are optimal w.r.t some statistical criterion. This is connected to the variance-covariance matrix of the model.

D optimal design: D refers to the determinant of the information matrix, and the D optimal design is maximizing the determinant of the selected regression model. It is a computer-generated algorithm, and it is very flexible as it can sense the irregularities in the space. N selected elements out of the full factorial candidate design will try to maximize the determinant of the information matrix and have the largest experimental space. The D optimal design is of interest when there is some kind of restriction or constraint modifying or chopping off the experimental region. To limit the number of designs over qualitative factors, we use a D optimal design.

A optimal design: Both A optimal and D optimal are contemporary, and they differ w.r.t working, i.e., the A optimal design minimizes the variance compared to D optimal design.

Sobol design: The Sobol design is used to create samples of multiple parameters which are uniform as possible over multi-dimensional space. The sample values are chosen based on previous sample values and thus avoids clusters and gaps [23].

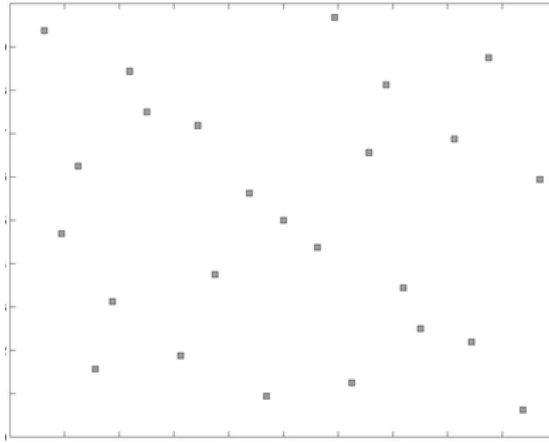
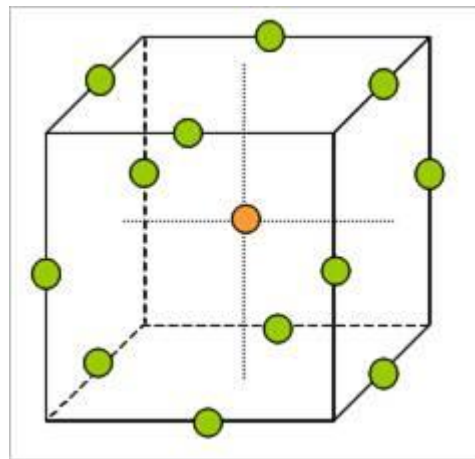


Figure 10 Sobol design

Box Behnken: The Box Behnken design is one of the most proficient amongst three-level factorial design when compared with central composite design, and this design is sufficient to fit a quadratic design[24].



Simplex design: It is a first-order design, and therefore it is difficult to determine the lack of fit.

Central Composite: This central composite design is a response surface methodology used to create second-order quadratic models with two-level designs.

GT power uses full factorial, D optimum, D optimum Latin hypercube design, and Simplex designs. AVL CAMEO uses all mentioned before, along with Space fill design, Box Behnken, and Central Composite Design. MATLAB, ETAS ASCMO & Orion IAV utilizes D optimal, Space-filling, and full factorial designs.

Overall, the DOE says how the design operating space is utilized by the above mentioned designs taking into account the application requirements. In the present thesis, Full factorial design was used to generate the dataset for common-mixer and MPFI system as the further optimization procedures are very crucial.

3.Measurement

Once the models are created, they are to be parameterized, and we need to perform steady-state measurements on the engine test bench. The accuracy of the model is dependent on the quality

of measurement performed in the test cell. While performing measurements in the test cell, it is obvious that we establish the necessary constraints and perform measurements [25]. For example, the turbine inlet temperature cannot exceed a particular temperature limit. Good automation practices are used for this purpose, and it involves iterative adjustment of the inputs. Here it is important not to violate any test space limits. Care needs to be taken that the engine and test bench are not stressed too much.

Types of data acquisition: Static and Dynamic Data Acquisition

- At first, the adjustment parameters are set to desired value via automatic control in the control time (CT). These adjustments influence the measurement variables.
- Stationary Data Acquisition: For any measurement taken, there are two timings, i.e., stabilization time (ST) and averaging time (AT). The whole measurement time is the sum of both. [26]
- This concept is present due to some factors of measurement having low dynamics and some with high dynamics. For example, the temperature of the engine waits in order to reach a stabilized value.
- Depending on the measurement dynamics and the noise on the measurements, the stabilization can take some significant time.
- In recent years, to avoid this time-intensive procedure, several non-stationary measurements were developed, and where the measurements are performed in such a way that dynamic behavior of the systems are suppressed, and the stationary values are calculated [26]
- By using dynamic measurements, one can save a significant amount of time as well as

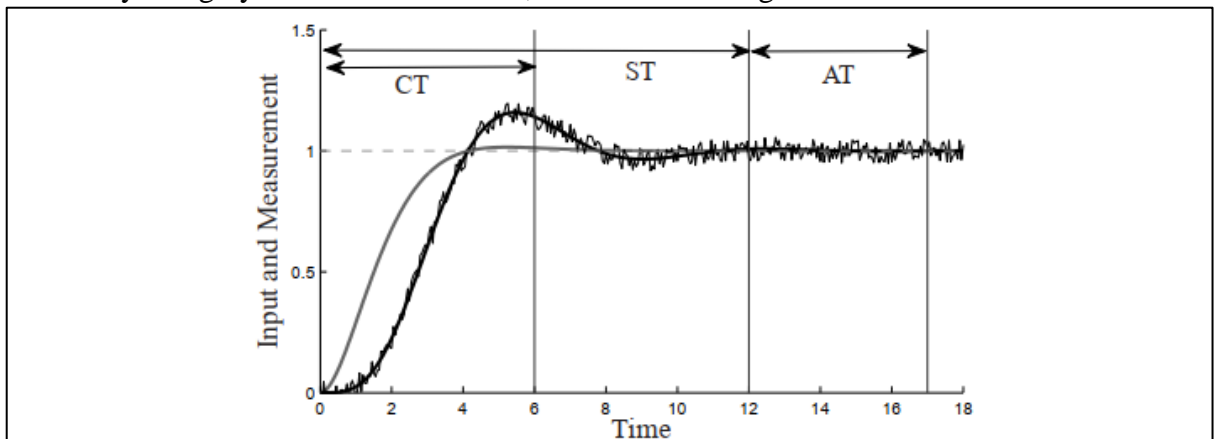


Figure 11 Stationary Measurements: Control (CT) , Stabilization (ST) and Averaging Time (AT)

represent the dynamic state of the engine [26].

- In this present moment, IAV GmbH, and GT-Power are designed for office use and they don't have direct connection to the test bench [26]. In comparison, others are developed for working with test benches. MATLAB customized in-house can be connected to testbenches.

4. Modeling

Once the measurements have been performed, a steady-state model is created. This can predict the effects of the input has on the output. There are many model types in the present moment. We have Least-squares, Neural Networks, Radial Basis Functions, and Gaussian Process Modeling. The advantage of using them is they are able to predict nonlinearities [25], and the quality of the model is judged based on statistical characteristics like RMSE (root mean square error) and R2(coefficient of determination). To assess the prediction capabilities of the model, we need measurements that validate and comparing the predicted values of the model with the measurements we can assess the model quality.

Once the model is found to be sufficiently accurate, it is used for optimization purposes.

In this present moment, AVL CAMEO uses Robust Neural Networks (RNN) and Polynomial Regression. ETAS ASCMO uses the previously mentioned along with Gaussian process modeling (GPM). GT Power utilizes Least Squares, Neural Networks, and Radial Basis Function. IAV Orion utilizes numerous Regression-based models.

For further understanding of the modeling and statistics involved, we can refer to [27],[28], and [29] manuals.

5. Optimization

Engine calibration aims to define engine maps that meet various criteria, namely, lower BSEC, statutory emission norms, drivability, etc. Here, in this stage, we can use the input of driving cycles and other calibrated engine maps to get optimization. Of course, there are always multiple outcomes of interest, and the calibration engineer has to give preference accordingly. For example, at lower RPMs preference can be given to minimize the BSEC than getting the maximum performance output.

For optimization purposes, AVL CAMEO offers the facility for optimization for inputting engine maps and drive cycles. Based on this, we can optimize the model to generate output plots.

Some of the additional tools offered in this segment are Intersection, 2D, 3D, and contour plots. They are especially helpful to perform optimization. All the other software packages too provide these facilities.

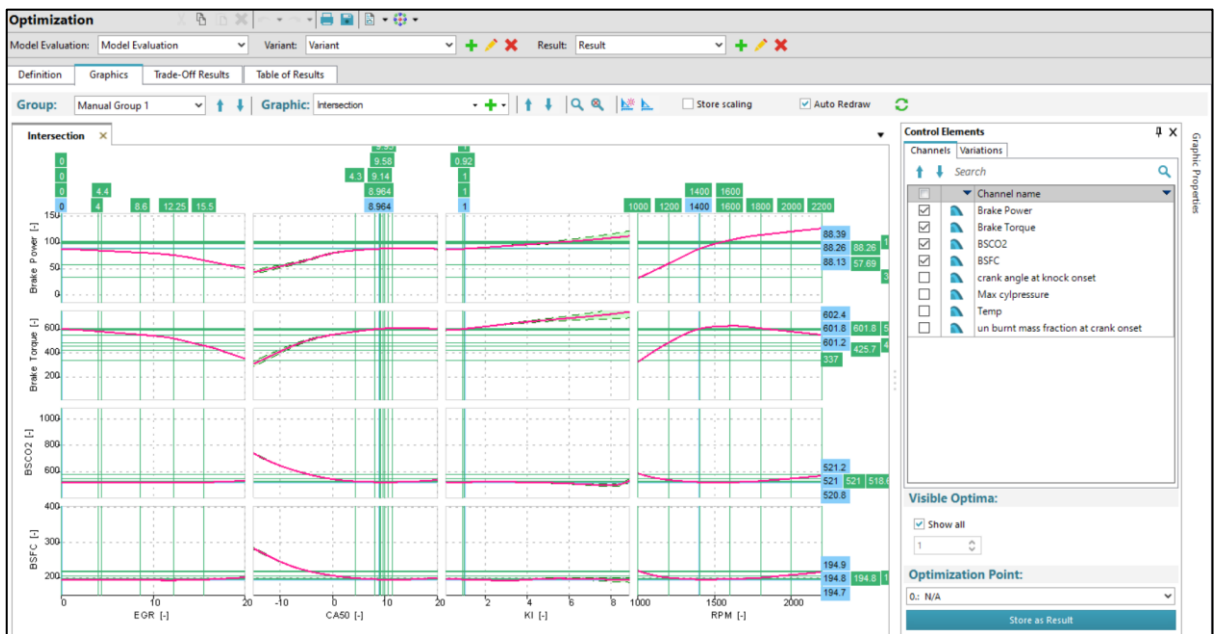


Figure 12 Parallel Optimization

6.Data filling in the ECU

Once the optimization has been performed, we generate a set of favorable operating points, and they will be stored in the ECU, which will be used during the engine operation.

The author of this thesis used GT-Power, assisted by AVL CAMEO. Although detailed steps for engine calibration have been discussed above, the author utilized GT power and AVL CAMEO for full load performance curve optimization in the present thesis. However, not all mentioned steps were utilized due to the lack of engine maps and in-depth measurements in the present stage of the thesis. It is further discussed in the further sections as to what kind of optimization & how the optimization has been performed.

| Software Package | Design of Experiments | Measurement | Modeling |
|------------------|--|--|--|
| GT Power | Full factorial, D optimum, D optimum, latin hypercube design and Simplex designs. | Designed for office use and they don't have direct connection to the test bench | Least Squares, Neural Networks and Radial Basis function |
| AVL CAMEO | Full factorial, D optimum, D optimum Latin hypercube design, and Simplex designs. Space fill design, Box Behnken and Central Composite design | Can have direct connection to the test bench | Robust Neural Networks (RNN) and Polynomial Regression |
| ETAS ASCMO | D optimal, Space filling and full factorial designs. | Can have direct connection to the test bench | Robust Neural Networks (RNN) and Polynomial Regression. Gaussian process modeling (GPM) |
| ORION IAV | D optimal, Space filling and full factorial designs. | Designed for office use and they don't have direct connection to the test bench | Regression based models. |
| MATLAB | D optimal, Space filling and full factorial designs. | Designed for office use and in-house customized products, it can be connected to test benches. | Least Squares, Neural Networks and Radial Basis function |

Table 1 Overview of the Automated Optimization Software with their different aspects

6. Engine Modelling in GT Power

6.1 GT Suite software

The simulation in this thesis is performed using the GT-Suite simulation program. GT suite [9] is a package of simulation tools and libraries that have a wide range of uses, from road and rail transport applications to ship applications.

The software package can be divided into categories as follows.

- Integrated systems: For energy management, emission simulations, battery and fuel cell designs.
- Temperature management systems: For vehicle cooling, air conditioning, heating, and waste heat recovery.
- Mechanics: For 3D vehicle mechanics, timing mechanisms and crank mechanisms
- Drive Systems: For engine modeling, combustion, emissions, and exhaust gas after-treatment systems.
- Fluid systems: Compressors, pumps, fuel injection, tribology, friction and lubrication systems.

6.1.1 GT-Power

GT-Power is engine simulation software used by the world's leading car manufacturers for the design and development of their engines. It offers comprehensive engine simulations with a high accuracy prediction. The GT-Power simulation solver is based on the 1D solution of non-stationary and nonlinear Navier-Stokes's equations [10]. In addition, other solvers are also present dealing with thermodynamics and models dealing with empirical relationships to capture the effects of combustion, heat transfer, turbulence, and other phenomenon. The combination of solvers then offers a highly accurate output.

6.1.2 GT- SPACECLAIM

GT-SPACECLAIM is a 3D CAD tool that allows us to create, edit and simplify a 3D model for simulation needs. For example, it can generate negatives of cavities in a body and can import further to the GEM3D preprocessor or COOL3D. GT-SPACECLAIM supports CAD formats, namely STEP, NX, IGES, and files from other 3D modeling software like Solid Works, CATIA, etc.

6.1.3 GEM3D preprocessor

The GT-SPACECLAIM is directly connected to the GEM3D graphics preprocessor. It basically converts a 3D geometry into a 1D model so that it can be used in GT-Power. It can be used to simplify basic elements such as pipes, branches, shells, catalysts, pumps, and much more.

6.2 Engine model and its aspects

The engine to be simulated is initially a diesel turbocharged four-cylinder Z 1605 tractor engine. It is having a displacement of 4156 cm³. This engine is used for the Zetor Forterra 135 tractors. This engine has been converted from a diesel engine into a SI engine presently running on methane gas. The simulation model of this engine model was built by accurate dimensioning by converting 3D geometries into 1D inside GT-Power [11]. The entire engine assembly was available in the form of a 3D model. Using the CAD software Creo, the necessary components

were imported inside GT-Suite using GT-Space Claim, converted from a 3D element to a 1D element Gem 3D, and then exported to 1D format[11].

Further, additional measurements were carried out by the author of this thesis to accurately model the engine and capture the effects of bends and tapers inside the model. The specifications of the Z 1605 engine are as follows.



Figure 13 Zetor 1605 Diesel Engine

| Parameter | Specification |
|------------------------------|--|
| No. of cylinder | 4 |
| Bore mm | 105 mm |
| Stroke mm | 120 mm |
| Engine Design | In-line, vertical, water-cooled |
| Max Power kW | 95kW/129 HP @ 2200 RPM |
| Max Torque Nm | 544 Nm @ 1400 RPM as per Zetor Datasheet |
| BSFC g/kWh | 244 |
| Displacement cm ³ | 4,156 |
| Max Engine speed RPM | 2200 |

Table 2 Engine Specification

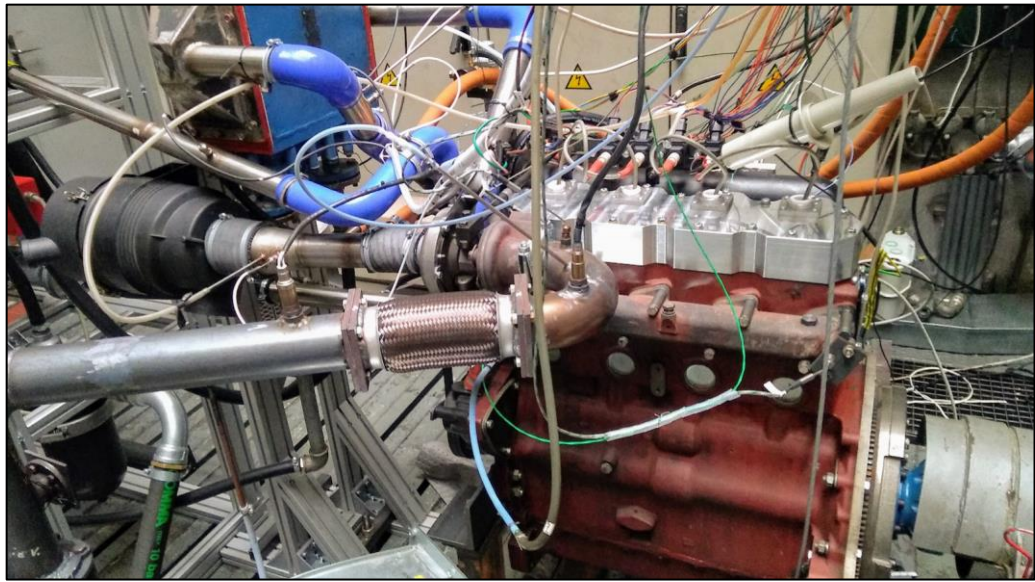


Figure 14 Engine Testcell

6.3 Environment

The object environment is one of the basic elements that every engine model in GT-Power must contain. It is necessary to define the inlet (intake) environment and outlet (exhaust) environment. Therefore, these two identical objects define the boundary conditions at the inlet and outlet of the engine environment. We define the temperature, pressure, and composition of the gas mixtures to be 25°C, atmospheric pressure, and air, respectively.

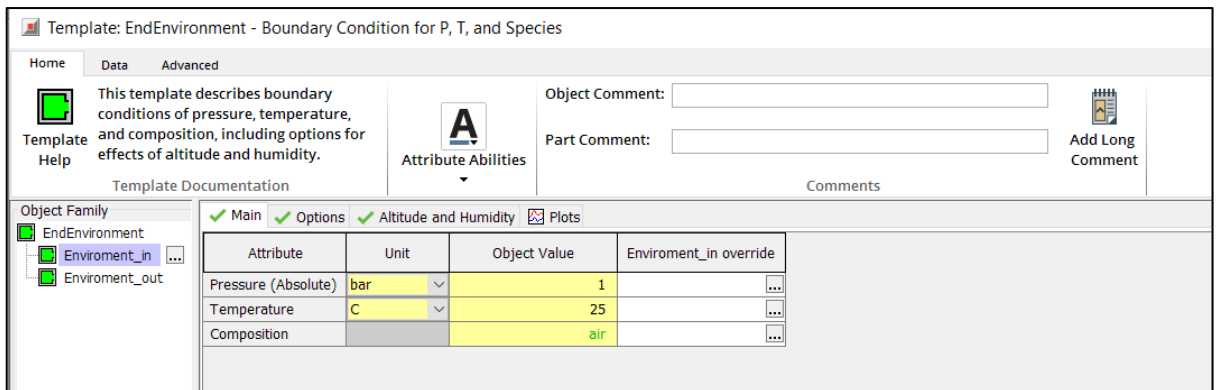


Figure 15 GT-Suite Environment Block

6.4 Cylinder object

The cylinder is the basic building block of the engine model, and the appropriate tuning of the model decides the correctness of the whole simulation. We need to define the initial state-input conditions, the reference wall temperature, the heat transfer object, and the combustion object. The wall temperature reference object is defined using the geometric dimensions and properties of the cylinder, piston, and valves of the Zetor engine.

The EngCylCombSIWiebe burning model was selected for the combustion object. The Wiebe function uses three parameters to define the combustion, i.e., Anchor angle 50% (CA50), duration (10% to 90%), and Wiebe exponent. The CA50 is the angle at which 50% of the mass fraction has been burnt, and it is the angle that is calculated after the TDC of the engine. The duration (10% to 90%) defines the burning duration of the combustion phase of the fuel mixture in the cylinder [11]. This duration has been defined based on the experimental data. The Wiebe exponent is the curve exponent selected to be 1.5.

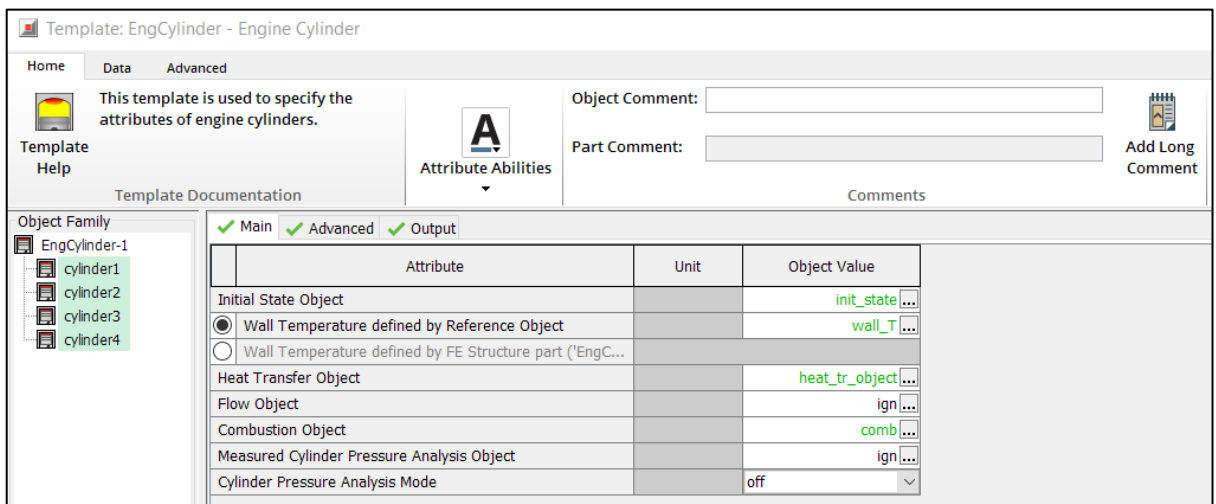


Figure 16 Cylinder Block

It is important to understand that the CA50 not only defines the 50 % mass fraction burnt but based upon changing this parameter, we can practically change the combustion lead or the spark angle. For initial simulation purposes, 12 ° ATDC is used as CA50 input. The Combustion duration of 10%-90% is taken as input from [10]. The duration was defined based on the dependency of cylinder pressures on combustion duration adjustment. Hence, it requires no further calibration.

A functional form used to represent the mass fraction burned versus Crank-angle curve $x_b(\theta)$ is the Wiebe function, and it is given by equation 5.

$$x_b = 1 - \exp \left[-a \left(\frac{\theta - \theta_0}{\Delta \theta} \right)^{m+1} \right]$$

Eq 5 Mass fraction burned

where θ is the crank angle, θ_0 is the start of combustion, $\Delta \theta$ is the total Combustion duration ($x_b=0$ to $x_b=1$) and a and m are adjustable parameters. Thus, varying a and m changes the shape of the curve significantly.

6.5 Crank train model

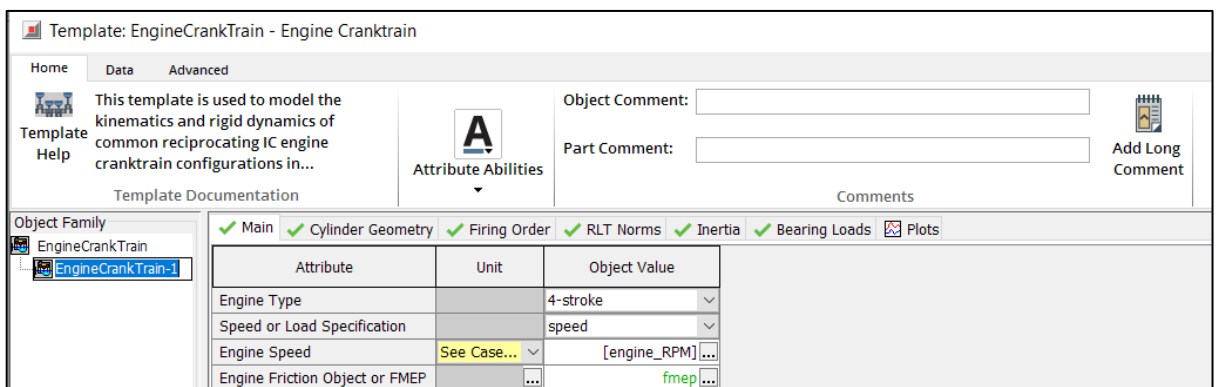


Figure 17 Crank train Block

The engine crank train model defines the crank mechanism. We define the geometry of the crank mechanism and engine cylinders, the firing order of the individual cylinder's and the last engine friction object or FMEP defines the engine friction losses using fixed FMEP or using a model taking into account. In our case, we defined the FMEP model based on [11], wherein we defined the Chen-Flynn model.

The Chen-Flynn model is defined using coefficients A, B, C, and constant component FMEP, which is entered based on the dependency of engine speed. With the help of GT-Power Help section, the recommended coefficients of A = 0.006, B = 0.09 and C= 0. Then, using the Max Pressure data and mean piston speeds for various engine speeds, the constant part of the FMEP was defined. This data is based upon measurement data in the Zetor engine.

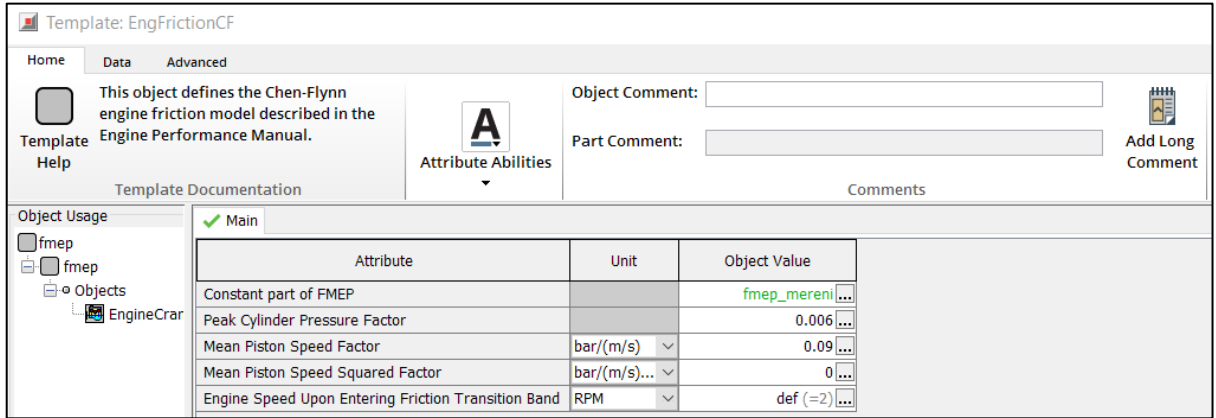


Figure 18 Engine Friction Block

The following equation is used to calculate the final FMEP of the engine.

$$FMEP = FMEP_{Const} + A \cdot P_{Cyl,max} + B \cdot c_{p,m} + C \cdot c_{p,m}^2$$

FMEP const is the constant component of friction losses in bars.

A is the coefficient of Maximum pressure in the cylinder.

B is the coefficient of Mean Piston Speed.

C is the coefficient of the quadratic Mean Piston Speed.

$c_{p,m}$ is the Mean Piston Speed.

$P_{cyl,max}$ is the maximum cylinder pressure in bars.

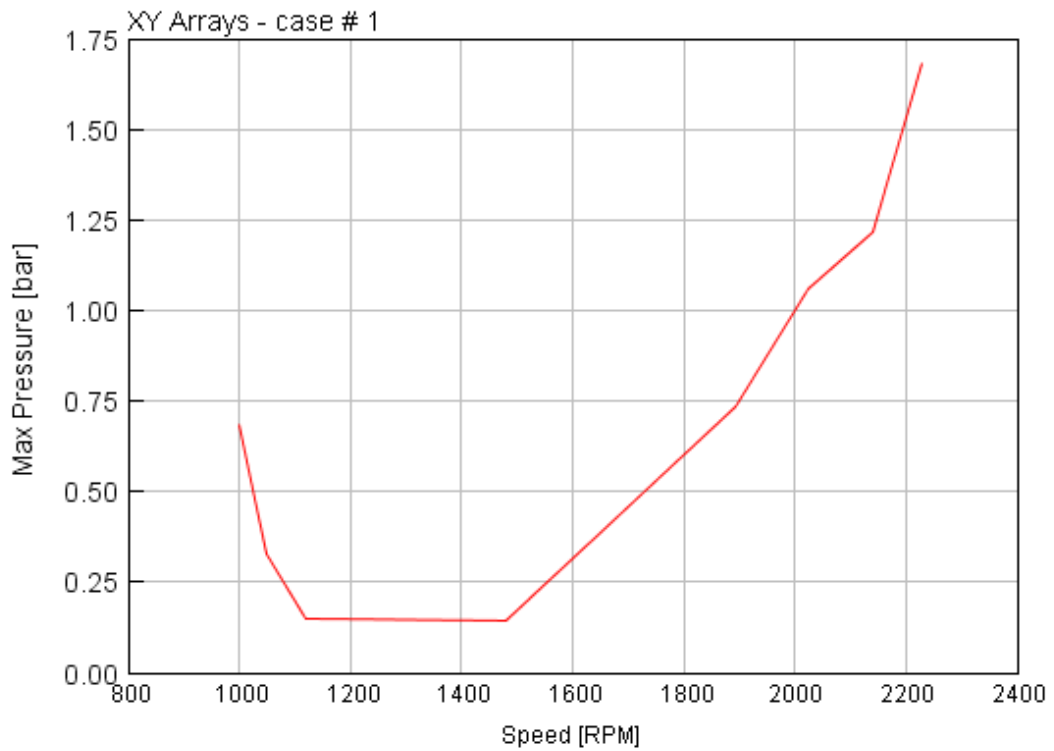


Figure 19 FMEP Curve

For this thesis work, an already calibrated FMEP model based on measurement performed in the engine is taken as input [10]. Hence, it requires no further calibration.

6.6 Piston object

It is important to define the piston cup geometry details as this is a converted engine. We have a diameter of 65mm and a depth of 5mm.

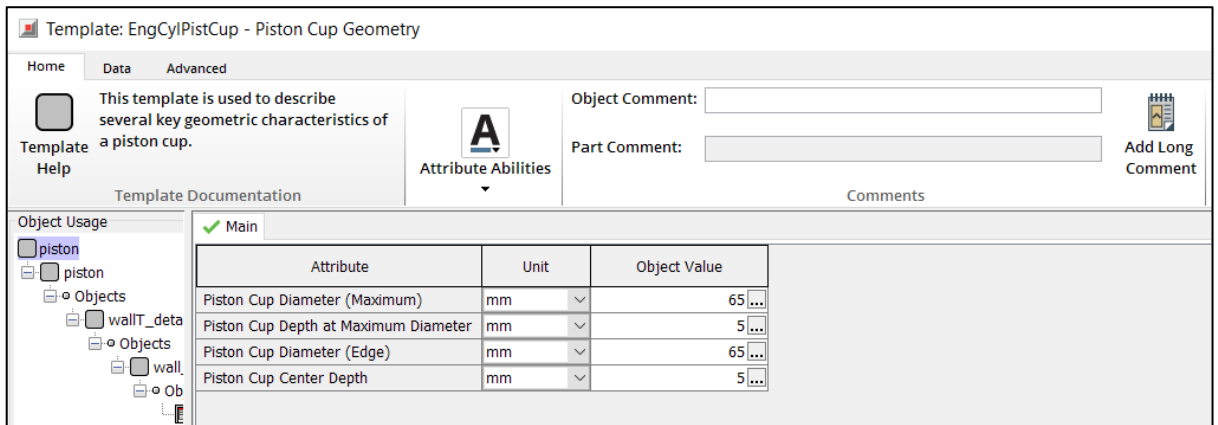


Figure 20 Piston Geometry Block

6.7 Valve object

Defining the valve object consists of two parts, the first part is the suction, and the second part is setting the exhaust. Based on the setting of the suction valve, the software analogously selects the others. The timing and stroke of the suction were according to the data provided by the company. The valve lift vs. the crank angle can be seen in the graph.

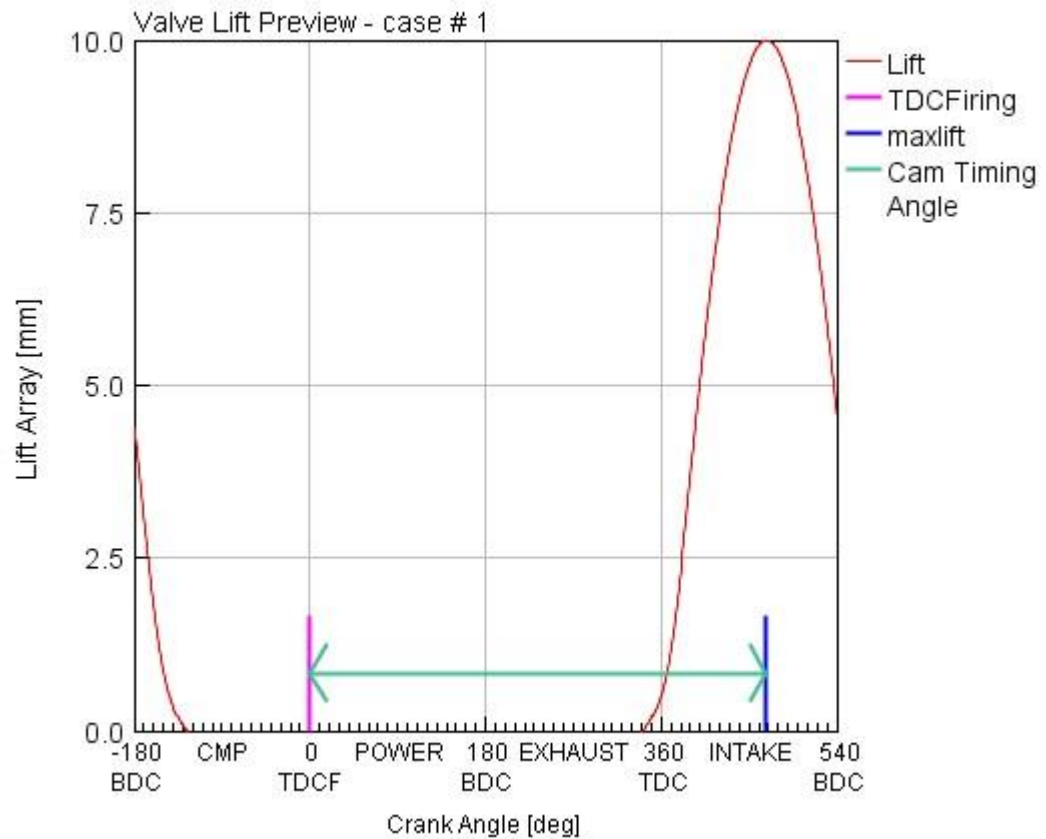


Figure 21 Valve Lift Profile

Furthermore, the forward and backward flow coefficients were entered based on the measurement data depending on the valve stroke ratio and diameter. The diameter of the suction valve and exhaust valve are 32.5mm and 28mm, respectively. In the present thesis, the valve timings are left untouched and used as per the manufacturer's configuration. This is done to avoid complexities.

6.8 Injector object

The injector object was required for injecting the fuel into the combustion chamber. However, in this thesis, we have two ways of injecting fuel into the combustion chamber. They are as follows,

- A. Common Mixer system
- B. MPFI system

In the common mixer system, we inject the Methane fuel (gaseous state) into a chamber presence before the compressor system. In this chamber, filtered air from the air filter mixes with the fuel. Therefore, the air-fuel mixture is homogenous before entering the combustion chamber.



Figure 22 Common Mixer Fuel Injection System

In the MPFI system, we have injectors directly injecting fuel into the intake ports, and in the present simulation, we have two intake ports per cylinder. The mixing of the air and fuel mainly happens inside the cylinder. Therefore, the common mixer system is more homogenous than the MPFI system.

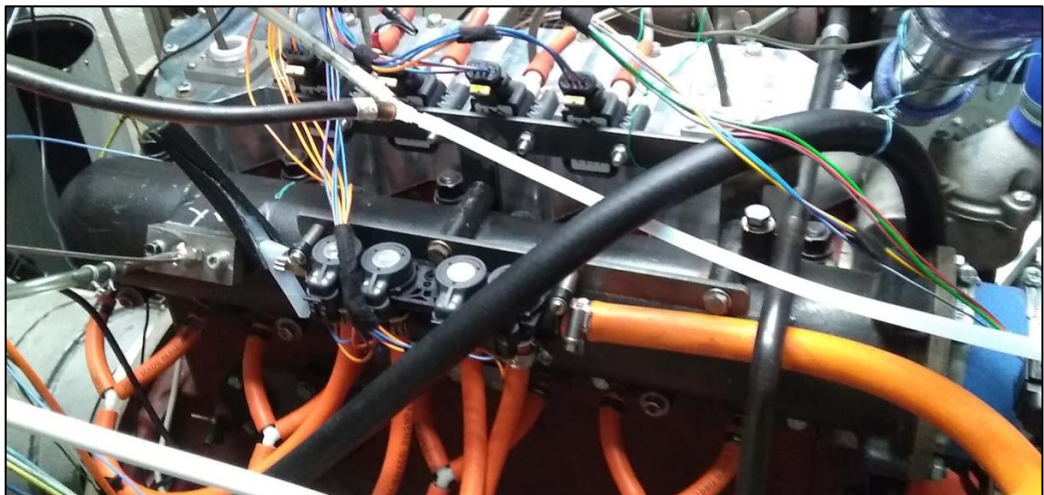


Figure 23 MPFI system

The components ,design and working of the MPFI system proposed for this engine can be understood from [31].

In the present simulation, the Air Fuel ratio is maintained at stoichiometric conditions. Based on this and the valve timings configuration, the GT-Power adjusts the injection to maintain an air excess ratio of 1.0.

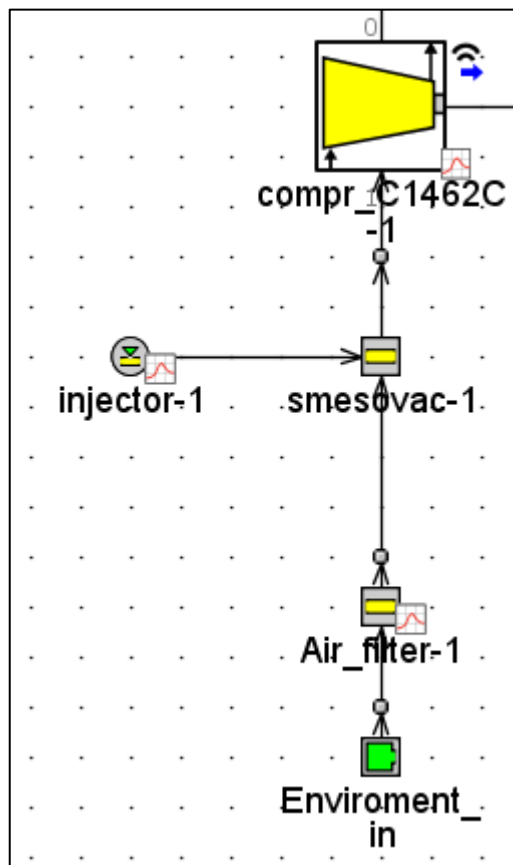


Figure 24 Common Mixer Injector System

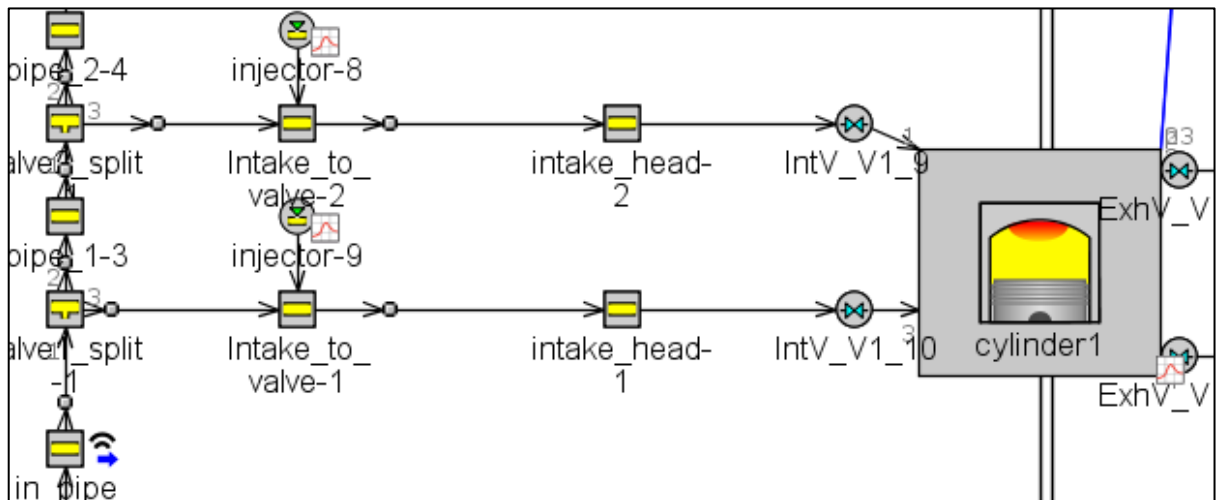


Figure 25 MPFI System

6.9 Air filter

The air filter object is defined as a round pipe element with a diameter of inlet, outlet end, and length of 95mm, 50mm, and 450mm, respectively. The losses are solves using the forward loss coefficient set to 3.

| <input checked="" type="checkbox"/> Main <input checked="" type="checkbox"/> Thermal <input checked="" type="checkbox"/> Pressure Drop <input type="checkbox"/> Plots | | | |
|---|------------------------|-------------|--------------|
| | Attribute | Unit | Object Value |
| Basic Geometry and Initial Conditions | | | |
| | Diameter at Inlet End | mm | 95 |
| | Diameter at Outlet End | mm | 50 |
| | Length | mm | 450 |
| | Discretization Length | See Case... | [dx_intake] |
| | Initial State Name | | init_state |

Figure 26 Air Filter Block

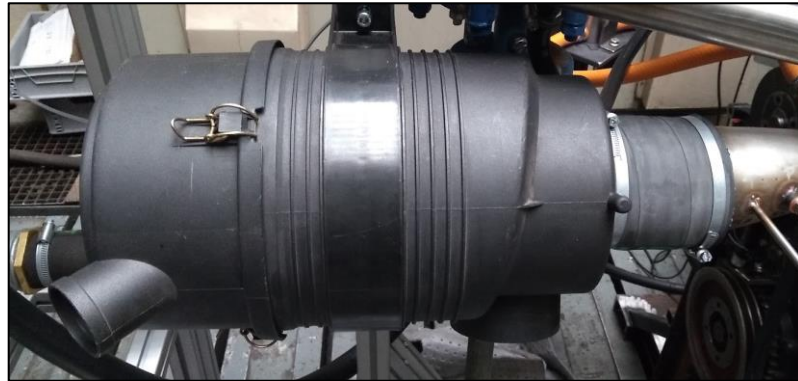


Figure 27 Air Filter engine test cell

6.10 Compressed air Intercooler

The compressed air cooler is a tube in a heat exchanger. It consists of 1700 aluminum tubes with a diameter of 5mm and a length of 385mm[10]. The cooling medium is water pumped from the tank at the test room with an estimated temperature of 25°C. This system is from Janaka Radotin engineering company.



Figure 28 Intercooler System

When modeling such a system inside GT-Power, there should be no pressure drop across the system but temperature drop. The latter is beneficial but the former is not from performance perspective.

6.11 Turbocharger system

The Zetor 1605 engine is turbocharged by the ČZ Strakonice C14-63 turbocharger, which uses a wastegate control (Turbocharger bypass valve). The turbocharger model in GT-Power was part of the material that was provided for this thesis. Therefore, there were no modifications performed with this model. The simulation model of the turbocharger consists of the compressor and turbine connected to their respective inlet and exhaust sides. Both turbine and compressor operations are defined in terms of their maps. The turbine map defines the interdependencies of the reduced mass flow rate, pressure ratio, and efficiency at reduced speeds. The compressor map uses pressure ratio and speed efficiency dependent on the pressure ratio. The graph shows the clear dependence of filling pressure on the mass flow with the isocurves in speed and efficiency.

In the simulation, the compressor RPM is monitored in the software, and it should not exceed 160000 RPM.



Figure 29 CZ C14-63 Turbocharger

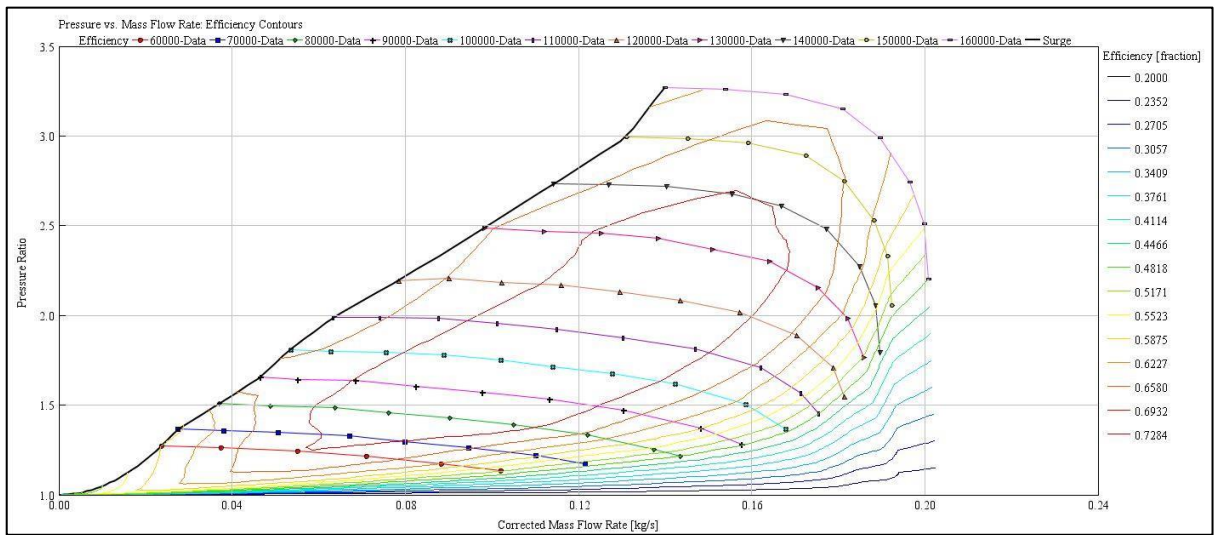


Figure 30 Compressor Map

The shaft object forms a mechanical connection between the turbine and compressor. We define the shaft moment of inertia, and it is an important factor that decides the response of the turbocharger to the changing engine operating modes.

6.12 Wastegate control

The ČZ C14-63 turbocharger uses a bypass valve to regulate the boost pressure. It regulates the flue gas pressure in the exhaust pipe by venting part of the flue gas behind the turbine wheel. The ČZ turbocharger is equipped with an internal wastegate, which is part of the cabinet turbochargers. It consists of a flap, a system of rods, and an actuator that controls the boost pressure.

In the simulation model, the wastegate diameter is controlled by monitoring the boost pressure at the compressor outlet via a sensor. In the image, we can see the illustration of the principle mentioned above.

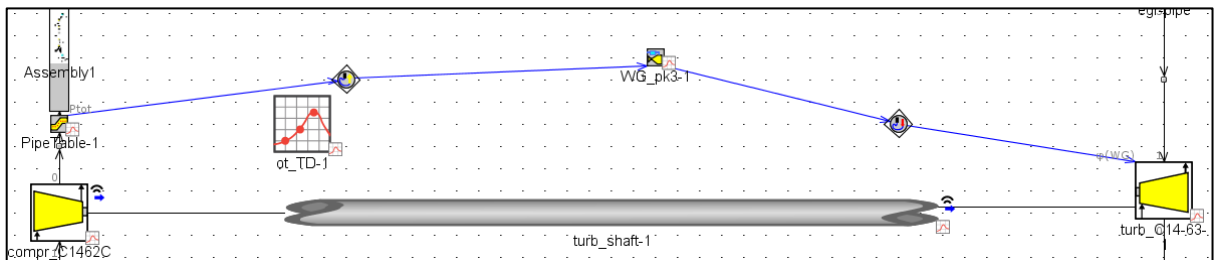


Figure 31 Waste Gate Control

6.13 Thermocouple temperature sensor model

The performance of an SI engine is limited by knock and the turbine inlet temperature [11]. Therefore, to address the latter issue, a thermocouple model was created prior to the turbine inlet. The mass averaged turbine inlet temperature is limited to 700 °C. The thermocouple, in reality, is made of Stainless-steel material. The sheath diameter, length, and thickness are 3mm, 64mm, and 0.5mm, respectively.

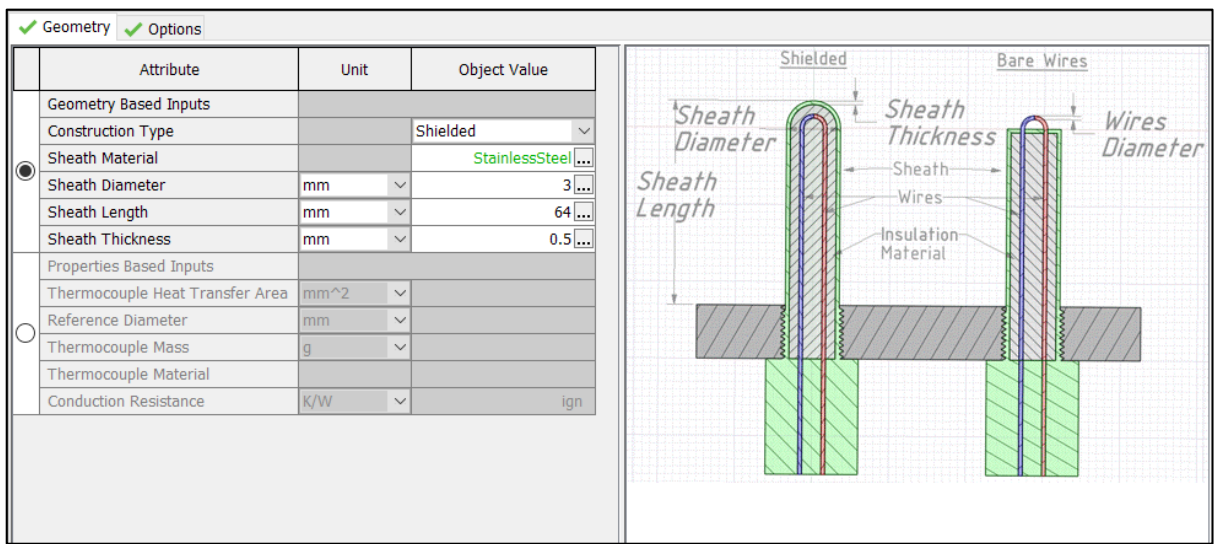


Figure 32 Thermocouple Model

6.14 Knock control

The auto-ignition of the air-fuel mixture before the arrival of the flame front is known as a knock. The performance and efficiency of an SI engine are limited by knock as it places a limit on the compression ratio of the engine [12]. Additional reasons for addressing knock is that it can lead to quick engine damage if the knock is severe.

Whenever a knock happens in an engine, the pressure in the cylinder reaches a peak value, and then it decays with an oscillating amplitude. The amplitude of oscillation detects the severity of the knock event after passing through a high pass filter. The heat release rate (HRR) increases with the flame propagation stage with a short-term drop due to piston movement towards the BDC and heat transfer [12]. Due to the compression heating effect of the burned gas and the piston movement towards TDC during the compression stroke, the unburnt mixture temperature increases [12].

Knocking is more prominent at lower engine speeds due to lower flame speeds and lower turbulence levels. This results in the end gas being exposed to higher temperatures for a significant period of time, overcoming the chemical delay. [12]

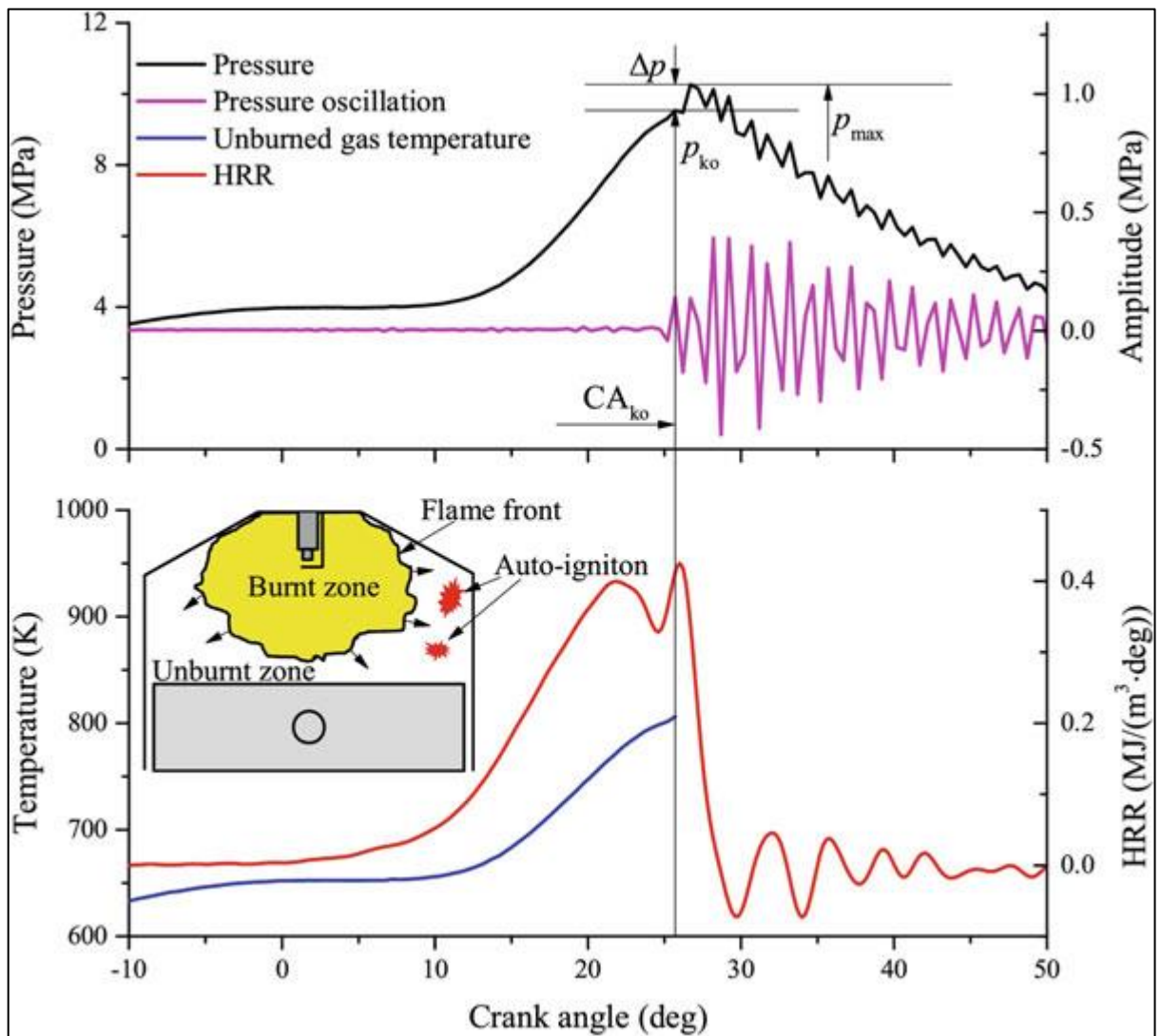


Figure 33 Knock Illustration

One of the viable solutions to reduce knock is by having a cooled EGR system, as this will reduce knock tendency. This is addressed in the next section.

In GT-Power, we address the issue of knock by the following factors.

Maximum cylinder pressure, Knock Induction time integral, the Crank angle at knock onset, and Unburnt mass fraction are the factors used to detect and mitigate knock.

6.14.1 Maximum cylinder pressure

The maximum cylinder pressure of this engine is 140bar. In severe knock, the in-cylinder pressures can exceed this limit and potentially damage the engine. Therefore, we monitor this parameter continuously throughout the simulation.

6.14.2 Knock Induction time integral

Phenomenological models use a one-step reaction model instead of detailed chemical kinetics to predict the end gas's auto-ignition. [12]

$$\tau = C_1 * p^{-c_2} * \exp \left(\frac{C_3}{T} \right)$$

Eq 6 Arrhenius Equation

The present SI gas engine uses natural gas as the fuel, and specific to this fuel, we have the kinetics fit natural gas model. This model specifies the induction time for natural gas as the fuel.

$$\tau = M1 * 1.9858 * (10^{-9}) * \exp\left(\frac{18659}{(M2 * T)}\right) * \left(\frac{MN}{100}\right)^{0.978} * FUEL^{-0.578} * O2^{-0.28} * Diluent^{0.03}$$

Eq 7 Induction time for Natural gas fuel

where M1 is the Knock Induction Time Multiplier, MN is the Fuel Methane Number, M2 is the Activation Energy Multiplier, Fuel], [O2], and [Diluent] are concentrations expressed in mol/m³, the diluent concentration is the sum of concentrations of N₂, CO₂, and H₂O.

To predict the onset of knock, we can use the simple Livengood and Wu integral. All the induction mentioned above time models culminate in this integral to predict the onset of knock.

$$I(t) = \int_{t_{ivc}}^{t_{knock}} (1/\tau) dt$$

Eq 8 Knock Induction Time Integral

This equation relies on the ignition delay of the current and changing thermodynamic states of the end gas mixture. Here t_{IVC} and t_{knock} represent the time of intake valve closing (IVC) and knock onset time. The knock occurs when the integral reaches the value of 1.

6.14.3 Unburnt mass fraction

Along with the knock induction time integral, we have to also monitor the unburnt mass fraction. There will be a certain unburnt mass fraction at the time of knock. If there is no knock, all the mass fractions will be completely burnt.[13]

6.14.4 Crank angle at knock onset

This parameter assists the parameters mentioned above in knowing the crank angle at which knock begins. This is measured in degrees Crank Angle (CA).

6.14.5 Knock Index

The knock index is a phenomenologically based parameter, and it can be scaled to the loudness of knock as heard in the lab conditions using the Knock Index Multiplier.

The simulation uses a Kinetic Fit Natural gas model developed for natural gas considering the above-mentioned knock-related parameters. This model used a single zone as a multi-zone requires the 3D spatial coordinates of the engine spark and flame model.


```

MAIN DRIVER: Case# 1 Period# 17 Freq/RPM=16.6667 1000. Time=1.92
INFO Knocking predicted:cyl# 1 CA= 3.4 Index= 208.2 MassFr=0.097
INFO Knocking predicted:cyl# 3 CA= 0.3 Index= 371.7 MassFr=0.135
INFO Knocking predicted:cyl# 4 CA= -0.9 Index= 455.2 MassFr=0.153
INFO Knocking predicted:cyl# 2 CA= 1.4 Index= 304.1 MassFr=0.120
Flow Step 160000, dt = 1.307E-05, t = 2.0241
COMP: CMP=compr_ RPM= 52485. PRmap= 1.162 Mass= 0.034 Power= 0.80 Ef=0.641

```

Figure 34 Knocking Predicted by model

Figure 28 shows the sample knock predicted by the model for a spark advance. The main details of crank angle, knock intensity, and mass fraction burnt are the details here.

6.15 Exhaust Gas Recirculation System (EGR)

Additional ways to avoid knock apart from the retardation of the spark timing is to have a cooled Exhaust Gas Recirculation (EGR) system. EGR increases the heat capacity of the system and therefore decreases the laminar burning velocity. In the present engine, we can use up to 20% of cooled EGR. Based on the pressure difference between the sampling and feeding location, the EGR system can be of two types, i.e., High-pressure EGR and Low-pressure EGR systems. [14]

6.15.1 Low-pressure EGR

A low-pressure EGR system typically appears after the turbocharger system as per the figure (typically after a DPF). This is preferred when the demand for EGR is lower for the engine. An additional problem associated with low-pressure EGR system is that the system cannot respond to the quick change of EGR rate. [14]

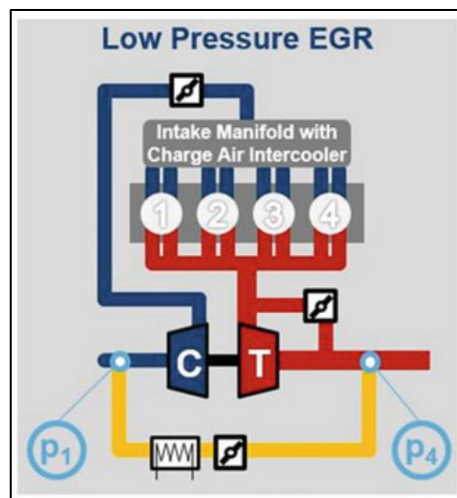


Figure 35 Low-Pressure EGR System

6.15.2 High-pressure EGR

In the present system, we are utilizing a high-pressure EGR system. This EGR system can achieve higher EGR rates at higher speeds and is more responsive to the changing EGR rates.

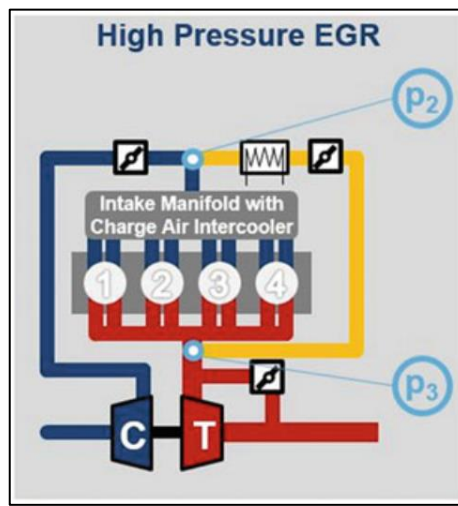


Figure 36 High-Pressure EGR System

The high-pressure EGR system mainly consists of the EGR cooler system with pipes connecting the cooling system to the exhaust and intake sides. The cooler is a heat exchanger with water as the coolant. The cooled recirculated exhaust gas temperature is 85°C.

In the present GT Power model, the measured dimension of the EGR cooler is 25.2mm. This EGR system is modeled so that there is no pressure drop across the system but temperature drop. Therefore, when a high-pressure EGR line is built, there must be no backflow of the exhaust gases due to lower pressures or pressure drop in the EGR line. In order to avoid this backflow of the gases modeling solutions are taken into consideration.

A. Building a venturi system

A venturi system is often used to increase flow from a secondary stream into the mainstream. This is achieved by making a connection at the throat of the venturi. The venturi is modeled with a flow split added at the throat to allow the secondary flow into the stream. This flow split would be very small to represent the volume of the throat where the secondary stream joins the mainstream. Both orifice systems have to be bell mouth orifice systems.

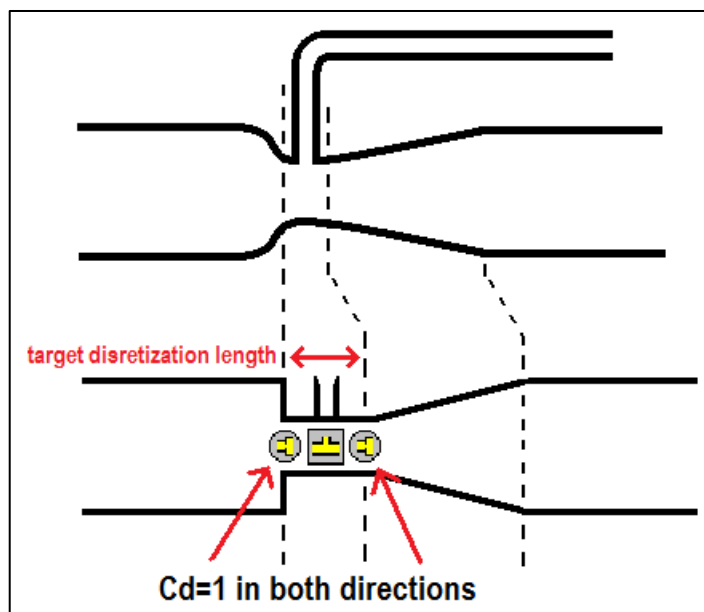


Figure 37 EGR Venturi System

This approach, however, has many-dimensional intricacies, and the resultant flow didn't have the required amount of EGR %. Therefore, this method wasn't successful.

B. Using an exhaust throttle flap system

In this system, an exhaust throttle flap was used after the turbine system (usually at vehicle level, there is sufficient back pressure) in order to have sufficient recirculation pressures. The throttle valve (Throttle conn in the figure) is controlled for a positive high-pressure exhaust recirculation. Experiences reveal that this exhaust flap is required mainly at lower speeds where the recirculation is poorer due to lower pressures.

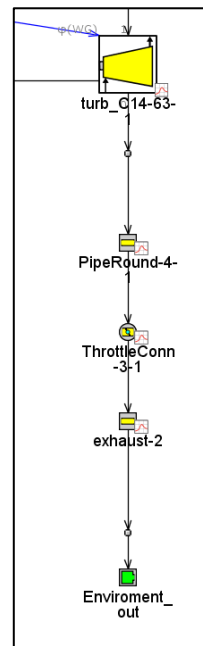


Figure 38 Exhaust Throttle Flap

6.15.3 EGR control

To control the amount of EGR inside GT-Power, a closed-loop control system has been implemented. A simple controller senses and compares the average mass flow rate inside the crank train (in kg/s) and EGR line (in kg/s). Based on this, the controller actuates the orifice to control the amount of EGR getting recirculated.

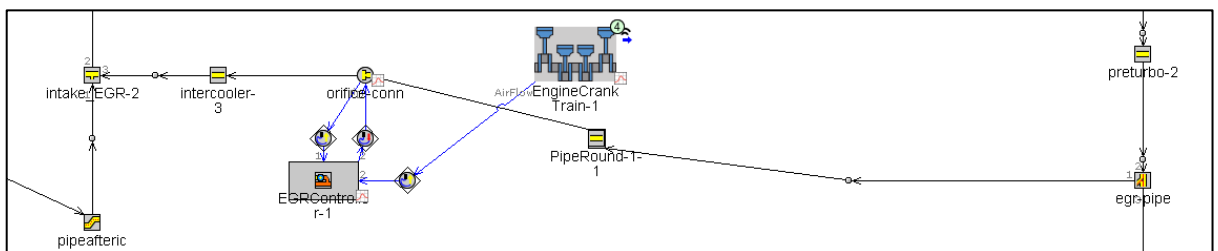


Figure 39 Closed Loop EGR System

6.15.4 EGR % recycled

The EGR % recycled is defined as the percentage of the total intake mixture which is recycled exhaust. It is given by

$$\text{EGR}(\%) = \left(\frac{m_{\text{EGR}}}{m_i} \right) \times 100$$

Eq 9 EGR %

m_{EGR} is the mass of exhaust gas recycled, and m_i is the total mass of EGR and air-fuel mixture.

6.15.5 EGR mass flow rate

Equation 10 gives the EGR mass flow rate across the EGR cooler system

$$\dot{m}_{egr} = \rho_c * A_c * \omega_c$$

Eq 10 EGR mass flow rate

Where ρ_c is the density of exhaust gas recycled, A_c is the area of the EGR cooler, and ω_c is the velocity of the flow through the EGR cooler system.



Figure 40 EGR Cooler 25.4mm Diameter Inlet/Outlet

6.16 Throttle position control

In a SI engine, the load is varied by controlling the amount of throttle. Both fuel and airflow are varied accordingly so that the mixture composition is uniform [11]. In the present system, the throttle is controlled by a similar close loop system. This system senses both engine BMEP (bar) and speed (rpm). Based on this, the throttle valve is actuated at the required angle.

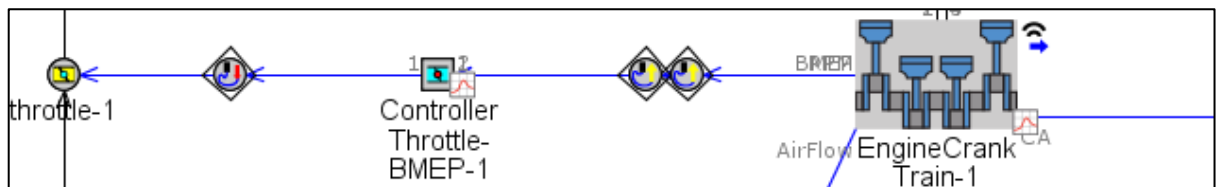


Figure 41 Closed Loop Throttle Control System

The throttle angle vs. the discharge coefficients data has been input inside the throttle valve.

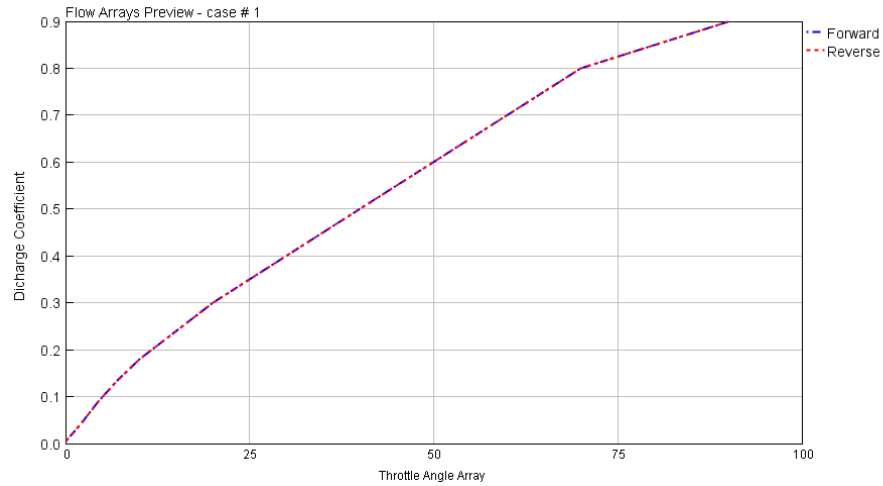


Figure 42 Discharge Coefficient vs Throttle Angle

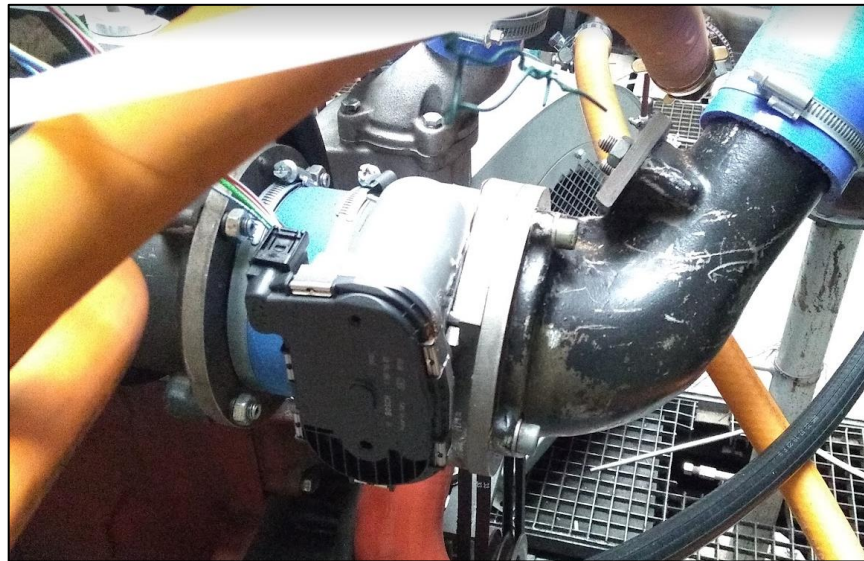


Figure 43 Throttle 88mm Diameter

6.17 Heat Transfer Object

A WoschniGT model evaluates the in-Cylinder heat transfer. This model is suitable compared to other models like WoschniClassic, Woschni Swirl, etc., due to the simplicity and non-requirement of measured swirl data. This calibrated model with parameters was available as part of data obtained for simulation.

6.18 NO_x model

The Extended Zeldovich mechanism evaluates the formation of NO, and this calibrated model with parameters was available as part of data obtained for simulation.

6.19 Discretization Length for simulation

The solver divides pipes into sub- volumes, upon which calculations are performed. The sub-volume length is called the discretization length. The recommended value of the discretization length is $0.4 \times (\text{cylinder bore diameter})$ on the intake side, and $0.55 \times (\text{cylinder bore diameter})$ on the exhaust side[32]. Intake side is 42mm. Exhaust side is 57.75mm.

7. Engine model & design of experiments

7.1 Common Mixer model

Refer section 15.1 for the GT-Power simulation model.

7.2 MPFI system model

Refer section 15.2 for the GT-Power simulation model.

The only difference between the common mixer system and the MPFI system is that the injector location has been changed from a single injector located before the compressor to two injectors per cylinder that injects fuel in the cylinder's intake port.

7.3 Design of Experiments (DOE)

This diploma thesis aims to optimize the full load performance curves of both the common-mixer and MPFI systems. For that purpose, an experiment is performed varying the input parameters to get the required output parameters. For full load curve optimization,

- Wide-open throttle (WOT) is maintained at all conditions
- Air fuel equivalence ratio is maintained at stoichiometric conditions (Lambda 1 condition)
- Maximum Cylinder pressure is limited to 140 bars.
- Mass Averaged Turbine inlet temperature is 700°C
- The maximum amount of EGR is limited to 20%
- Run the engine at the knock border (Knock Integration time =1) & monitoring Unburnt mass fractions, knock index and crank angle at knock onset.
- Turbocharger speed limit of 160000 RPM with a wastegate control system.
- Combustion phasing is performed by CA50 variation

Therefore, CA50 is varied from -20° BTDC to +20° ATDC parallelly with EGR varied from 0 to 20% to capture the system's total behavior. This entire procedure generated around 1200 points of data depending on the level of accuracy required. For this procedure, the Full Factorial method was utilized in order to get good quality of data. This entire procedure was carried out using the DOE setup of the GT-Power software.

The procedure mentioned above was carried out for both the common mixer and MPFI system.

8. Optimization

8.1 AVL CAMEO software

AVL CAMEO is an intelligent automated environment suitable for all engine optimizations. The software is equipped with a model-based approach that can design, Test, Simulate and perform measurements with engine test cells. The software has the main workflow and sub-work flows that guide the user through the calibration process [16].

In the present scenario, the DOE data generated inside GT-Power is imported inside AVL CAMEO. Once imported, the data can be categorized into input and output. For example, this

can be seen in figure 45, wherein CA50, engine speed (RPM), Knock Integration time, and EGR% were categorized as input and the rest as output parameters.

Once imported, the software evaluates the quality of experiment data. The model quality is evaluated based on goodness of fit, average value, repetition points, model standard deviation, root mean square error, and F-tests.

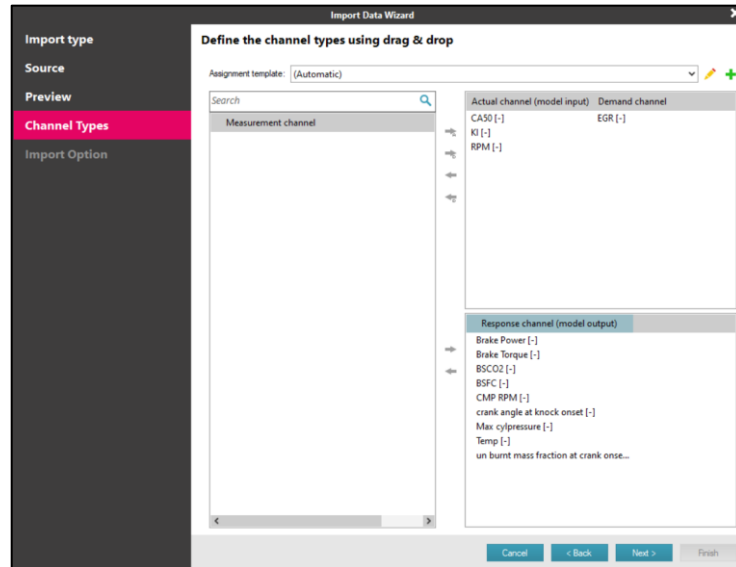


Figure 44 CAMEO I/O System

8.2 Common Mixer full load DOE data evaluation.

The figure shows that the data generated in the DOE procedure matches the software's linear model, and there is a 99.98% correlation.

- R² coefficient of determination (Value range 0 to 1): If $R^2 \geq 0.95$, then the goodness of fit is very good. In our case, we have a 0.99 correlation.
- R²Adjusted (value range $-\infty$ to 1): If $R^2_{Adjusted} \geq 0.95$, then the goodness of fit is very good. In our case, we have a 0.99 correlation.
- R²Predicted (value range $-\infty$ to 1): If $R^2_{Predicted} \geq 0.90$, then the goodness of fit is very good. In our case, we have a 0.99 correlation.
- Root Mean Square Error (RMSE): It is the square root of the mean square error. Therefore, a lower RMSE value reflects greater accuracy. In our cases, the RMSE values are significantly lower.
- Normalized Root Mean Square Error %(NRMSE %): The RMSE value normalized the difference between the maximum and minimum observation. This is evaluated in %, and to the degree it is lower, the model is accurate. In our case, the NRMSE % values are less than 2%.

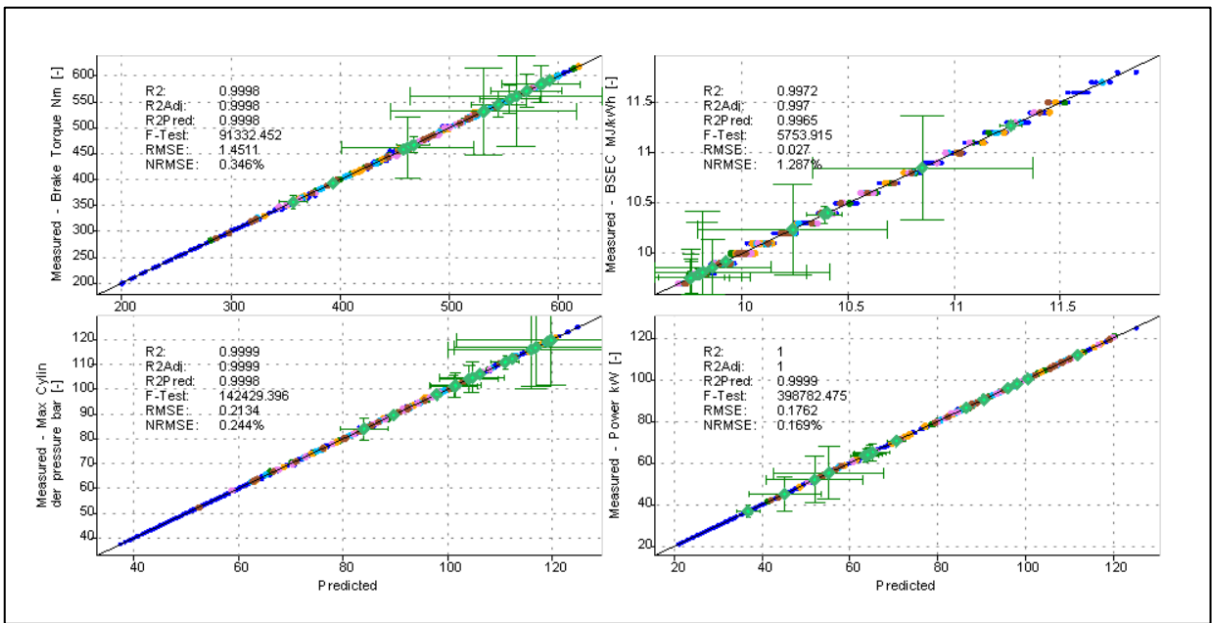


Figure 45 DOE Data Fit - Common Mixer System

The DOE data generated from GT-Power for the common mixer is imported inside AVL CAMEO, and optimization is performed considering the conditions mentioned in the DOE section.

8.3 MPFI system full load DOE data evaluation.

The MPFI system follows a similar statistical trend similar to the common mixer system, and hence the goodness of fit is very good.

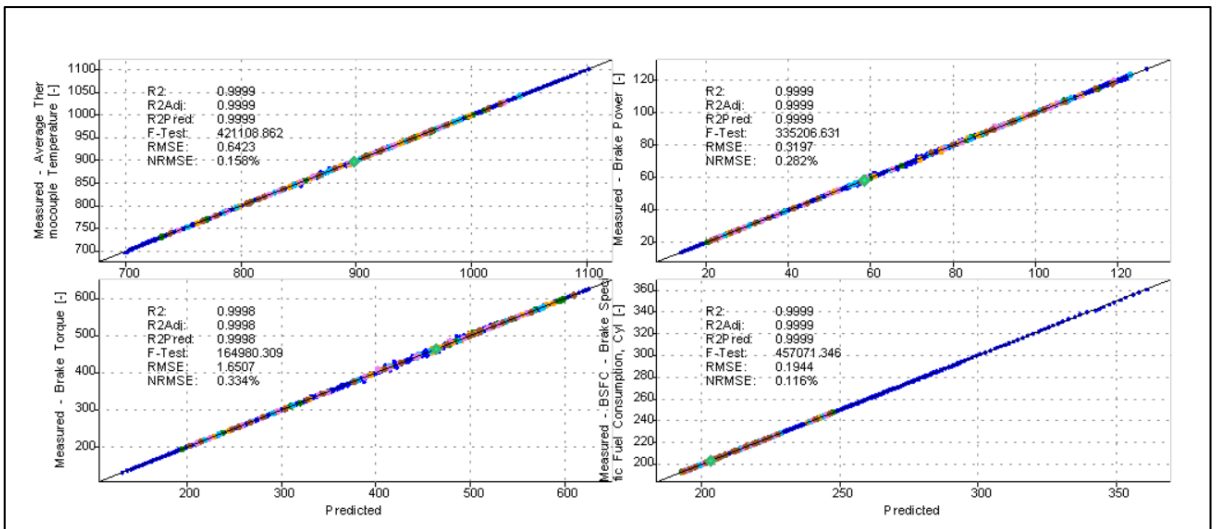


Figure 46 DOE Data Fit - MPFI System

9. Results & Conclusion

The full load curve optimization is performed following the conditions mentioned in the DOE section. The optimization is carried out by parallel optimization of CA50, EGR%, KI for a particular engine RPM. The optimization is performed for all seven speeds ranging from 1000 RPM to 2200 RPM to maximize the engine's performance, i.e., how well the engine can perform, satisfying all the necessary boundary conditions. The optimized points are noted and plotted as graphs in MATLAB.

Section 15.3 shows for both Common-Mixer and MPFI system, the engine Torque Vs. Speed RPM with various isolines as Power kW, CA50, EGR %, Knock Induction time integral, BSEC MJ/kWh, Mass Averaged Turbine inlet temperature K, Max Cylinder Pressure-bar and BS CO₂ g/kWh.

9.1 Comparison of Common Mixer and MPFI system performance

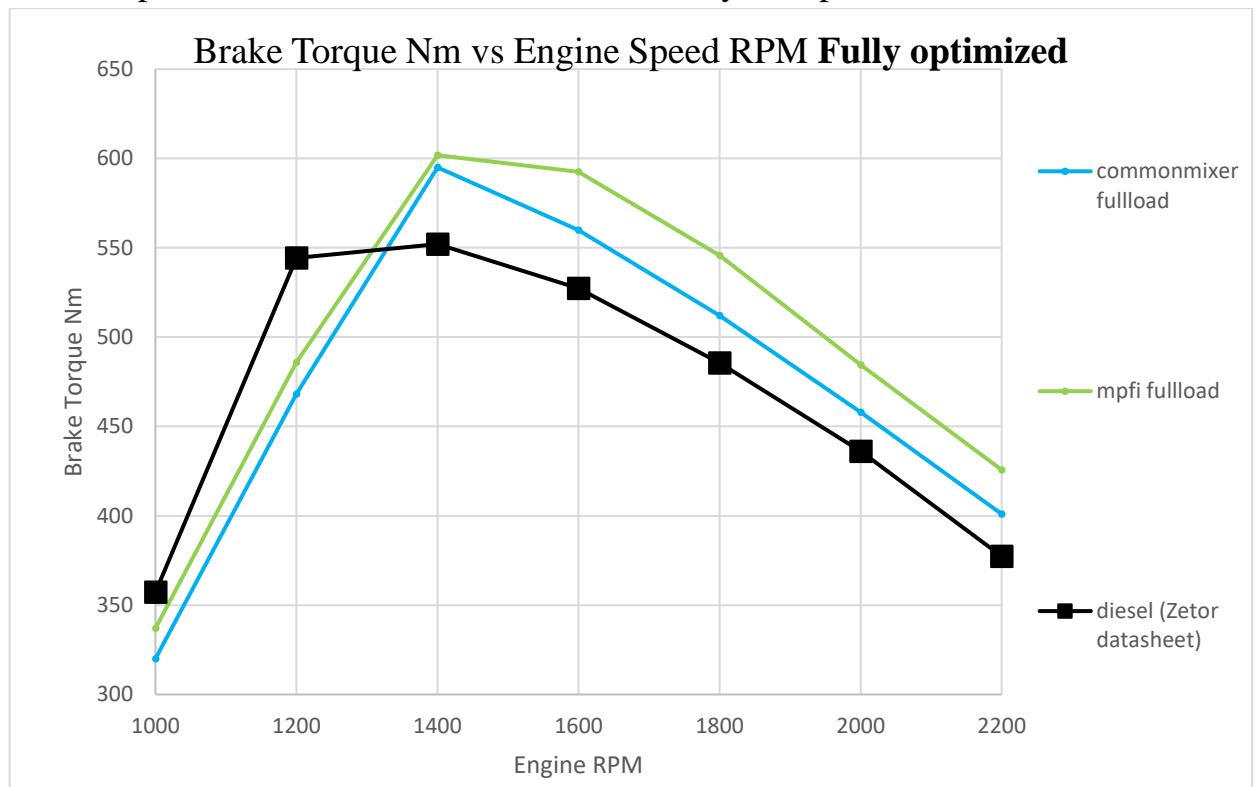


Figure 49 Brake Torque Vs. Speed RPM

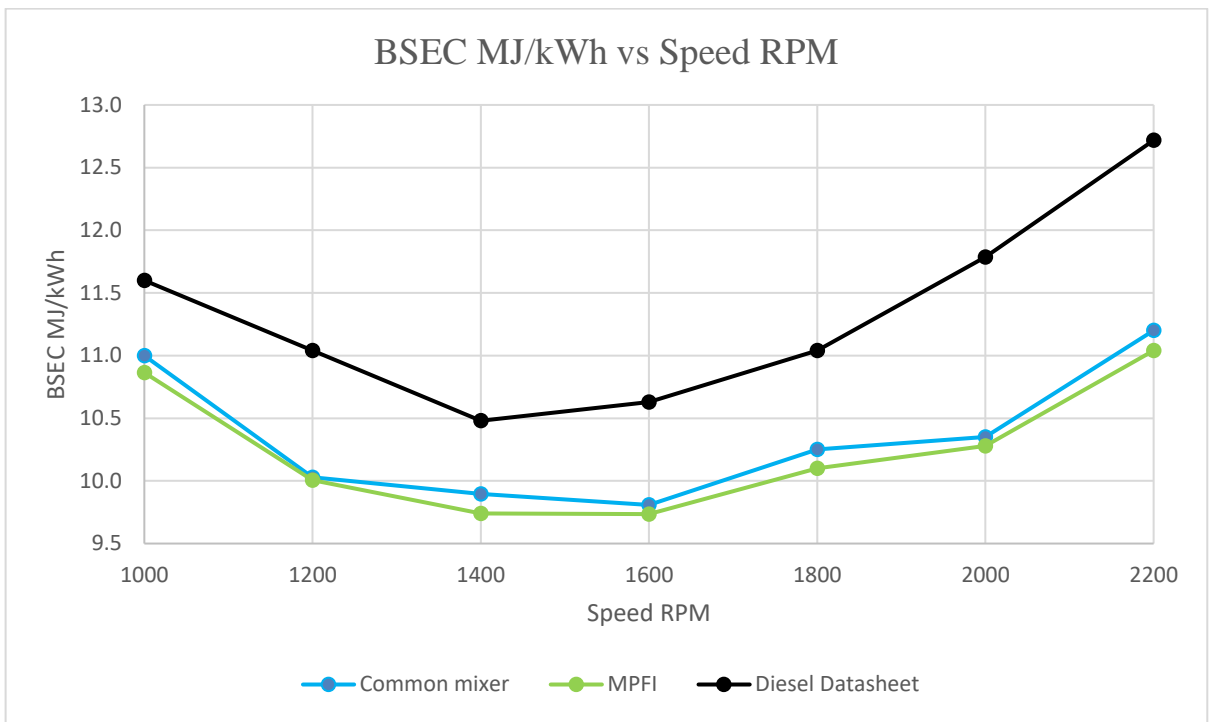


Figure 50 BSEC Vs. Speed RPM

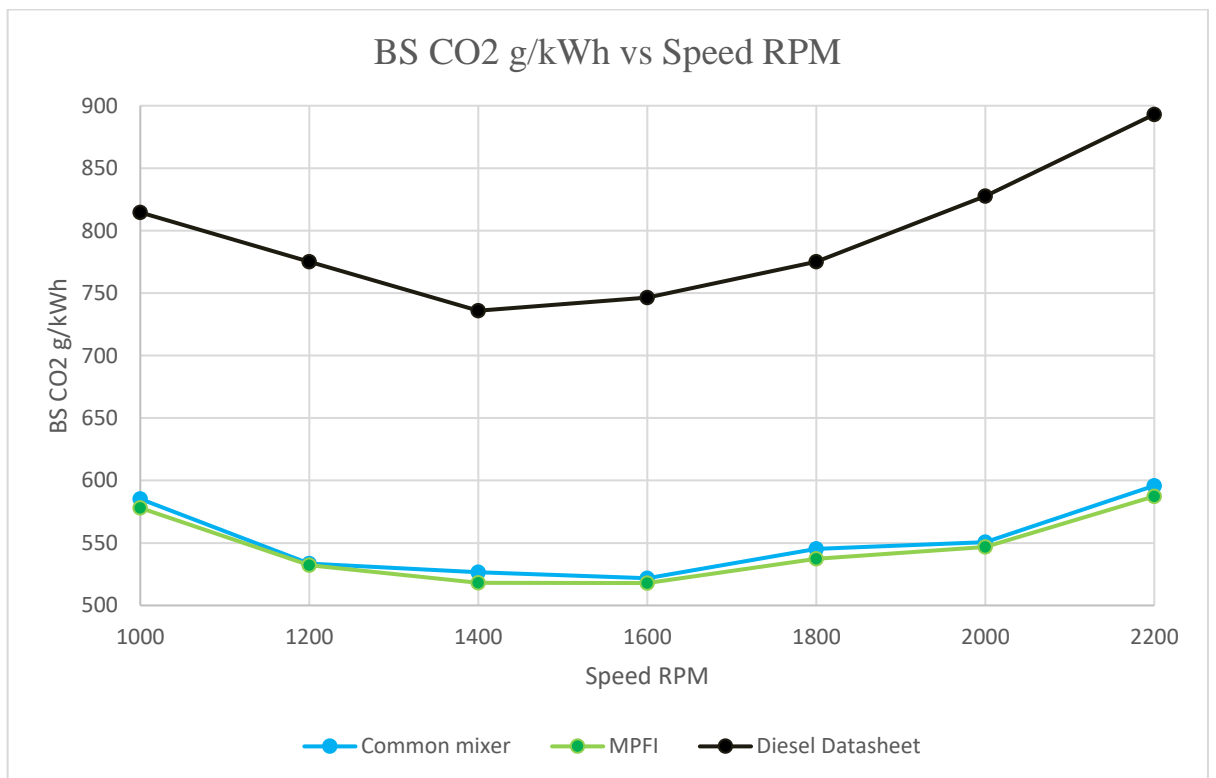


Figure 51 BS CO₂ Vs. Speed RPM

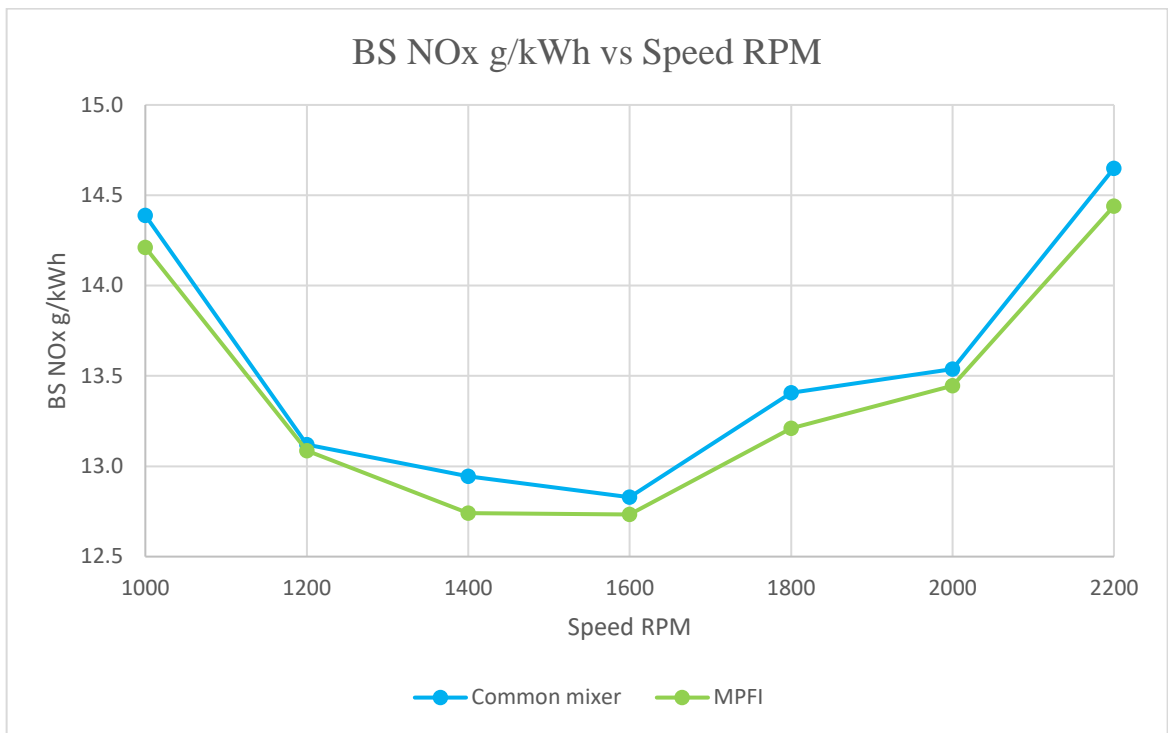


Figure 5247 BS NO_x Vs. Speed RPM

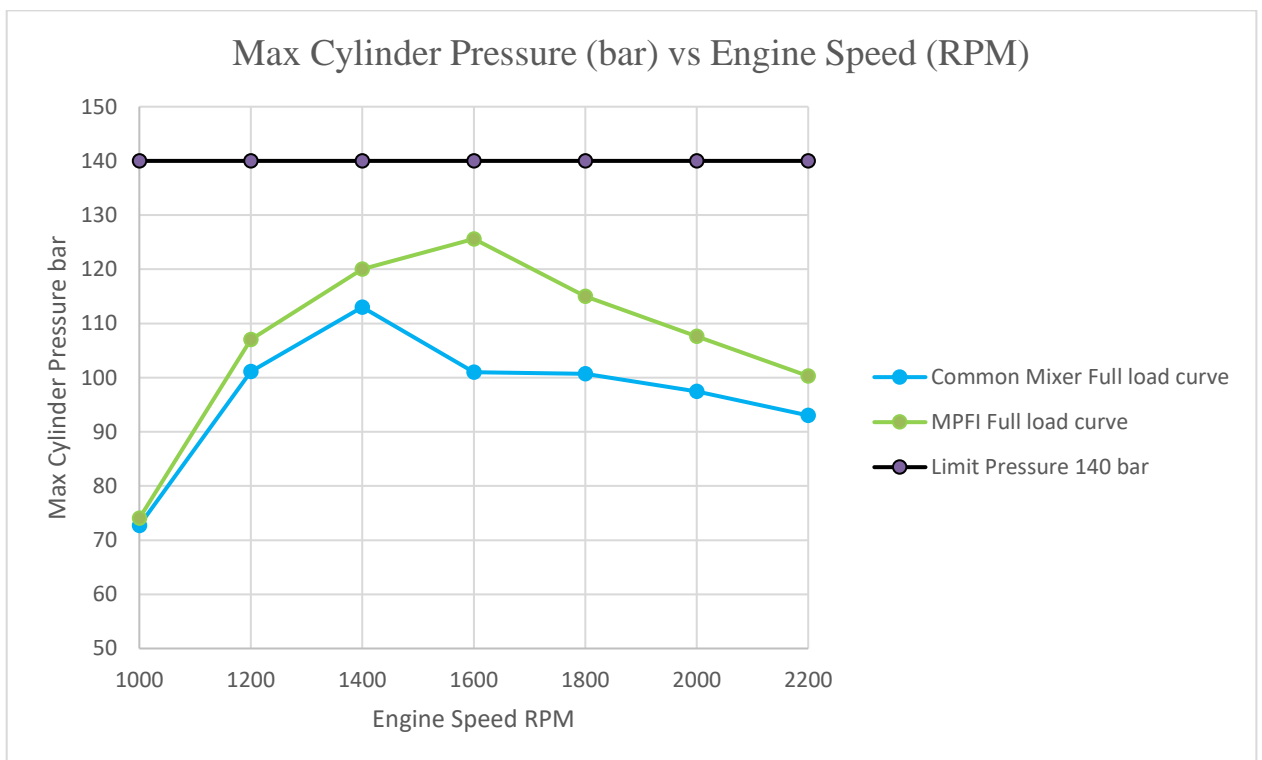


Figure 53 Max Cylinder Pressure (bar) vs. Engine Speed RPM

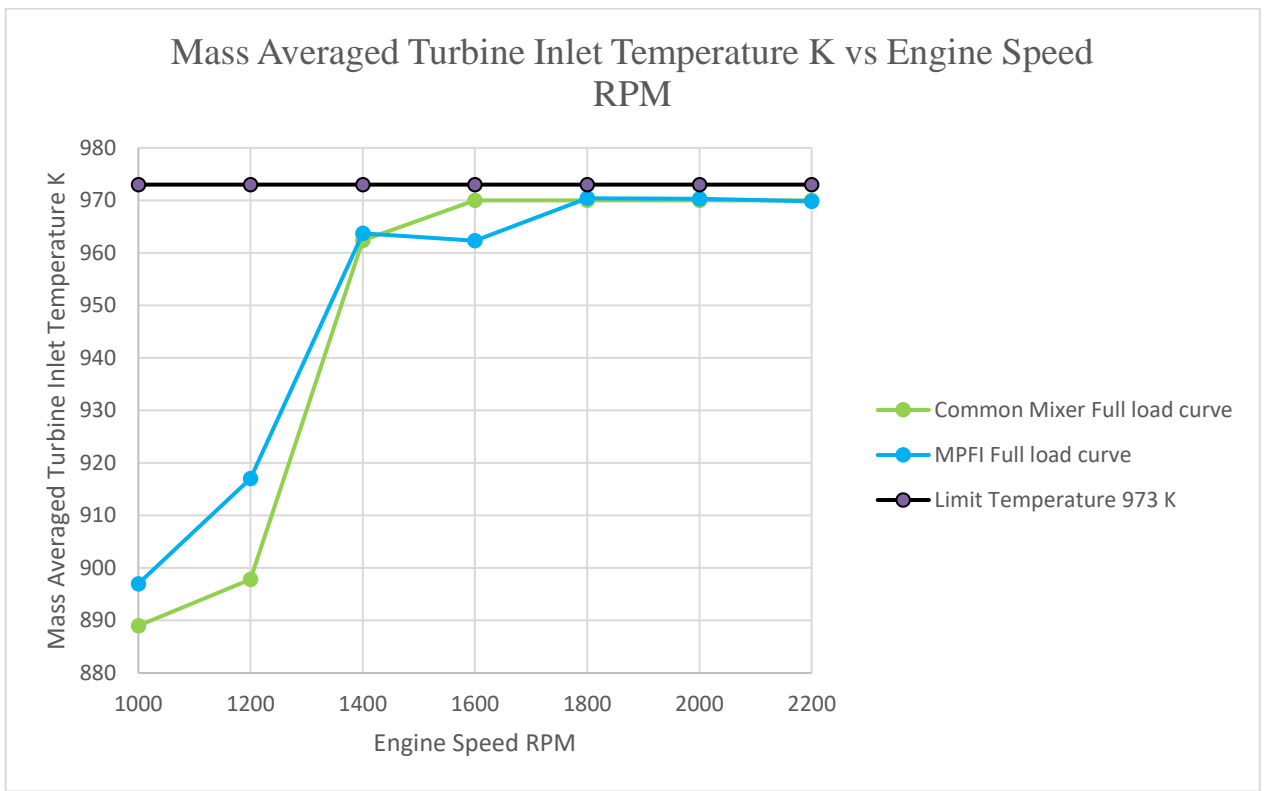


Figure 5448 Mass Averaged Turbine Inlet Temperature K vs. Engine Speed RPM

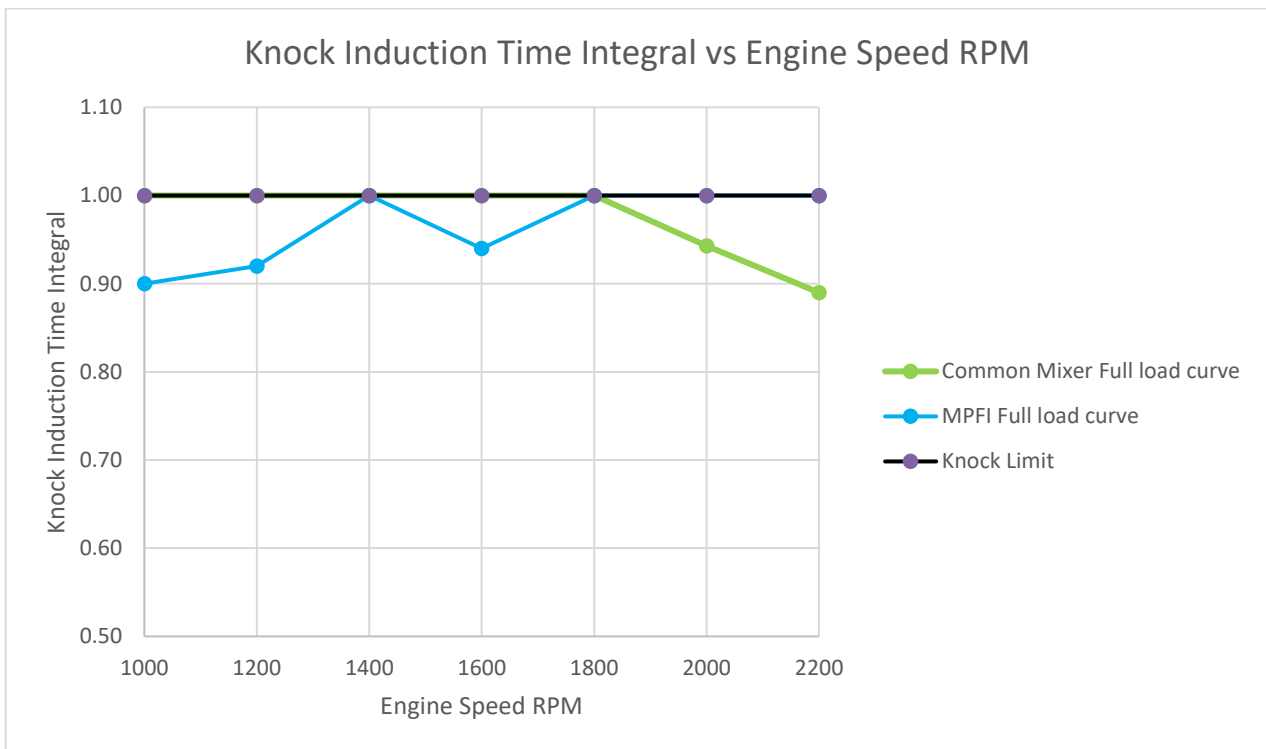
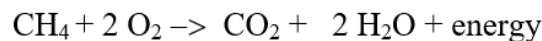


Figure 55 Knock Induction Time Integral vs. Engine Speed RPM

The following conclusions can be understood from the graphs mentioned above:

- From figure 49, we find that the MPFI system is performing better than the common mixer system. The lower performance of the common-mixer is mainly due to the volumetric loss at the compressor as part of the volume is occupied by fuel gas. For example, at 2200 RPM in the common-mixer system, we find from the simulation model that the compressor average mass flow rate to be 27.11 g/s and out of which 1.49 g/s is the fuel flow rate. This accounts for a 5.49% loss of air which is available for air in the MPFI system. The torque is directly proportional to the mass flow rate in the engine. Therefore, we find higher torque in the MPFI system.[11]
- Further, at higher RPMs, the MPFI performance is higher than the common mixer system. Also, the performance of both systems is better than the diesel version of the system at middle and higher speeds.
- From fig 50, A 13.38% decrease in brake specific energy consumption (BSEC) can be observed at 2200RPM upon comparing the MPFI system with the diesel version.
- From fig 51, The Common-Mixer system has a higher amount of BSCO₂ than the MPFI system as it follows the trend of BSEC.
- The GT-Power controls the amount of injection according to the speed in order to maintain air excess ratio 1.0. Therefore, especially in MPFI system, there exists variation in the amount of injections. But the total air excess ratio of 1.0 is maintained. Therefore, results of the total simulation is considered and AVL CAMEO offers the optimized result from this total simulation result.
- The common mixer system provides a much better homogeneous mixture compared to the MPFI system, wherein the air-fuel mixture undergoes mixing inside the cylinder. The inhomogeneity might be an issue for the MPFI system compared to the common-mixer system but the GT-Power cannot capture this.
- CO₂ is a product of complete combustion. As per the below chemical reaction, 1 kg of Methane reacts with 4 kg of Oxygen to form 2.75 kg of CO₂ and 1.25 kg of H₂O. Therefore, the BS CO₂ follows the same trend as of BSEC.



- Further possible reasons for CO₂ increase can be the burning of a certain amount of rich fuel that travels towards intake due to piston movement towards TDC. The fuel metering calibrations change if the fuel sticks onto the walls of the intake system [11]. These rich mixtures can reach the combustion chamber in successive strokes and can contribute to an increase in CO₂. This effect cannot be observed in GT-Power but in 3D CFD simulation it can be observed.[31]
- Even after the fuel injection is completed, there are potential chances of the presence of rich mixtures near the injector nozzle. This could undergo successive combustion and can contribute to the cause.
- From fig 52, the BSNO_x follows a similar trend of BSCO₂.
- From the maximum cylinder pressure graphs(fig 53), we observe for both systems; the optimized pressure levels are below the maximum pressure limit of 140 bars.
- From the temperature graph(fig 54), we observe the optimized temperature levels are below the mass averaged turbine inlet temperature of 973K. We see a reverse trend at 1600RPM because the knock limits (unburnt mass fraction limits reached) are much closer for the MPFI system as we observe the knock induction time integral. Further

increase in knock induction time integral can lead to unburnt mixtures during combustion.

- As we maintain the knock border, we can potentially have higher performance out of the engine. Although the temperatures of the system increase, a positive compensation is further offered by the cooled high-pressure EGR system. An additional degree of freedom for further increase in the performance is CA50. By controlling the CA50, we are indirectly controlling the spark timing of the engine.
- This kind of optimization is much easier to perform in AVL CAMEO. It offers the freedom to control the user required several variables, making it a much more potential software than GT-Power.
- The market survey shows that as years advance, much more complex systems are implemented in a simplified manner to make engine calibrations easier. As a result, incorporating machine learning algorithms for engine performance optimization is a newer trend in the automotive industry [17].

10. Further Scope

- Based on a similar methodology, we can perform part-load optimization for parameterization of the engine in part-load regimes.
- The performed optimizations can be verified further with the engine test cell to validate the models.

11. References

1. Jason B. Quinn, Thomas Waldmann, Karsten Richter, Michael Kasper and Margret Wohlfahrt-Mehrens : “Energy Density of Cylindrical Li-Ion Cells: A Comparison of Commercial 18650 to the 21700 Cells.” Available: [10.1149/2.0281814jes](https://doi.org/10.1149/2.0281814jes)
2. Extending the ICE age: SAE Automotive engineering 2019 August edition.
3. Samuel Wiseman, Martin Rieth, Andrea Gruber, James R. Dawson, Jacqueline H. Chen. “A comparison of the blow-out behavior of turbulent premixed ammonia/hydrogen/nitrogen-air and methane-air flames”. Volume 38, Issue 2, 2021, Pages 2869-2876 Available: [10.1016/j.proci.2020.07.011](https://doi.org/10.1016/j.proci.2020.07.011)
4. Pavlos Nikolaidis, Andreas Poulidakas. “A comparative overview of hydrogen production processes. Renewable and Sustainable Energy Reviews”. Volume 67, January 2017, Pages 597-611. Available: [10.1016/j.rser.2016.09.044](https://doi.org/10.1016/j.rser.2016.09.044)
5. Natural gas vehicles. Alternative fuels data center. Energy efficiency & renewable energy.
6. J. Vavra, M. Takats and V. K. a. M. Skarohlid, “Influence of Natural Gas Composition on Turbocharged Stoichiometric SI Engine Performance,” *SAE International*, no. ISSN:0148-7191, 2012.
7. <https://www.worldometers.info/gas/>
8. <https://www.worldometers.info/oil/>
9. GAMMA TECHNOLOGIES, LLC. *GT-SUITE Overview* [online]. [vid. 2020-04-03]. Dostupné z: <https://www.gtisoft.com/gt-suite/gt-suite-overview/>
10. Ing. Ondřej Pavlíček: “Engine characteristics of turbocharged natural gas engine with a scavenged prechamber” Available: <http://hdl.handle.net/10467/90188>
11. John B Heywood Internal combustion engine fundamentals. New York, ISBN 0-07-028637-X, 1988.
12. Rakesh Kumar Maurya. “Reciprocating engine combustion diagnostics”. Available: [10.1007/978-3-030-11954-6](https://doi.org/10.1007/978-3-030-11954-6)
13. Ing. Oldřich Víték Ph.D. Lectures of Theory of Internal combustion engines.
14. EGR systems: <https://x-engineer.org/automotive-engineering/internal-combustion-engines/ice-components-systems/exhaust-gas-recirculation-egr-complete-guide-architectures/>

15. GAMMA TECHNOLOGIES Flow theory manual.
16. AVL CAMEO 4 working manual
17. ETAS Optimisation of Gasoline Engines Automation and Machine Learning Techniques in Calibration
18. A.C.Alkidas, "Combustion-chamber crevices: The major source of engine-out hydrocarbon emissions under fully warmed conditions," *ScienceDirect*, vol. 25, no. 3, pp. 253-273, 1999. Available: [https://doi.org/10.1016/S0360-1285\(98\)00026-4](https://doi.org/10.1016/S0360-1285(98)00026-4)
19. M. Perin and T. Okoniewski, "Lean Burn Engines," *SAE International* , no. 2013-36-0402, 2013. Available: <https://doi.org/10.4271/2013-36-0402>
20. A. Kamane, "Gaseous Fuel Injection For Engine With A Scavenged Pre-Chamber," Diploma Thesis: Department of Automotive, Combustion Engine and Railway Engineering, Czech Technical University, Prague, 2019. Available: <http://hdl.handle.net/10467/85131>
21. Karsten Roepke. IAV. DOE in Engine Development. Available: [10.1002/qre.941](https://doi.org/10.1002/qre.941)
22. Cory Natoli Sarah Burke, Ph.D. Computer Experiments: Space Filling Design and Gaussian Process Modeling. Available: https://www.afit.edu/stat/statcoe_files/Computer%20Experiments-%20Space%20Filling%20Designs%20and%20Gaussian%20Process%20Modeling.pdf
23. Model based calibration toolbox for use with MATLAB & Simulink
24. Box Behenken Design
https://en.wikipedia.org/wiki/Box%E2%80%93Behnken_design
25. Karsten ROEPKE. Design of Experiments for Engine Calibration JL. Available:004/14/5304–0322 C 2014 SICE
26. Benjamin Berger. Modeling and Optimization for Stationary Base Engine Calibration. Semantic scholar. Available: Corpus ID: 116770020
27. GT power DOE POST manual
28. AVL CAMEO 4 R2 User Guide basics
29. IAV ORION manual
30. Zetor Datasheet. Available: <https://www.zetor.com/data/files/traktor-forterra-en.pdf>
31. Ing.Shubham Bawkar. "Mixture Homogeneity Evaluation for a CNG Port Fuel Injection on a Gas Engine". Available : <http://hdl.handle.net/10467/90398>

32. GT-Power Performance tutorial manual

33. Battery weight of Tesla Model S. Available:
https://en.wikipedia.org/wiki/Tesla_Model_S

34. Fred Schlachter. “Has the Battery Bubble Burst?”. American Physics society.
August/September 2012 (Volume 21, Number 8).

12. List of Figure

| | |
|--|----|
| Figure 1 Chemical Efficiency vs. Air excess [13]..... | 13 |
| Figure 2 sample engine control volume[11]..... | 13 |
| Figure 3 Energy balance for a spark-ignited gasoline engine as a function of load. Operating Conditions:2000 rpm, bmep from 100 to 920 kPa [11]..... | 14 |
| Figure 4 Bosch L-Jetronic Multi point PFI. [11]..... | 15 |
| Figure 5 Emission Vs A/F Ratio[11]..... | 16 |
| Figure 6 Schematic of Flow process during a) blowdown phase b) exhaust stroke[11]..... | 17 |
| Figure 7 Space Filling Design | 19 |
| Figure 8 Latin Hypercube design | 19 |
| Figure 9 Stratified Latin Hypercube sampling | 20 |
| Figure 10 Sobol design | 21 |
| Figure 11 Stationary Measurements: Control (CT) , Stabilization (ST) and Averaging Time (AT)..... | 22 |
| Figure 12 Parallel Optimization | 24 |
| Figure 13 Zetor 1605 Diesel Engine | 27 |
| Figure 14 Engine Testcell..... | 28 |
| Figure 15 GT-Suite Environment Block | 28 |
| Figure 16 Cylinder Block | 29 |
| Figure 17 Crank train Block | 29 |
| Figure 18 Engine Friction Block | 30 |
| Figure 19 FMEP Curve | 31 |
| Figure 20 Piston Geometry Block | 31 |
| Figure 21 Valve Lift Profile | 32 |
| Figure 22 Common Mixer Fuel Injection System..... | 33 |
| Figure 23 MPFI system | 33 |
| Figure 24 Common Mixer Injector System..... | 34 |
| Figure 25 MPFI System..... | 34 |
| Figure 26 Air Filter Block | 35 |
| Figure 27 Air Filter engine test cell..... | 35 |
| Figure 28 Intercooler System | 35 |
| Figure 29 CZ C14-63 TC | 36 |
| Figure 30 Compressor Map | 37 |
| Figure 31 Waste Gate Control..... | 37 |
| Figure 32 Thermocouple Model..... | 38 |
| Figure 33 Knock Illustration | 39 |
| Figure 34 Knocking Predicted by model..... | 41 |
| Figure 35 Low-Pressure EGR System..... | 41 |

| | |
|---|----|
| Figure 36 High-Pressure EGR System | 42 |
| Figure 37 EGR Venturi System..... | 42 |
| Figure 38 Exhaust Throttle Flap..... | 43 |
| Figure 39 Closed Loop EGR System | 43 |
| Figure 40 EGR Cooler 25.4mm Diameter Inlet/Outlet | 44 |
| Figure 41 Closed Loop Throttle Control System | 44 |
| Figure 42 Discharge Coefficient vs Throttle Angle | 45 |
| Figure 43 Throttle 88mm Diameter..... | 45 |
| Figure 46 CAMEO I/O System | 47 |
| Figure 47 DOE Data Fit - Common Mixer System..... | 48 |
| Figure 48 DOE Data Fit - MPFI System | 48 |
| Figure 52 BS NO _x Vs. Speed RPM | 51 |
| Figure 54 Mass Averaged Turbine Inlet Temperature K vs. Engine Speed RPM | 52 |
| Figure 60 Torque Vs. RPM with EGR Isolines..... | 63 |
| Figure 61 Torque Vs. RPM with Knock Induction Integral Isolines | 63 |
| Figure 63 Torque Vs. RPM with Temperature Isolines | 64 |
| Figure 65 Engine Torque vs. Speed RPM with BSCo ₂ g/kWh isolines | 65 |
| Figure 66 Torque Vs. RPM with Power Isolines | 66 |
| Figure 69 Torque Vs. RPM with Knock Integral Isolines..... | 67 |
| Figure 71 Torque Vs. RPM with Cylinder Pressure Isolines | 68 |
| Figure 72 Torque Vs. RPM with maximum cylinder pressure..... | 70 |
| Figure 73 Torque Vs. RPM with BSCO ₂ g/kWh..... | 71 |

13. List of Tables

| | |
|--|----|
| Table 1 Overview of the Automated Optimization Software with their different aspects | 25 |
| Table 2 Engine Specification..... | 27 |

14. List of Files in Attached CD

- Master thesis report
- GT Power models
- Calibration results excel file.

15. Appendix.

15.1 Common Mixer system

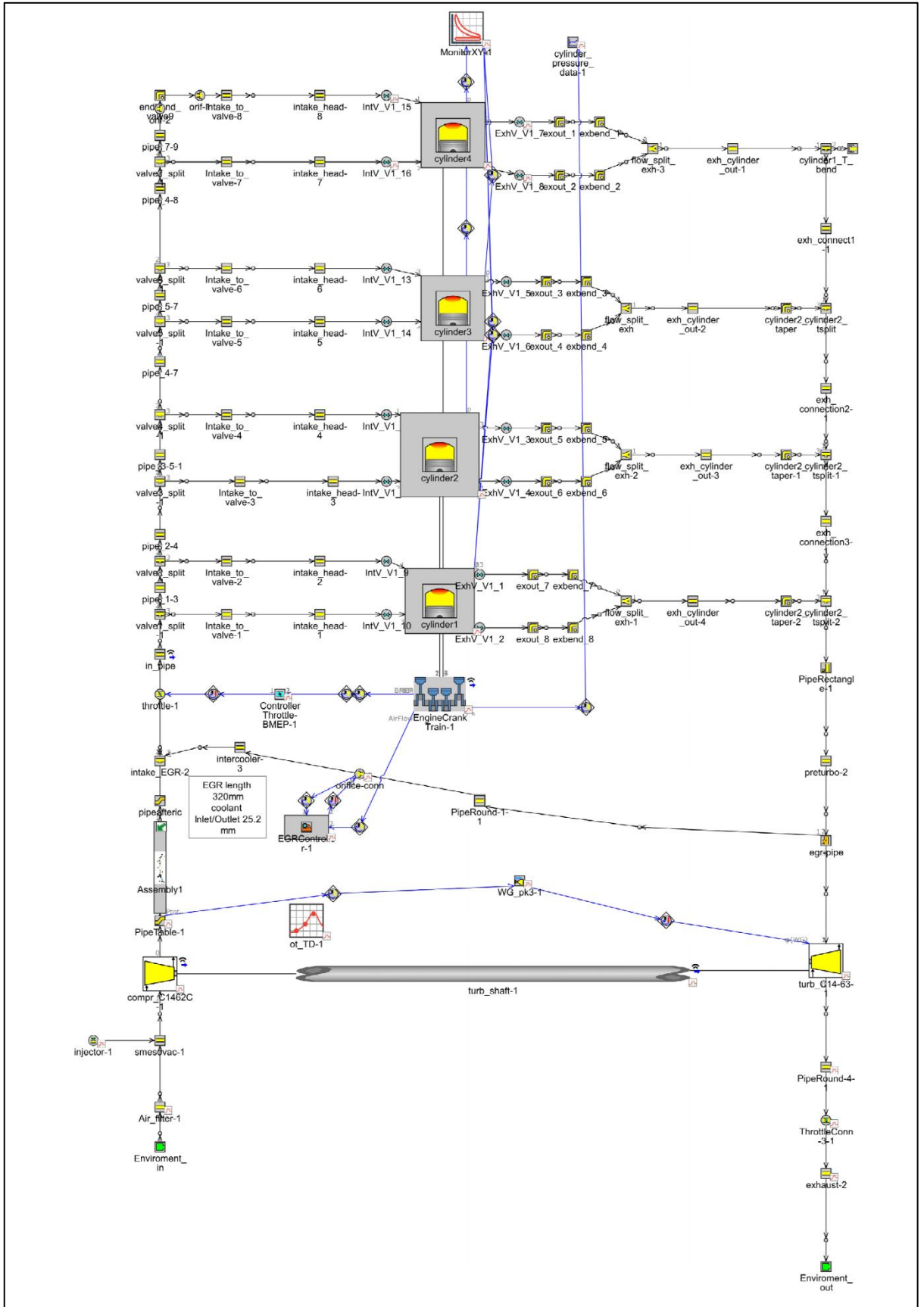


Figure 56 Common Mixer GT Power Model

15.2 MPFI system

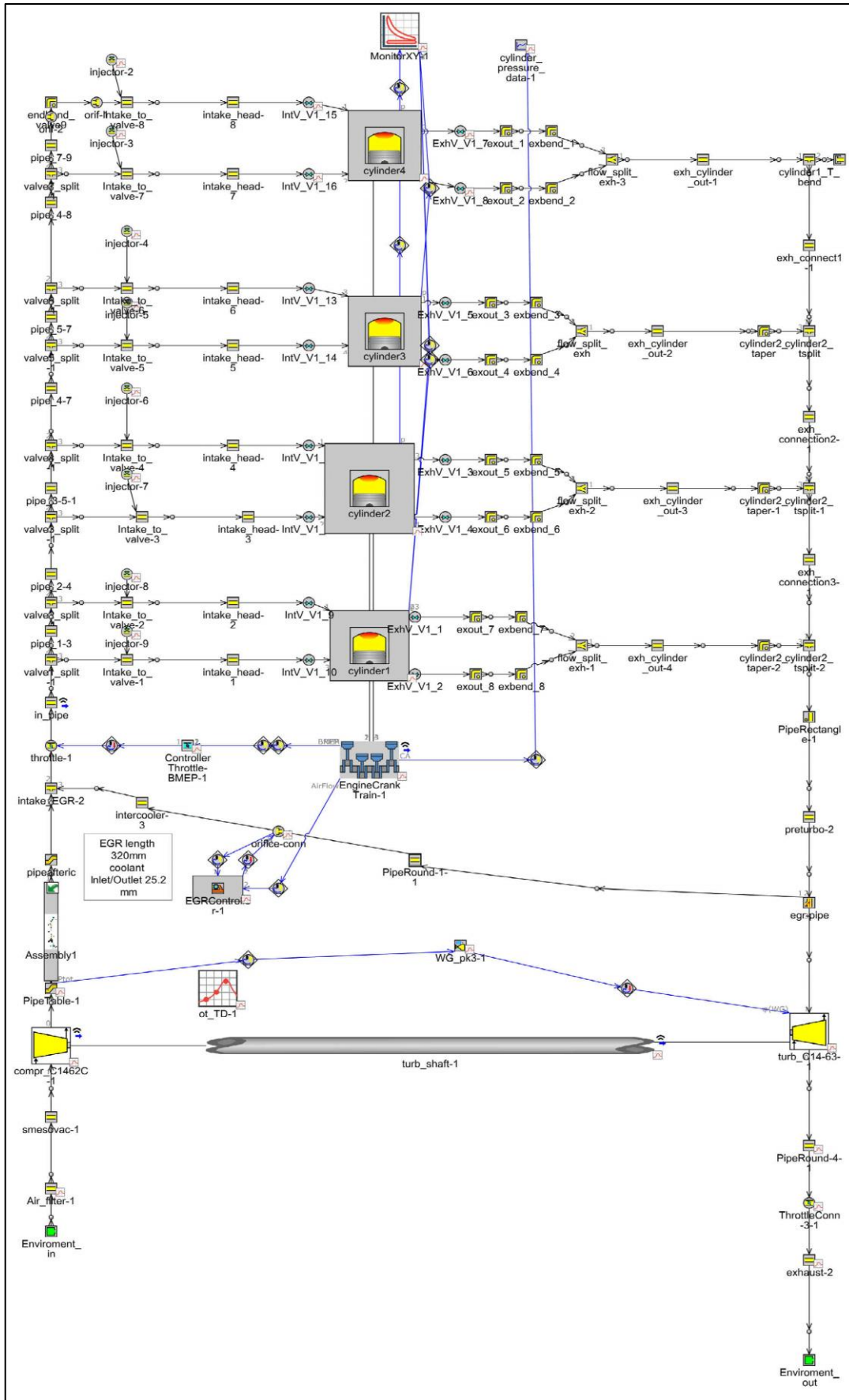


Figure 57 MPFI GT-Power Model

15.3 Simulation graphs

15.3.1 Common Mixer system

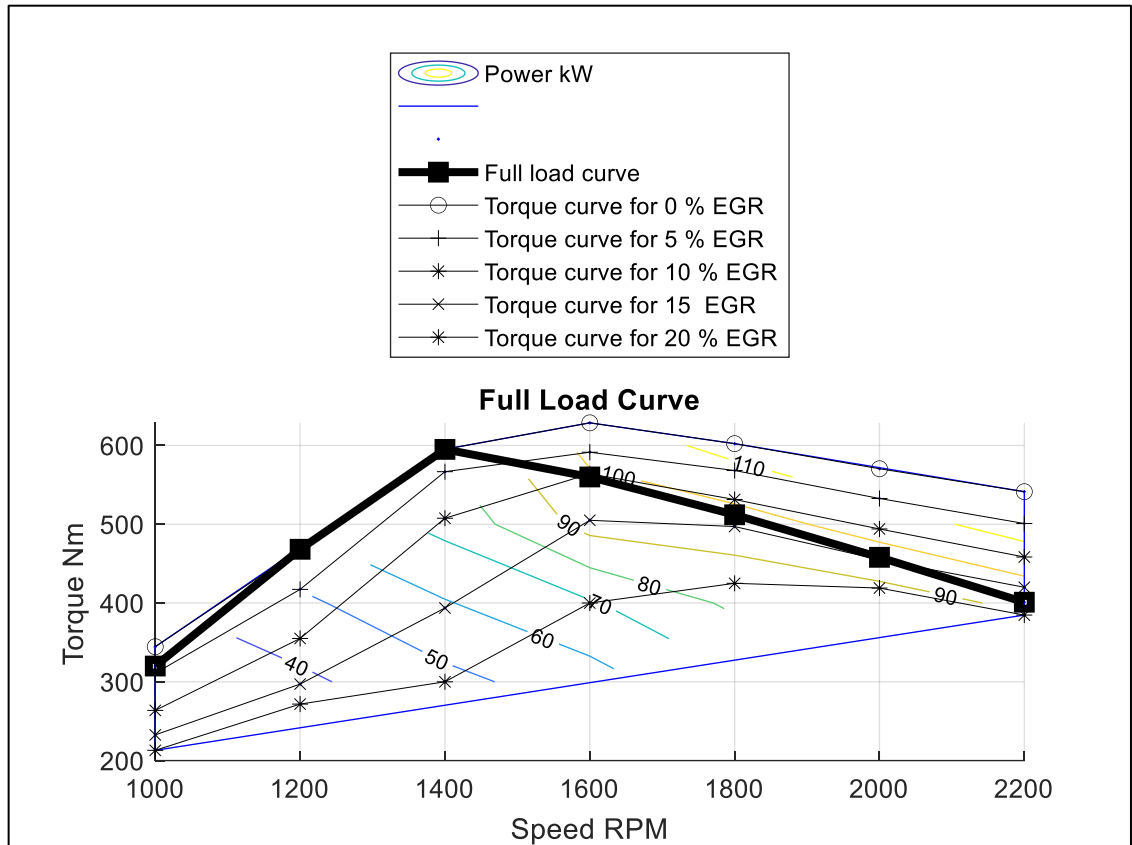


Figure 58 Torque Vs. RPM with Power Isolines

The common-mixer system reaches a peak power of 101kW at 1600RPM.

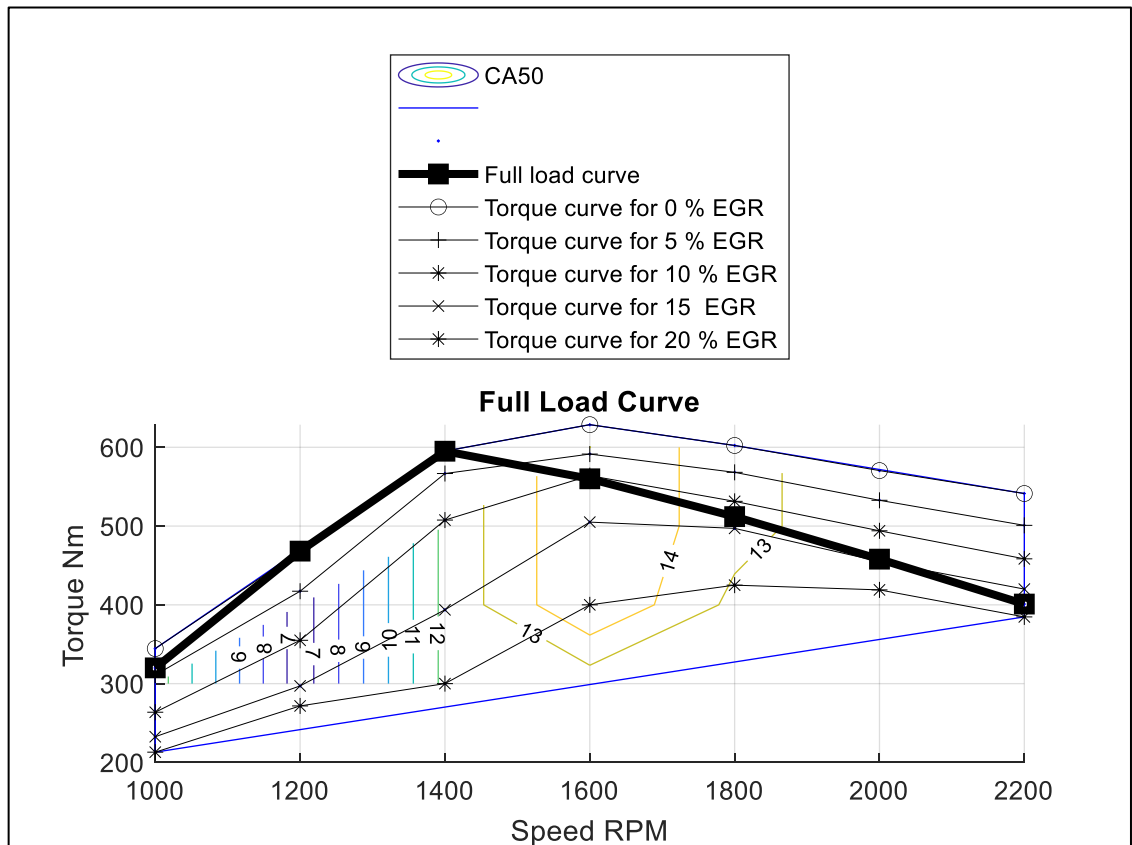


Figure 59 Torque Vs. RPM with CA50 Isolines

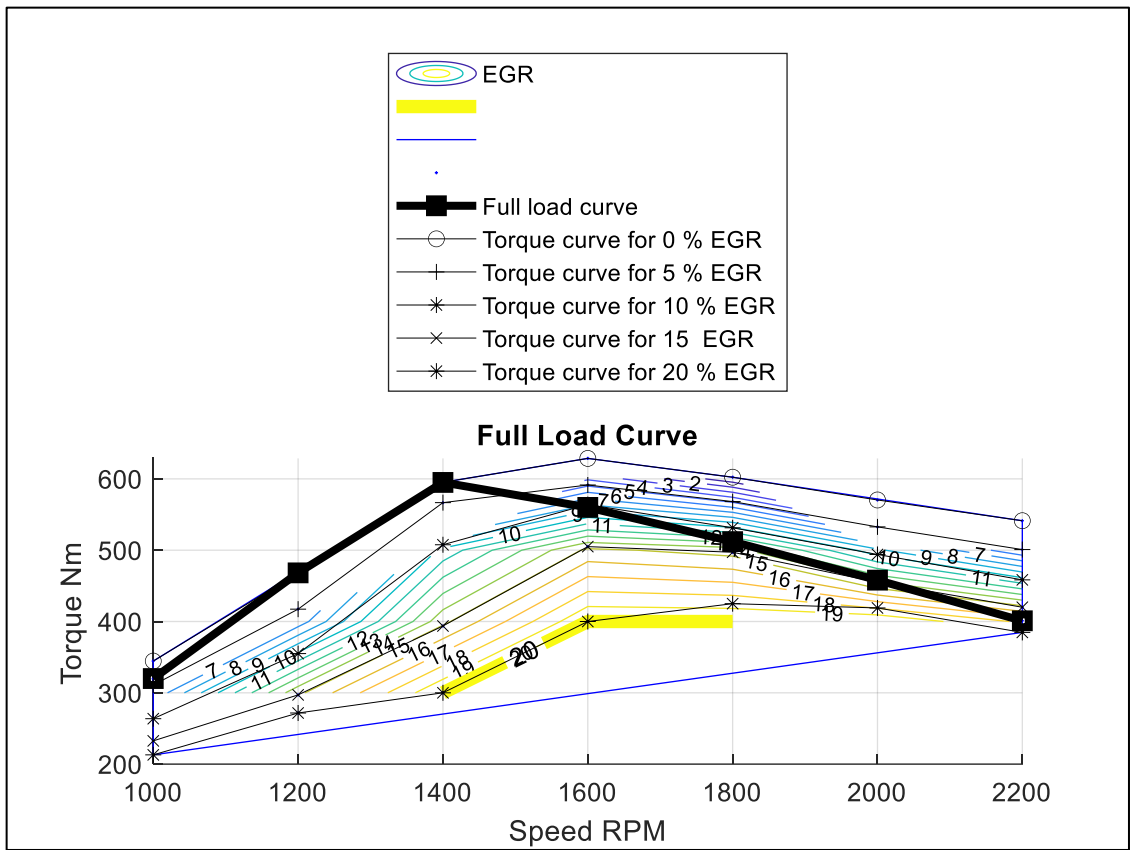


Figure 60 Torque Vs. RPM with EGR Isolines

The maximum EGR percentage is limited to 20%, and it can be seen by the yellow isolines.

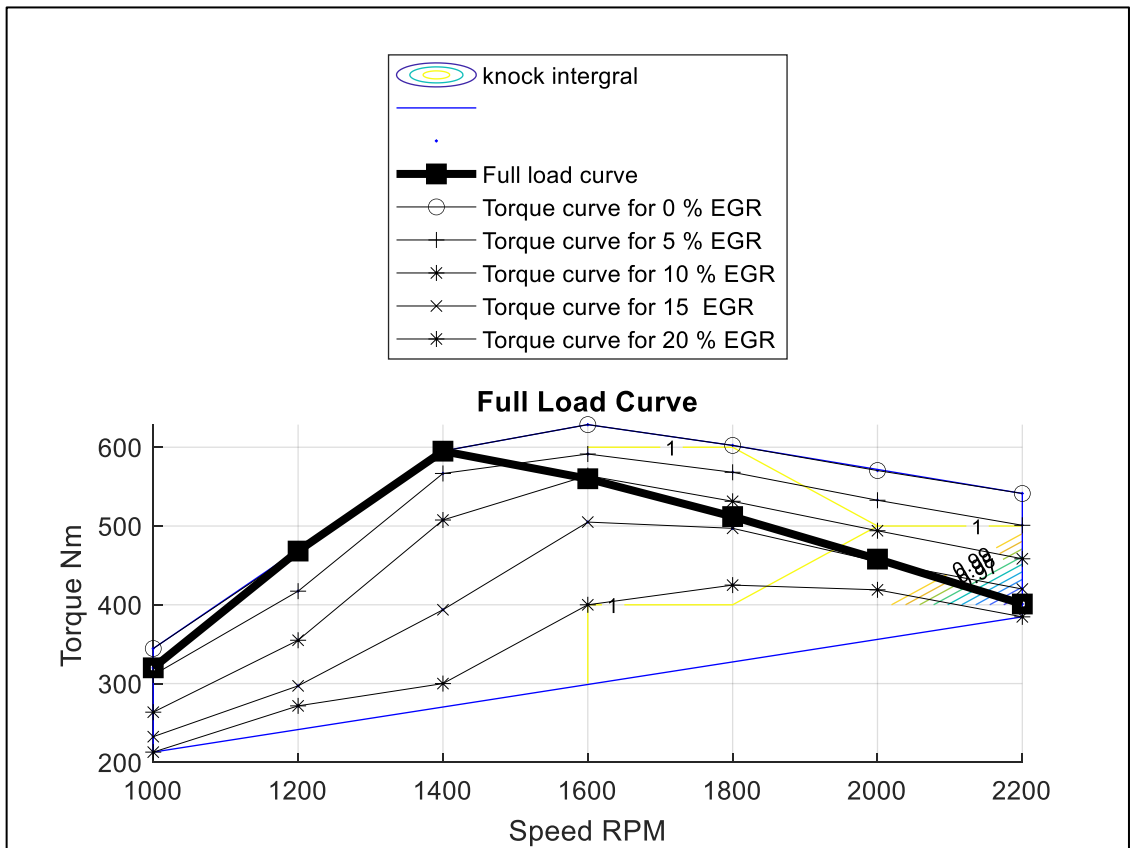


Figure 61 Torque Vs. RPM with Knock Induction Integral Isolines

The Knock induction time integral value border limit is 1, and the full load curve follows this limit.

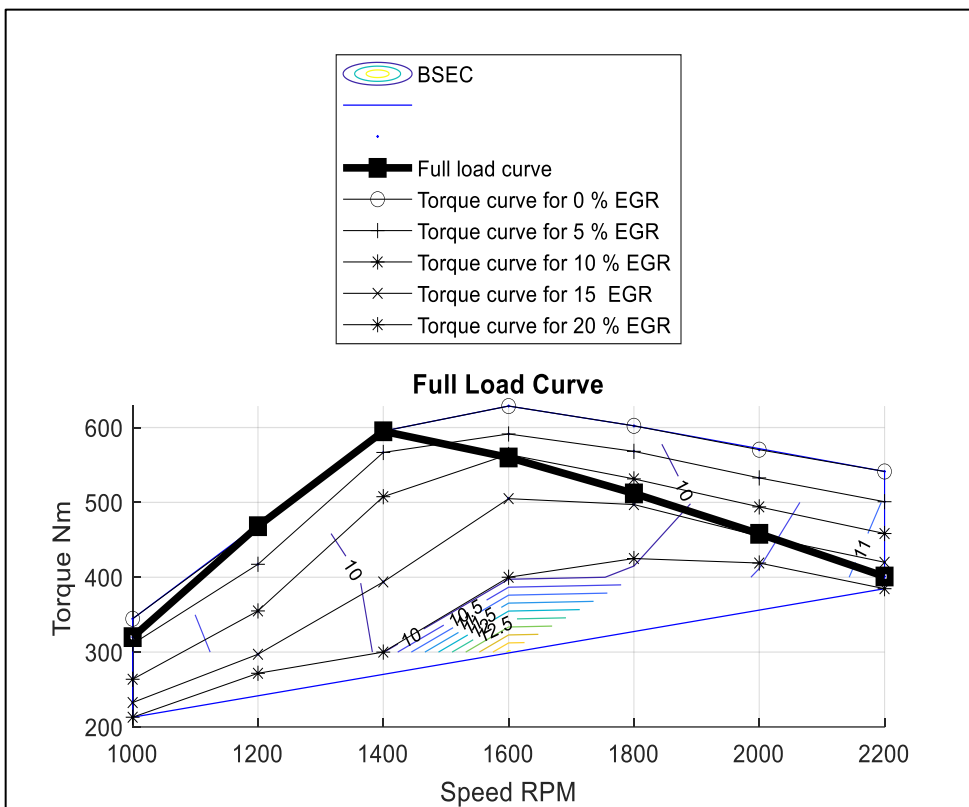


Figure 62 Torque Vs. RPM with BSEC Isolines

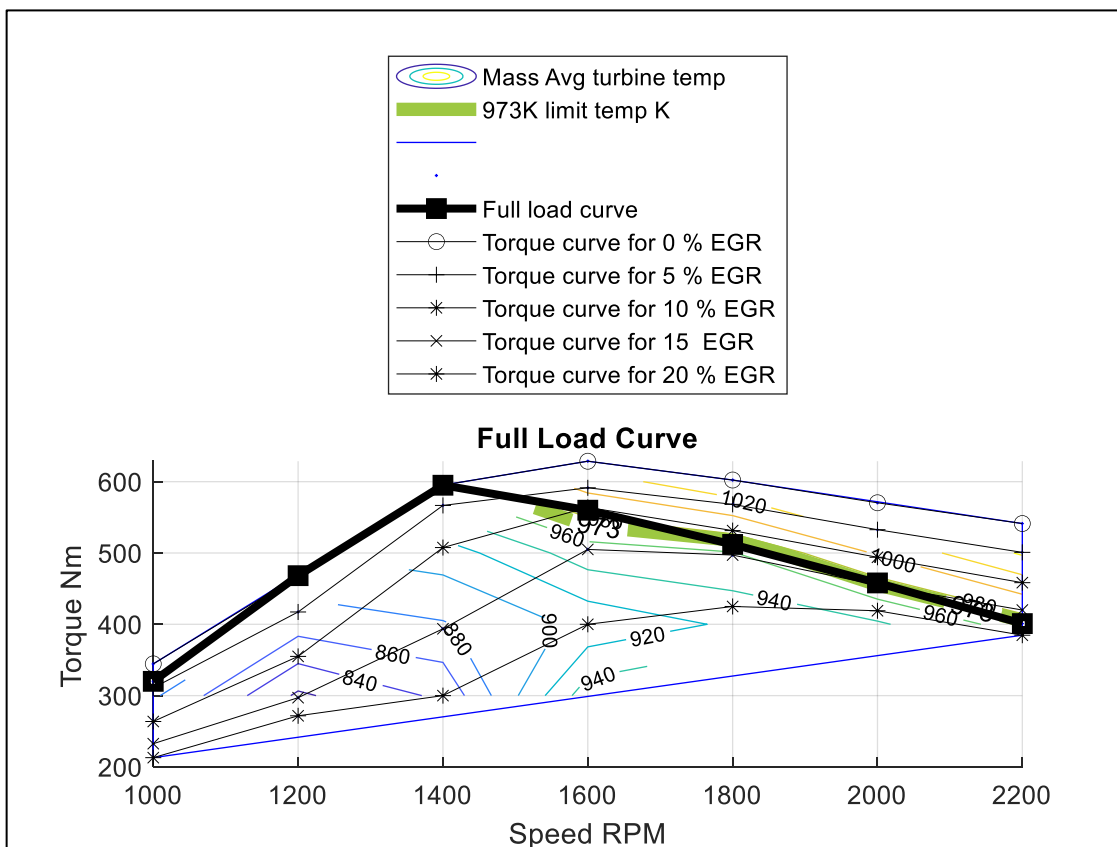


Figure 63 Torque Vs. RPM with Temperature Isolines

The mass average turbine inlet temperature is limited to 973K, denoted by the green borderline.

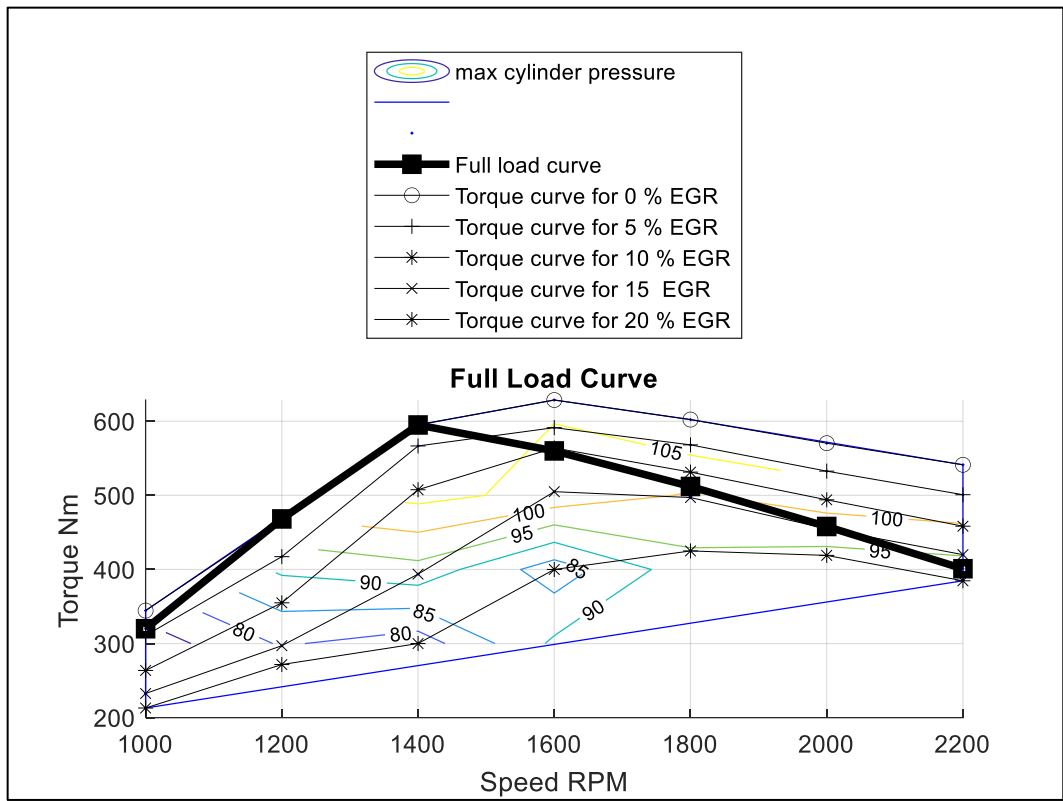


Figure 64 Torque Vs RPM with Cylinder Pressure Isolines

The maximum cylinder pressure limit is 140 bar and from figure 54, all the pressure values are within this limits.

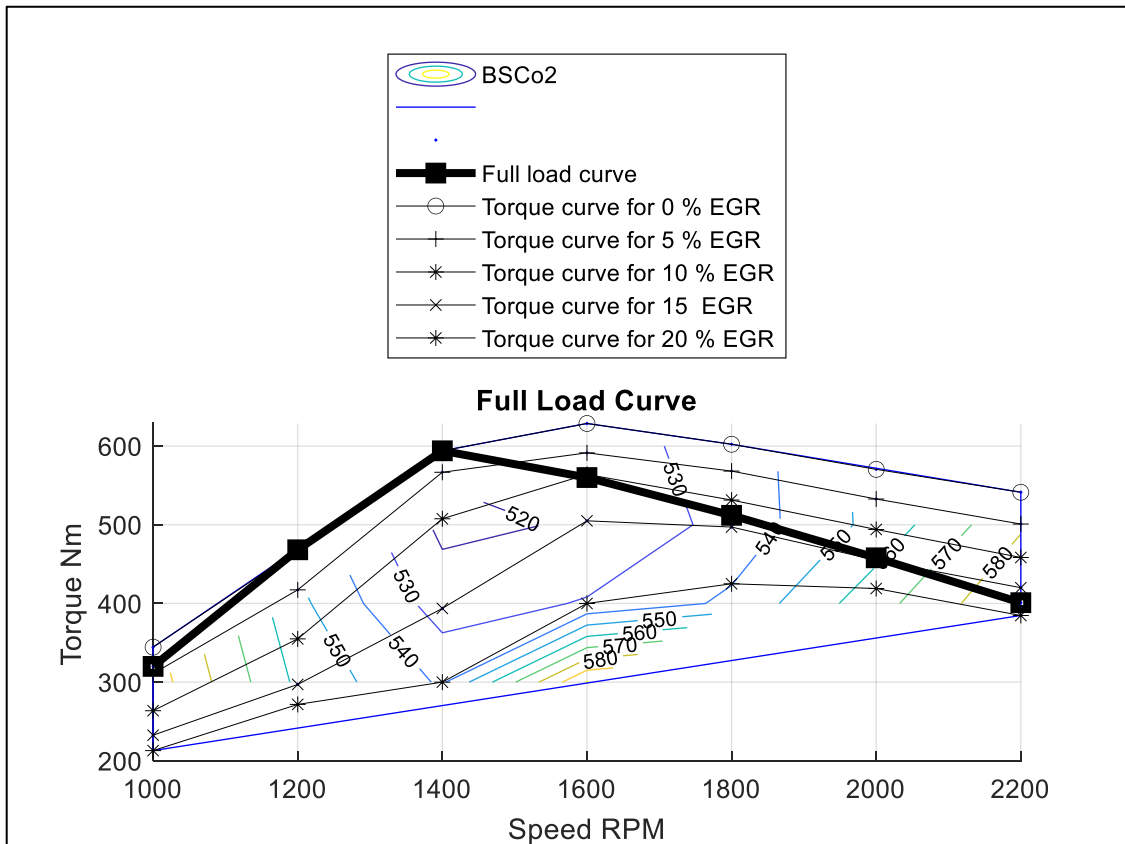


Figure 65 Engine Torque vs. Speed RPM with BSCo2 g/kWh isolines

15.3.2 MPFI system full load optimization

The same procedure of common-mixer was applied for the optimization of the MPFI system. The results are as follows.

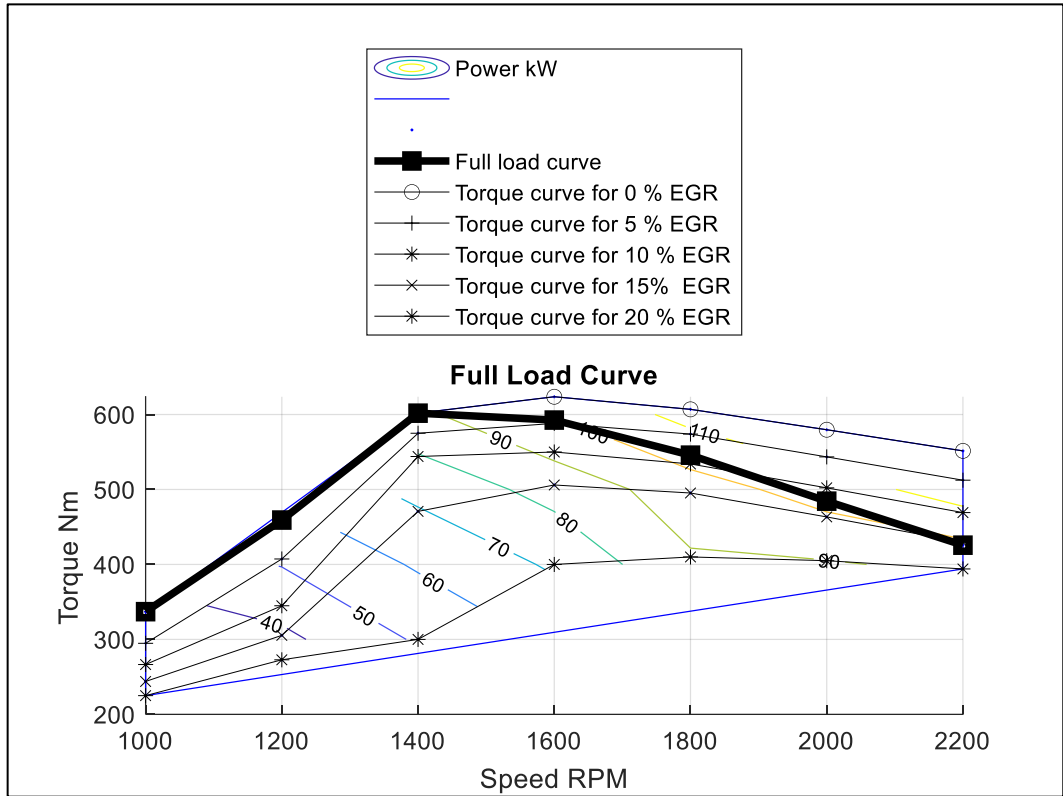


Figure 66 Torque Vs. RPM with Power Isolines

The MPFI system offers a power output of 103kW at 1800RPM.

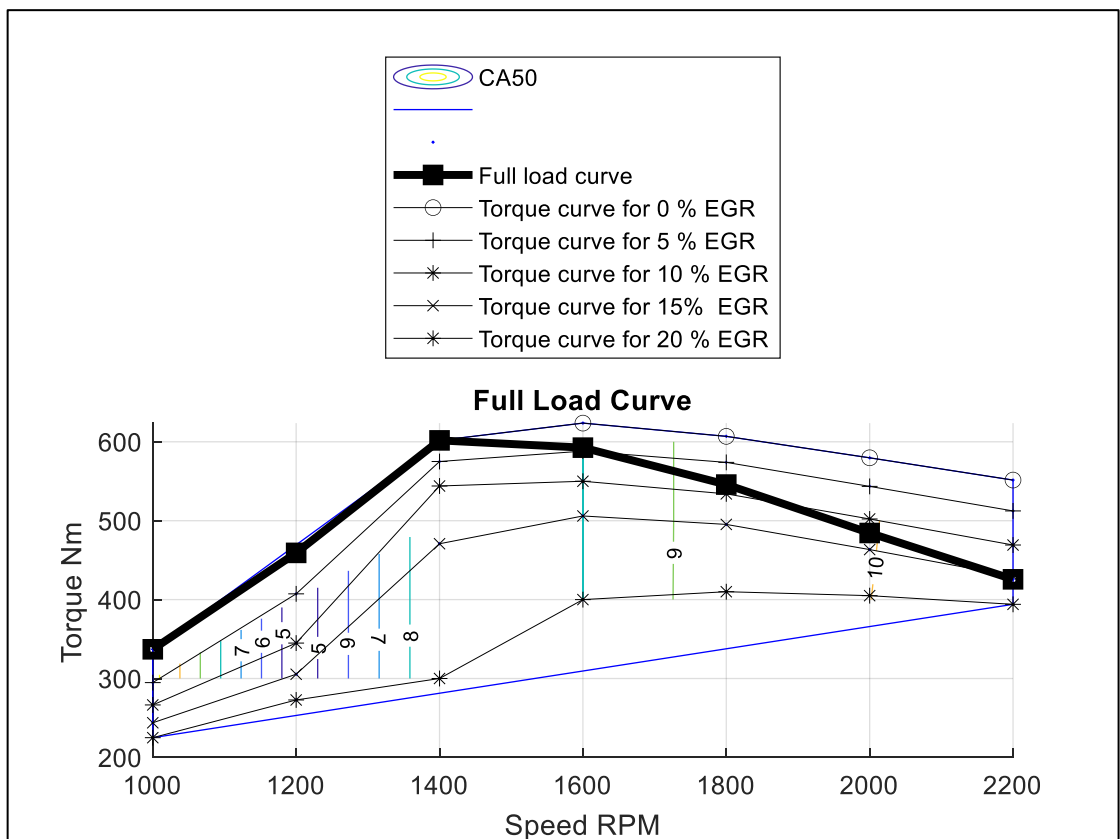


Figure 67 Torque Vs. RPM with CA50 Isolines

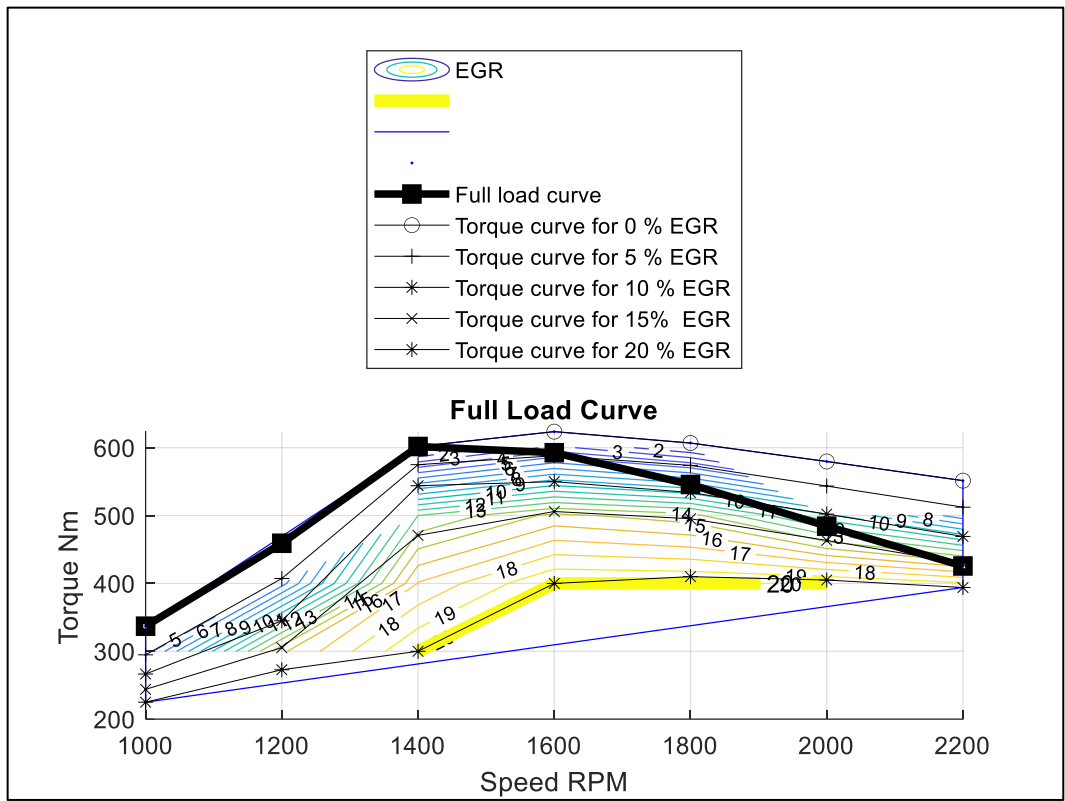


Figure 68 Torque Vs. RPM with EGR Isolines

From fig 68, The maximum EGR percentage is limited to 20%, and it can be seen by the yellow isolines.

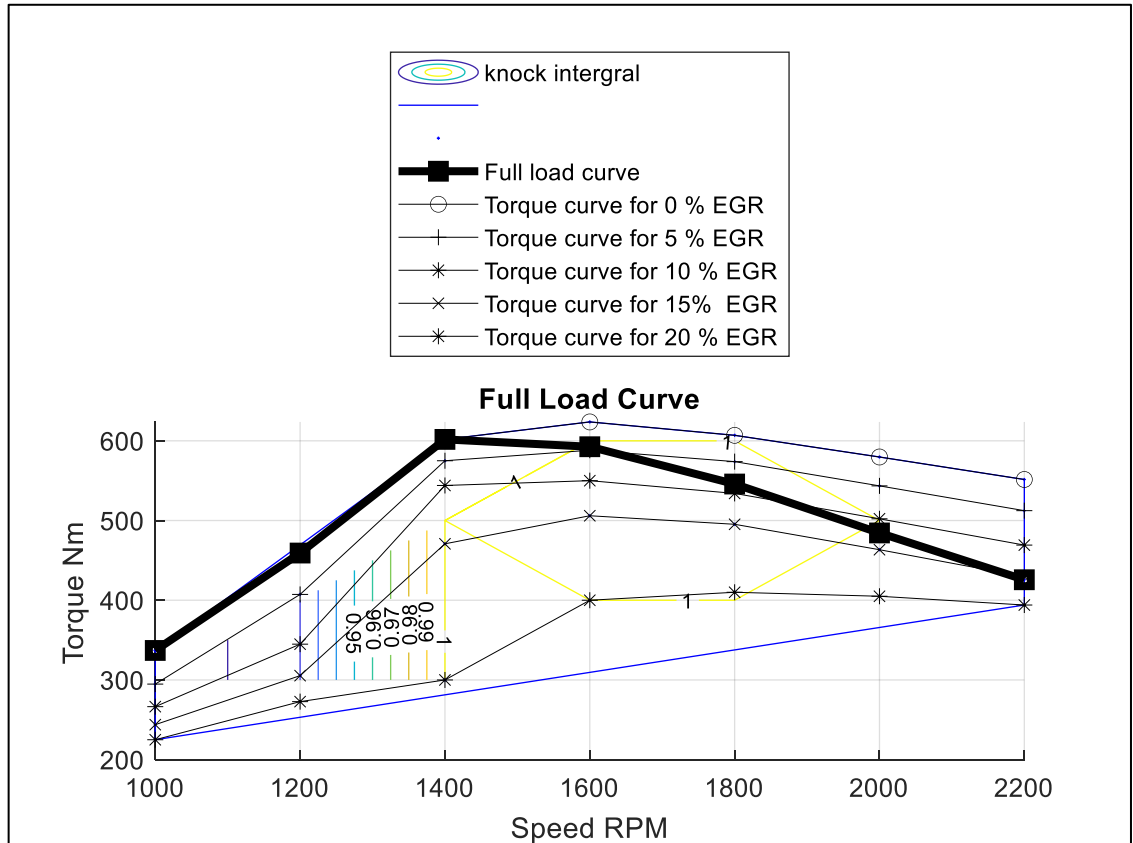


Figure 69 Torque Vs. RPM with Knock Integral Isolines

From fig 68, The Knock induction time integral value border limit is 1, and the full load curve follows this limit.

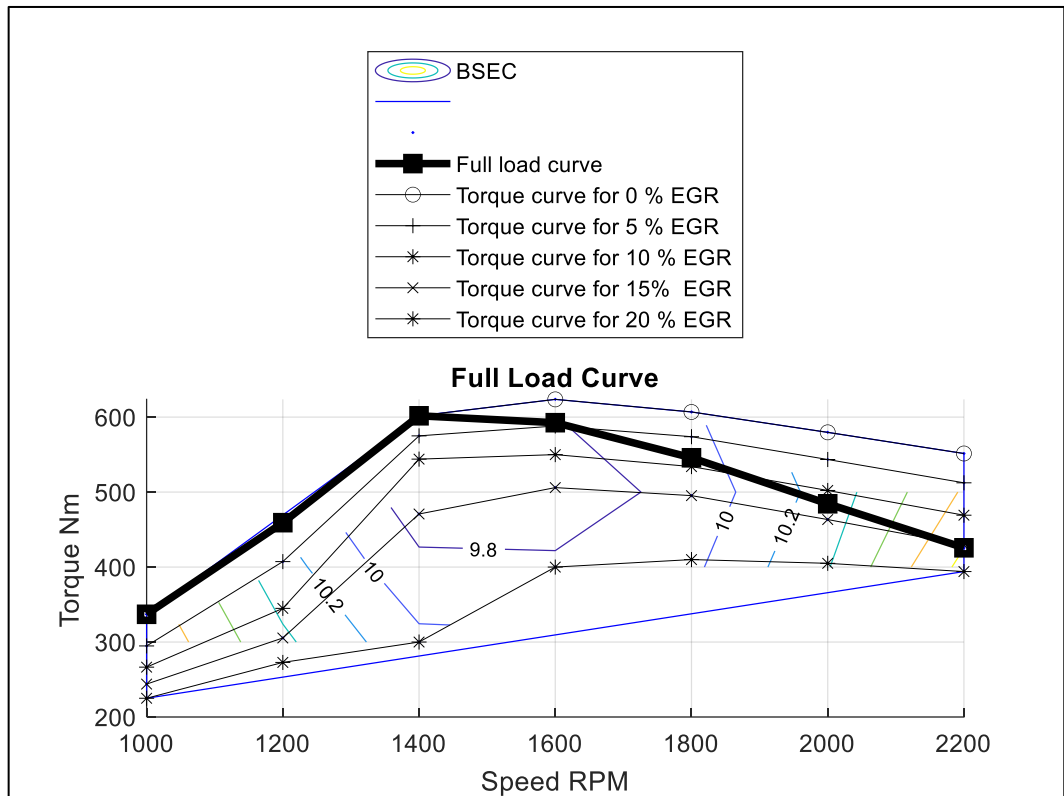


Figure 70 Torque Vs. RPM with BSEC Isolines

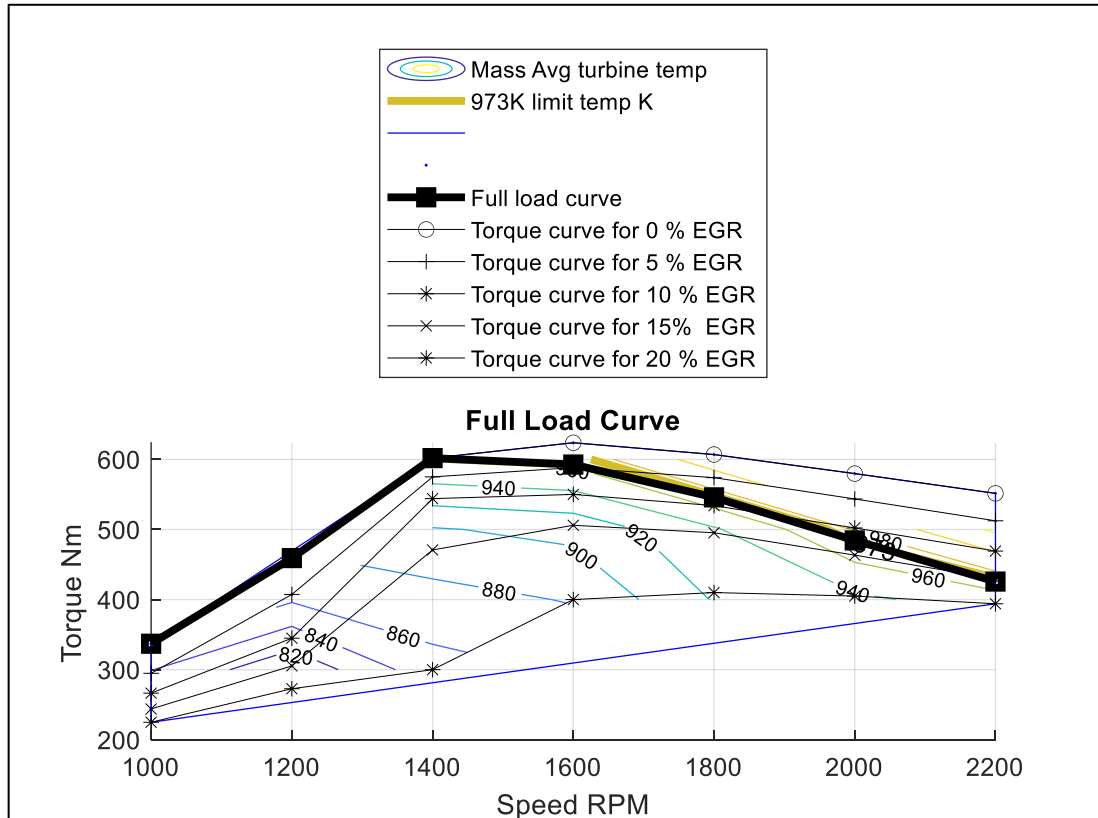


Figure 71 Torque Vs. RPM with Cylinder Pressure Isolines

From fig 71, The mass average turbine inlet temperature is limited to 973K, denoted by the green borderline.

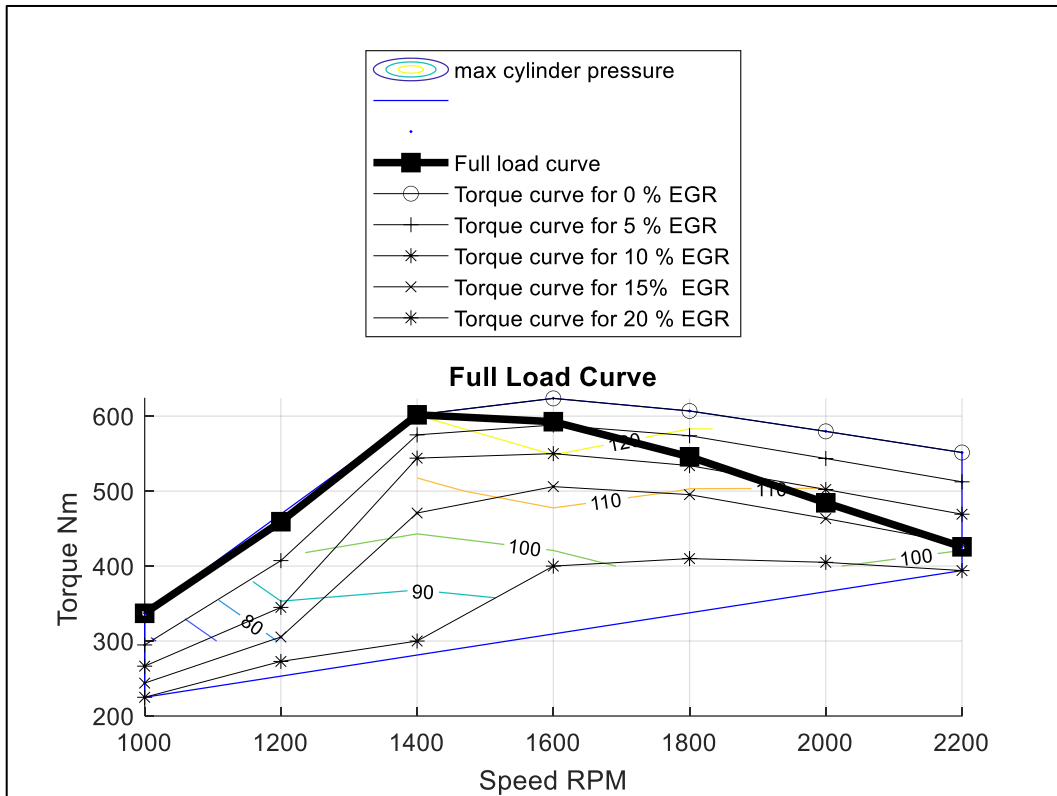


Figure 72 Torque Vs. RPM with Cylinder Pressure Isolines

The maximum cylinder pressure limit is 140 bar, and from figure 72, all the pressure values are within this limit.

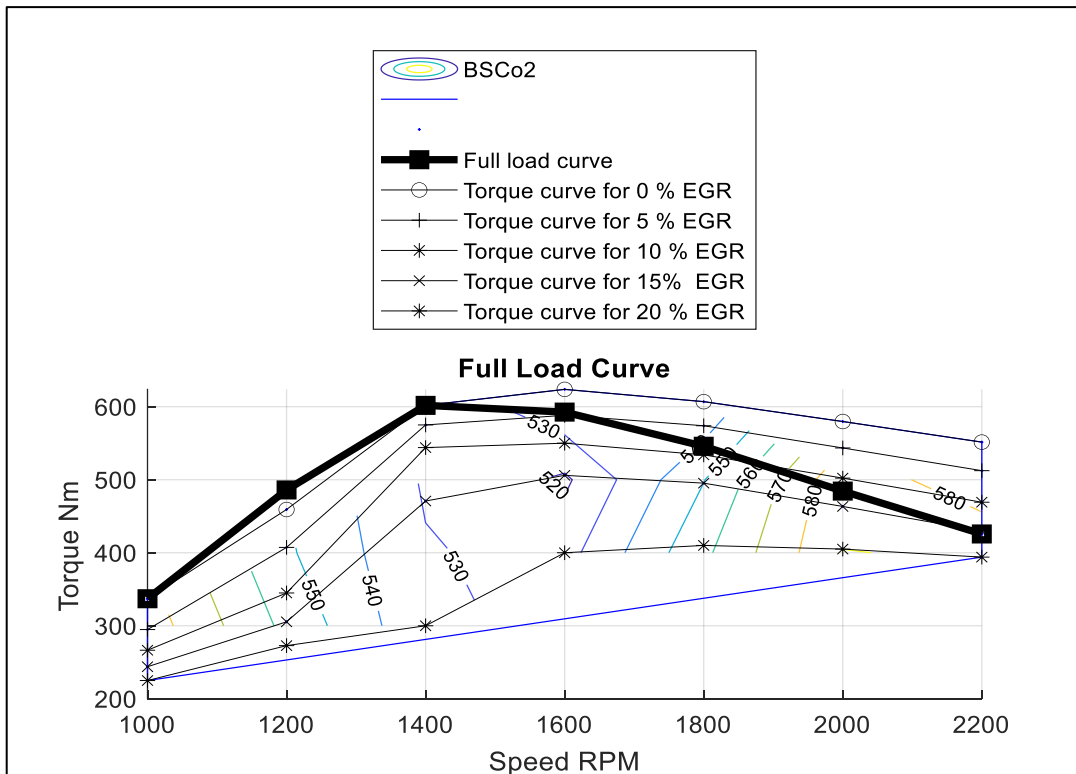


Figure 73 Engine Torque Vs. Speed RPM with BSCO2 g/kWh isolines

15.4 Zetor Forterra 135 Diesel Datasheet[30]

SIMPLE BUT NOT STUPID

www.zetor.com

ZETOR FORTERRA 135

| | |
|--------|---------------------------------|
| Width | 222 cm |
| Length | 501 cm (incl. front linkage) |
| Height | 279 cm (exhaust stack) |



TECHNICAL DATA

Engine | 95kW/129 HP to ECE R24 at 2,200 rpm; water-cooled four-cyl Zetor 1605 engine (Stage IIIA) with turbocharger, intercooler and four valves per cylinder; 4,156 cm³ displacement; 180-litre fuel tank.

Transmission | 24F/18R speeds, four main gears, two ranges, three powershift steps, synchronised shuttle, 40 km/hr.

Brakes | Wet disc brakes at rear, hydraulic engagement, front disc brake on propshaft; mechanical hand brake; air brake system is supplied as standard.

Electrics | 12 V, 165 amps battery, 100 amps alternator, 3.2 kW/4.4 hp starter power.

Linkage | Category II, ELC with draft link control and shock absorption, standard slip control option. Optional front linkage and front pto package.

Hydraulics | Gear pumps with 70-litre/min capacity + 30-litre/min flow for steering system, 190 bar; three double-acting spools with float position are standard; available oil for external use by trailed and mounted implements is 22 litres.

PTO | 54D/1,000 or 54DE/1,000 and ground speed pto with 24/18 speeds; 1 3/8in, six splines.

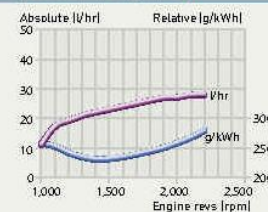
Axles and running gear | Planetary axle with multi-plate differential lock, pneumatic 4WD and differential lock engagement; RD-70 Mitas test tyres 420/70 R24 at the front and Mitas RD-B2 520/70 R38 at the rear.

Service and maintenance | 11.0 litres of engine oil (500-hour intervals), 52 litres of gearbox/hydraulic oil (1,500 hours), 22.5-litre cooling system.

Output and torque



Fuel consumption



RESULTS FROM THE TEST STATION

| | |
|------------------------------|---------------|
| Pto output | |
| Max (1800 rpm) | 89.8 kW |
| At rated speed | 85.2 kW |
| Fuel consumption | |
| Specific at max draft output | 24.4 g/kWh |
| Specific at rated speed | 27.9 g/kWh |
| Absolute max/rated speed | 26.2/28.4 l/h |

| | |
|-------------------|---------------------|
| Torque | |
| Max | 54.4 Nm (1,400 rpm) |
| Torque rise | 47.1 % |
| Engine speed drop | 36.4 % |
| Start-off torque | 96 % |

| | |
|----------------------------------|----|
| Transmission | |
| No. of gears in 4-12 km/hr range | 10 |

| | |
|--|-----------------------|
| Rear lift capacities (90% max oil pressure, cor.) | |
| Bottom/middle/top | 5,049/5,931/6,039 daN |
| Lift height under load | 69.0 cm (20-89.0 cm) |

| | |
|---|------------------------|
| Front lift capacities (90% max oil pressure, cor.) | |
| Bottom/middle/top | 2,979/3,393/3,924 daN |
| Lift height under load | 66.5 cm (20.5-87.0 cm) |

| | |
|-------------------------|-------------------------------|
| Hydraulic output | |
| Operating pressure | 192.9 bar |
| Max flow | 70.7 l/min |
| Max output | 18.4 kW (62.1 l/min, 178 bar) |

| | |
|----------------------|---------------------|
| Drawbar power | |
| Max (1,800 rpm) | |
| At rated speed | 78.9 kW (298 g/kWh) |

| | |
|---|-----------------|
| Noise level (Under load at driver's ear) | |
| Cab closed/open | 80.0/84.0 dB(A) |

| | |
|-----------------------|----------------------|
| Braking | |
| Max mean deceleration | 5.8 m/s ² |
| Pedal force | 27 daN |

| | |
|------------------------|---------------|
| Turning circle | |
| 4WD disengaged/engaged | 10.70/11.40 m |

| | |
|------------------------|------------|
| Test weight | |
| Front axle | 2,045 kg |
| Rear axle | 2,505 kg |
| Unladen weight | 4,500 kg |
| GVWR | 8,000 kg |
| Payload | 3,450 kg |
| Power-weight ratio | 4.8 kg/kW |
| Wheelbase | 233 cm |
| Track width front/rear | 172/174 cm |
| Ground clearance | 38 cm |

FUEL ECONOMY AT TYPICAL PERFORMANCE

| Working areas | Output | Speed | g/kWh | l/h |
|---------------------------|--------|-------|-------|------|
| Standard speed PTD 54D | 100 % | 1,911 | 251 | 26.9 |
| Economy PTD 54DE | 100 % | 1,563 | 232 | 23.7 |
| Standard speed PTD 1,000 | 100 % | 1,950 | 254 | 27.1 |
| Economy PTD 1,000E | 100 % | - | - | - |
| Engine in top speed range | 80 % | max | 305 | 24.9 |
| High output | 80 % | 70 % | 264 | 21.6 |
| Transport work | 40 % | 90 % | 310 | 12.7 |
| Low output, 1/2 speed | 40 % | 60 % | 267 | 10.1 |
| High output, 1/2 speed | 60 % | 60 % | 231 | 8.1 |

THE TEST RESULTS

| | |
|--|-----|
| Engine <input checked="" type="checkbox"/> | |
| Performance characteristics | 2.1 |
| Fuel economy | 1.5 |
| Pto output/drawbar power | 1.7 |
| Good performance characteristics and high drive power, but a low start-off torque. Fuel economy is nearly 6% better than the average for the Forterra 135's power class. | |

| | |
|---|-----|
| Transmission <input checked="" type="checkbox"/> | |
| Gearbox ratios/functions | 3.5 |
| Shifting | 2.8 |
| Clutch, throttle | 3.5 |
| Pto | 4.0 |

Basic gearbox with a large number of speeds. No forward/reverse powershuttle and only three powershift steps. Pto has two speeds, which are selected by turning the stub.

| | |
|---|------|
| Axles and running gear <input checked="" type="checkbox"/> | |
| Steering | 1.5 |
| Four-wheel drive and diff lock | 3.5 |
| Hand/foot brake | 2.0 |
| Suspension | n.a. |
| Weight and payload | 3.5 |

Manoeuvrable with a direct steering system, but no auto engagement of four-wheel drive and diff lock; powerful brakes; no front-axle suspension available; inadequate payload.

| | |
|---|-----|
| Linkage/hydraulics <input checked="" type="checkbox"/> | |
| Lift power and lift height | 2.0 |
| Operation | 1.5 |
| Hydraulic output | 3.7 |
| Spool valves | 4.0 |
| Hydraulic couplers | 4.0 |

Excellent lift capacities and operation; hydraulic output too low for this hp bracket; operation and labelling of rear spools need improving.

| | |
|--|-----|
| Cab <input checked="" type="checkbox"/> | |
| Space and comfort | 3.2 |
| Visibility | 2.5 |
| Heating/ventilation | 3.0 |
| Noise level | 4.0 |
| Electric system | 2.0 |
| Build quality | 2.0 |
| Maintenance | 2.0 |

Space and visibility are OK for a tractor in this power sector; 80dB(A) noise level under load is high and needs further designer attention.

| ABILITY | <input checked="" type="checkbox"/> | <input checked="" type="checkbox"/> | <input checked="" type="checkbox"/> | <input checked="" type="checkbox"/> | <input checked="" type="checkbox"/> |
|-------------------|-------------------------------------|-------------------------------------|-------------------------------------|-------------------------------------|-------------------------------------|
| Basic standards | | | | | |
| Average standards | | | | | |
| High standards | | | | | |
| Fieldwork | | | | | |
| Grassland work | | | | | |
| Transport work | | | | | |
| Ladder work | | | | | |

Grading system
 very good; good; average;
 below average; poor

The individual marks are extracts from our assessments and do not necessarily result in a mathematically conclusive overall mark.

PROFI TRACTORS 10/2011, www.profi.com

